Master Thesis carried out to obtain the following degrees:

Master Degree in Smart Cities and Communities (SMACCs)

&

Master Degree in Research in Energy Efficiency and Sustainability in Industry, Transportation, Building and Urban Planning (EESITBUP)

Title: A multifaceted analysis of COVID-19 propagation in confined spaces:

A techno-economic assessment of ventilation, heating, and renewables integration

Student: Abdulrahman Mohammed

Supervisor: Prof. Álvaro Campos-Celador

Academic Course: 2020/2021

Date: 13/07/2021

ABSTRACT

The outbreak of novel coronavirus disease 2019 (COVID19) has spread rapidly, affecting nearly all countries and territories around the globe, impacting every aspect of human life. Governments and various organizations worldwide have issued mitigation measures to counteract COVID-19 virus propagations, whether in indoor spaces or outdoors. Although the underlying uncertainty concerning COVID-19 transmission details, most international organizations such as WHO, ECDC, ASHRAE, REHVA, and CIBSE agree on the important role of ventilation to minimize the causes and reduce the viability of SARS-CoV-2 in confined spaces. Given that natural ventilation is variable, which depends on the intermittent wind source, mechanical ventilation systems provide stable airflow rates that ensure reliability and adequacy to meet the minimum ventilation rates for building users in a controlled environment. Thus, a paradigm shift in the mechanical ventilation system is needed to steer the focus from the predominant energy efficient space-based design to occupant-based design. This study will discuss the cost-related effects to ensure stable and adequate ventilation by setting up ventilation scenarios with parameters derived from the recommendations published in recent guidelines focusing on HVAC operations. A working methodology is applied to a case study on two zones, an office, and a nursery. The results show that maintaining a minimum of five and seven air changes per hour for office and nursery, respectively, with proper indoor air distribution can reduce the risk of infection by more than half while ensuring an economic balance between ventilation costs and infection risk. Additionally, the study suggests using photovoltaics installations to power ventilation rates higher than five air changes per hour which can save at least forty-five tons of CO_2 while reaching a payback period in thirteen years. Based on the achieved results, the paper presents recommendations to operate the two zones' ventilation, space heating, and photovoltaics cost-effectively while ensuring COVID-19 probability of infection reduction.

Keywords: COVID-19, Ventilation, Air distribution, Photovoltaics, Cost-effectiveness.

Abdulrahman Mohammed

21/06/2021

NOMENCLATURE

ACH	Air Change per Hour
ADU	Air Distribution Unit
AHU	Air Handling Unit
ASHP	Air Source Heat Pump
ASHRAE	The American Society of Heating, Refrigeration, and Air conditioning Engineers.
CAV	Constant Air Volume
CIBSE	Chartered Institution of Building Services Engineers
COVID-19	Corona Virus Disease 2019
COP	Coefficient of Performance
CFD	Computational Fluid Dynamics
DB	Design Builder software
ECDC	European Centre for Disease Prevention and Control
HEPA	High-Efficiency Particulate Air filter
HDDs	Heating Degree Days
HR	Heat Recovery
HVAC	Heating, ventilation, and air-conditioning
HX	Heat Exchanger
IRR	Internal Rate of Return
MERV	Minimum Efficiency Reporting Value
OA	Outside Air
PP	Payback Period
REHVA	Federation of European Heating and Ventilation Associations
RH	Relative humidity
SARS-CoV-2	Severe Acute Respiratory Syndrome Coronavirus 2
VAV	Variable Air Volume
WHO	World Health Organization

TABLE OF CONTENTS

LIST OF FIGURES

LIST OF TABLES

CHAPTER 1. INTRODUCTION

At the beginning of the pandemic, the World Health Organization (WHO) presumed the main transmission route of SARS-CoV-2 infection to be only via respiratory droplets. Nevertheless, on the 5th of October 2020 and the 9th of July 2020, the US Center for Disease Control (CDC) and WHO, respectively, both acknowledged that COVID-19 could be spread through airborne transmission.

Recent studies agree that the majority of the global SARS-CoV-2 infections have occurred indoors. Airborne transmission is one of several pathways for COVID-19 transmission routes and is linked to the pandemic quick spread in several “superspreading” events, especially in crowded spaces with poor ventilation rate and lack of proper air filtration; the probability of infection through aerosols is substantial.

The increased evidence and recognition about the important role long-range plays in spreading COVID-19 in indoor spaces has pushed several ventilation organizations such as REHVA and ASHRAE to address new interim guidance to mitigate the airborne transmission inside buildings through adjusting current HVAC settings.

These recommendations target the HVAC systems in buildings and pinpoint the importance of supplying adequate outdoor fresh air, filtration, and extending ventilation duration to increase the rate of air change and reduce the level of contaminants inside indoor spaces.

However, ensuring stable ventilation through natural means by opening windows, for instance, is not always applicable in settings like offices, schools, and healthcare buildings. Therefore, reducing indoor air pollution by applying the recommended measures for mechanical systems comes commonly with higher energy penalties. HVAC is already the major consumer of energy, according to the US department of energy, and it accounts for 35% of the total building energy consumption. Any further increase in ventilation rate to counteract COVID19 proliferation would result in more energy consumption.

CHAPTER 2. LITERATURE REVIEW

The following sections address both the medical and technical attributes related to COVID-19. The first section presents a synopsis of the nature of the virus and an overview of previous airborne transmission events. The technical aspect addresses the HVAC different configurations. Subsequently, the chapter concludes with the correlation between ventilation and modeling of COVID-19 probability of risk to link the medical with the technical side of this study.

2.1 COVID-19 OVERVIEW

This section provides insights into COVID-19's virus nature and presents known outbreaks caused by airborne transmission.

The SARs-CoV-2 is around 0.1 micron and is contained and carried within human respiratory fluids (Bar-On *et al.*, 2020). The projected pathogens particle disseminates through the air, typically by sneezing, coughing, shouting, breathing, and even toilet flushing (fecal-oral transmission). These generate large particles called droplets (> 5μm) and small, contagious particles, namely aerosols (< 5μm) (Bischoff *et al.*, 2013).

The transmission of COVID19 occurs mainly via droplets during close contact or contaminated surfaces or via inhaling infectious aerosols. Most droplets travel a shorter distance of 1~2 meters from the source, which eventually falls on the ground due to gravity and the large relative particle mass.

Unlike droplets, aerosols can travel a longer distance exceeding two meters, and stay in the air for three hours to infect the secondary host without contact with the primary source (van Doremalen *et al.*, 2020). Aerosols are also formed by the dispersion and evaporation of large droplets turning to nuclei at 1 to 100 μm (Liu *et al.*, 2017). Figure (2.1) depicts the short- and long-range transmission routes. The arbitrary distance of 1.5m separates the two ranges. In the short-range, a large number of ballistic particles are projected to susceptible persons in close proximity i.e., susceptible persons are exposed to large, short droplets and direct deposition of large droplets on nearby surfaces.

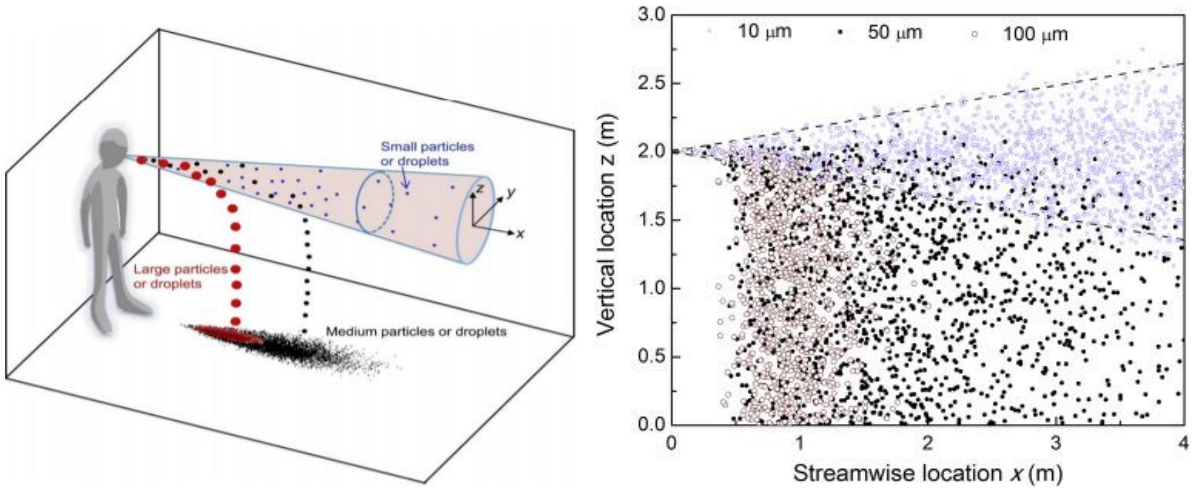

Figure 2.1: (Left) theoretical aerobiology trajectory of droplets and small airborne particles produced by an infected patient (right) Instantaneous dispersion pattern of particles (t = 100 s) in the buoyancy-neutral jet (mouth opening diameter D = 2 cm, initial velocity u0 = 10 m/s, Tamb = 25°C) (Wei and Li, 2015).

2.1.1 PREVIOUS OUTBREAKS

HVAC systems are suspected in a role of a series of outbreaks. There have been a number of events associated with COVID19 transmission in closed spaces with large gatherings such as factories, offices, dormitories, churches. Qian *et al.*, 2020, have studied three hundred and eighteen outbreaks in China. All these outbreaks happened in a confined environment except for one case.

Li *et al.*, 2020 have studied an outbreak in a restaurant in Guangzhou, China. The study results show that ten people who were infected ate at the same restaurant with no close contact. It concludes that poor ventilation (less than 2 l/s per person) was the primary reason for infection.

Other outbreaks also happened in meat-processing and poultry plants where poor ventilation and recirculating operation mode of inside air were two of the main reasons (Durand-Moreau *et al.*, 2020).

The increasing number of outbreaks implicate the effective role of aerosols for the SARS-COV-2 transmission particularly in enclosed environments (Leclerc *et al.*, 2020). Consequently, it is important for building operators in large buildings to review and adapt the HVAC system to ensure adequate air supply.

2.2 HVAC CONFIGURATIONS

HVAC systems are used to maintain thermal conditions like temperature and humidity. Also, to ensure good air quality conditions, including ventilation, pressure, and airflow.

HVAC systems have many classification criteria such as the system's function, reversibility, expansion type, heating/cooling medium, and others. Since this study is mainly targeted to ensure proper ventilation for COVID19, the installation must include an air system. HVAC systems can either be centralized or decentralized system.

2.2.1 CENTRALIZED SYSTEM

Central systems, also referred to as multizone single-supply systems, consist of generation units that produce thermal energy and are transported to different thermal zones. The centralized system is typically used in large buildings. The system typically includes the supply loop, AHU, and demand loop (distribution). (See figure 2.2).

Centralized systems are typically used in large buildings with multi thermal zones. However, it can also be combined with decentralized units.

The supply loop consists of heating and cooling plants. Examples of plants are:

- boilers
- chillers
- renewable energy sources; geothermal with GSHP and solar thermal with backup heater and storage tank.

The supply loop can use All-air or All-water or a combination of the two mediums. The Supply loop feeds up the heating/cooling coils located at the AHU. The AHU is the central machine that connects the supply with the demand loops. A typical AHU comprises of the outside grilles, dampers, mixing chamber, blow and return fans, coils, pumps, filters, de/humidifier, and economizer to allow outdoor air when weather conditions allow. A single AHU can supply multiple zones.

There are two basic mechanisms to vary the energy removed or supplied by air: CAV and VAV. The CAV working principle is to vary the temperature of the supply air (usually reheat coils are installed at zone level) while VAV varies the amount of air by using variable dampers.

A fraction of the return air is mixed with the supply stream in the mixing chamber at the AHU to achieve highly energy-efficient operations. The remaining of the return air is exhausted to the outdoors while utilizing some of the energy content by heat recovery devices.

The fraction of outdoor to recirculated air depends on factors such as the building use and the category of the indoor air quality level, energy efficiency design tolerance, number of occupants, and quality and temperature of the outdoor air. Nevertheless, many commercial systems typically use a range of 10% to 30% outside air of the total air supply to the zone. However, some systems provide 100% fresh air i.e., no recirculation (McDowall, 2006b).

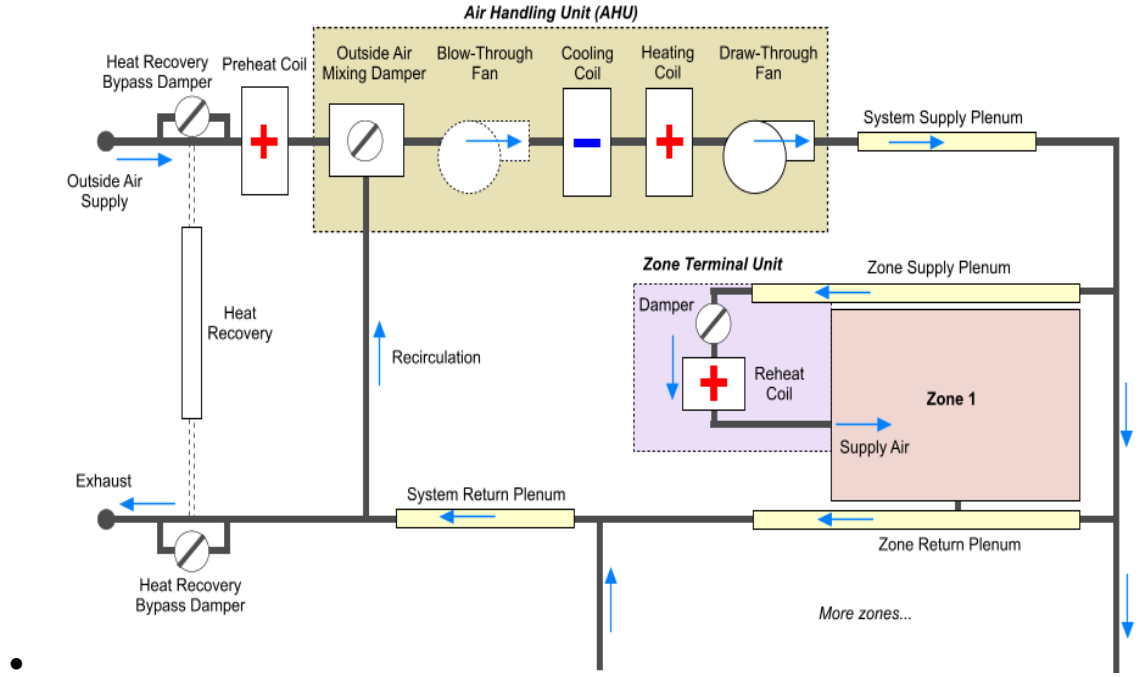

Figure 2.2: Centralized HVAC system (Courtesy: Design Builder Help Manual).

2.2.2 DECENTRALIZED SYSTEM

Decentralized systems, also called unitary zone systems, refer to devices that supply a single space. This system incorporates heating and cooling coils and fans as a packaged system or split system for simple applications and installations.

In large buildings, the packaged system, also called Fan Coil Unit (FCU), may either recirculate zone air, in which case a separate ventilation system is required (e.g., central AHU), or may introduce a proportion of fresh air through a dedicated supply duct that is mixed with the recirculated air.

FCU can be classified into two-pipe or four-pipe systems. The two-pipe system, also called a changeover system, uses one coil for heating or cooling. A four-pipe system includes two coils and four pipes, two pipes for each coil. This system is more expensive but can supply heating and cooling simultaneously to different zones. FCU is ideal for places like hotels, where rooms may be unoccupied for long periods.

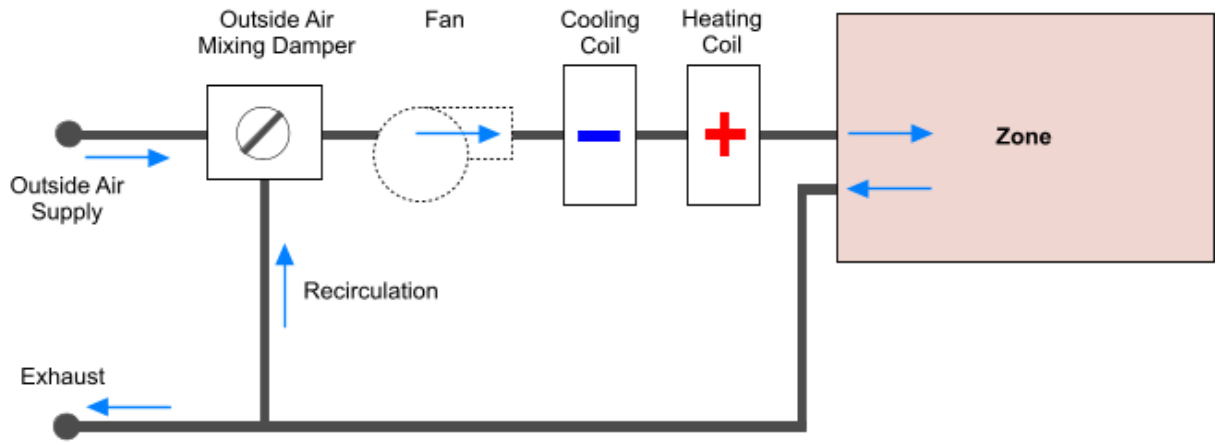

Figure 2.3: Decentralized HVAC system (Courtesy: Design Builder Help Manual)

2.3 HVAC AND COVID-19

The COVID-19 pandemic is a novel research subject, consequently, the literature is limited to provide generic recommendations and “good building practices” to reconfigure HVAC rather than solid numeric guidelines with high confidence levels based on proven facts or experiments designed explicitly for the COVID19 context.

This section begins by highlighting the position of this work in the COVID-19 context. The recommendations that REHVA, ASHRAE, CDC, and WHO put to address HVAC operations are presented thereafter.

2.3.1 HVAC GUIDELINES

In figure (2.4) is a representation of the control hierarchy from the US Center for Disease Control and Prevention (CDC). The idea is to focus on the methods at the top at first that are more effective, then follow the subsequent control measure.

This study scope falls in the *engineering controls category* which in essence does not remove the source but rather separates the occupants from the viral aerosols through ventilation, filtration, and other techniques. According to the control hierarchy, ventilation and other building systems measures are more effective to contain pathogens dissemination in space than using personal protective equipment (PPE) and administrative controls. Hence, it is important to consider ventilation and other building measures to reduce or eliminate airborne transmission.

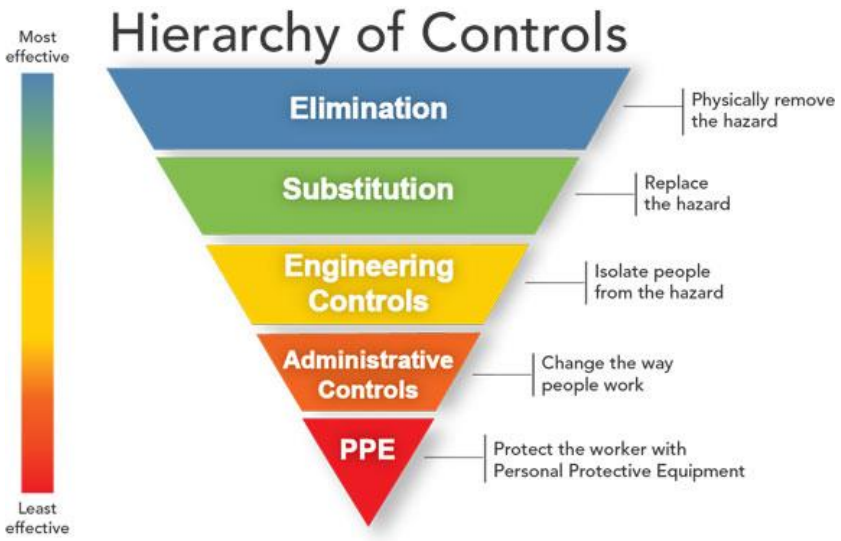

Figure 2.4: Traditional infection control pyramid (CDC, 2015)

It is worth noting that ventilation alone is not the only control measure to address the infection in enclosed spaces. Other non-HVAC measures recommended by WHO, such as social distancing, surface cleaning, and masks, are crucial to limit fomite transmission and break the

chain of infection. These non-HVAC measures abolish the infection source before turning to airborne aerosols. The dotted line in figure (2.5) shows the scope of this study in the COVID-19 context to cover only the airborne transmission mode while keeping in mind that other routes exist and are crucial to mitigate first.

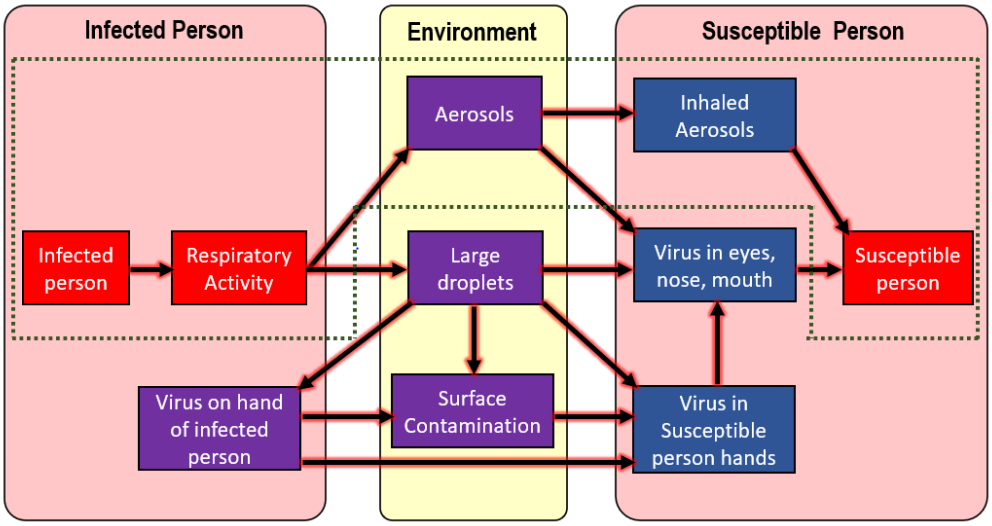

Figure 2.5: Study scope in the COVID-19 transmission routes, reproduced from (Otter et al., 2016)

2.3.1.1 VENTILATION RATE

ASHRAE Standard 62.1 defines ventilation " the process of supplying air to or removing air from space for the purpose of controlling air contaminants levels, humidity, or temperature within the space".

Although the ASHRAE standard 62.1 mentions controlling air contaminants, it was not designed to mitigate viral transmission such as COVID-19. During the COVID-19 outbreak, ASHRAE, REHVA, and various other ventilation agencies worldwide issued continuous updates to highlight the importance of ventilation and present provisional guidelines to reduce the COIVID-19 infection probability indoors.

In addition, previous studies before the COVID-19 pandemic, stress on increasing ventilation rates than normal to decrease the probability of exposure to pathogens and disrupt aerosols transmission pathways such as Gao *et al.*, 2016. It is nevertheless noteworthy that ventilation as a mitigation technique does not influence large droplet flow patterns. Remarkably, it can interrupt infectious aerosols dissemination (Pantelic, Kwok and Tham, 2013).

Although the many similarities between REHVA and ASHRAE guidelines which aim to dilute viral pathogens and lower their indoor concentration, each organization takes a slightly different approach on nonresidential buildings. REHVA guidance (REHVA, 2020) focuses on supplying as much fresh air as reasonably possible and recommends closing mixing chamber dampers to to avoid air recirulation and acquire higher indoor air renewal (see figure 2.6). However, if recirculation cannot be avoided, HEPA filters or ultraviolet germicidal irradiation devices (UGVI) would be recommended.

Conversely, ASHRAE stresses on keeping recirculation but to upgrading primary filters to at least MERV-13 or better filter level and allow maximum flow through the primary filter to remove as many infected aerosols as possible (ASHRAE, 2020).

Recirculation of air is inevitable when it comes to current existing HVAC systems design. The earlier focus was to achieve as high energy efficiency as possible without degrading the thermal comfort of occupants.

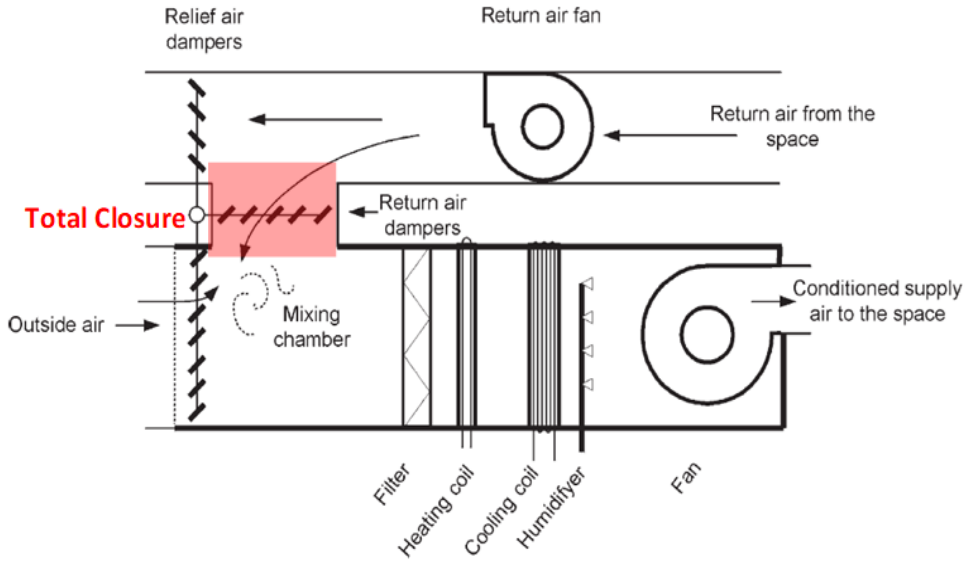

Figure 2.6: AHU with the closure of recirculation damper (McDowall, 2006a)

Moreover, ASHRAE standard 62.1 sets up the minimum ventilation requirement to maintain acceptable indoor air quality to occupants to minimize adverse health effects. According to section 6.2 in (ANSI/ASHRAE, 2019) for "*Ventilation for Acceptable Indoor Air Quality,"* the minimum primary airflow for a breathing zone ($V_{PZ\text{-}min}$) is obtained using the following formula:

$$V_{bz} = (R_p \cdot P_z) + (R_s \cdot A_z) \qquad [l/s] \qquad (1)$$

Where:

- Vbz[1] = breathing zone outdoor airflow

- Az = zone floor area [m^2]

- Pz = number of occupants.

-R_P and Rs are the minimum primary flow rate for ventilation per person and per unit area, respectively, and are determined using table 2.1. This method is referred to as the "Ventilation Rate procedure."

Table 2.1: Minimum ventilation rates in the breathing zone, reproduced from (ANSI/ASHRAE, 2019)

Occupancy category	People Outdoor air rate R_p (l/s/person)	Area Outdoor Air Rate R_a (l/s/m^2)	Occupancy Density # / 100 m^2	Air class
Office Buildings				
Breakrooms	5	0.3	50	1
Main entry lobbies	5	0.3	10	1
Office space	5	0.3	5	1
Outpatient Health Care Facilities				
General examination room	7.5	0.6	20	1

VRF is a perspective procedure based on the number of occupants and floor area. Each occupant and floor meter square requires a minimum ventilation rate indicated in the table above. The equation contains two components; a) ventilation requirements for occupants and b) ventilation requirements for pollution from the building and its systems. It is worth noting that the VRF procedure is only applicable for normal operating conditions but not to mitigate COVID-19 as the standard was developed before the pandemic and did not consider airborne disease transmission like COVID-19.

It is noticed from table 2.1 that spaces with higher activities and movements require more ventilation rates. For example, office spaces need a lower airflow rate (l/s/m^2) than breakrooms

[1] The breathing zone is defined as the zone in space between 0.2 and 1.8 meters from the floor and 0.6 meters from walls or air-conditioning equipment (McDowall, 2006b).

because of lower occupant activity characterized as sedentary, which returns relatively lower space-related contaminants.

Additionally, according to (REHVA, 2020), in its COVID-19 update, stated that to achieve an indoor air quality of category 2 (medium IAQ), a 1.5 - 2 l/s per m^2 (*10 – 15 l/s per person*) is needed in offices and 4 l/s per m^2 (*8 – 10 l/s per person*) in classrooms and meeting rooms.

Although some airflow rates in some spaces fall less than 4 l/s by some standards, it is recommended to have a minimum ventilation rate of 4 l/s per person throughout all building categories for health reasons (ISO, 2017).

Moreover, another parameter for ventilation is the *Air change per hour (ACH)***.** ACH is a unit to measure how many times the air volume is being added and removed from the space volume in one hour, i.e., five air changes per hour means that the air inside will be exchanged with clean air on average five times an hour, see equation (2). ACH is a metric typically used in healthcare buildings. The volume of the space is an important parameter and is inversely proportional to ACH. Although it quantifies the volume of air relevant to the volume of space, ACH is not an indication of the supply air type, whether outdoor fresh or recirculated.

$$ACH = \frac{Q_{air}}{V} \qquad [h^{-1}] \qquad (2)$$

Where:

- *V is the space volume [m^3]*
- *Q_{air} is the air volumetric flow rate[m^3/h]*

Dai and Zhao, 2020, have studied the required ACH needed in bus, classroom, aircraft, and office spaces (See figure 2.7). The study concludes that to get an infection probability of less than 1%, a ventilation rate is required above 8–25 l/s per infector and 83–278 l/s per infector for 0.25 h and 4h of exposure with mask-wearing, respectively.

The Center for Disease Control (CDC), table 2.2, presents the airborne contaminant removal time in minutes equivalent to air quantity supplied (ACH) when there is no aerosols generation source i.e, infectors inside the space. Healthcare facilities usually use stringent standards for indoor air quality, which proved resiliency to control cross-infection during the COVID-19 pandemic. ASHRAE recommends applying the healthcare standards if applicable to all other

facilities. According to CDC, 2003, healthcare facilities use *6 – 12 ACH*, equivalent to *40-80 l/s/patient* (Atkinson *et al.*, 2016). Therefore, based on CDC table 2.2, the recommended 6-12 ACH would take 46 – 23 minutes, respectively, to remove airborne contaminants with a 99% efficiency. The time durations show the required duration to dilute aerosols pathogens after space occupancy.

	Scenario	Bus		Classroom		Aircraft cabin		Office	
	Volume (m^3)	75		348		100		150	
	Exposure time (h)	0.5		2.0		4.0		8.0	
Infection probability		ACH (h^{-1})							
		Y	N	Y	N	Y	N	Y	N
2.0%		0.33	1.30	0.28	1.15	2.00	8.00	2.70	10.00
1.5%		0.48	1.80	0.40	1.70	3.00	11.00	3.30	14.00
1.0%	q = 14 h^{-1}	0.70	2.80	0.60	2.40	4.00	16.00	6.00	20.00
0.5%		1.40	5.60	1.20	4.80	9.00	33.00	10.00	43.00
0.1%		7.00	27.00	5.50	20.00	35.00	160.00	50.00	200.00
2.0%		1.20	4.80	1.00	4.00	7.00	30.00	10.00	36.00
1.5%		1.60	6.40	1.40	5.00	9.00	38.00	12.00	53.00
1.0%	q = 48 h^{-1}	2.40	9.60	2.00	7.00	15.00	55.00	18.00	80.00
0.5%		4.80	19.00	3.50	15.00	29.00	110.00	33.00	133.00
0.1%		24.00	93.00	20.00	71.00	125.00	550.00	200.00	666.00

*The ACHs in red text indicate that the ventilation rates could be achieved with a normal ventilation system or natural ventilation for the corresponding scenarios.

Figure 2.7: Air change rate (ACH) vs. infection probability (Y: with masks; N: without masks, one infector inside). (Dai and Zhao, 2020)

Table 2.2: Air changes per hour and time required for airborne-contaminant removal by efficiency. (CDC, 2003)

ACH	Time (mins.) required for removal 99% efficiency	Time (mins.) required for removal 99.9% efficiency
2	138	207
4	69	104
6	46	69
8	35	52
10	28	41
12	23	35
15	18	28
20	14	21
50	6	8

2.3.1.2 AIR FILTRATION

Unlike REHVA, ASHRAE COVID-19 guidance emphasizes on the importance of filters upgrade when most supply air is recirculated and when areas share the same central HVAC system.

The use of highly efficient filters recommended by ASHRAE Standard 52.2 in HVAC systems can reduce airborne infectious particles significantly. The main characteristics to distinguish filters are their efficiency in removing particles of varying size, resistance to airflow, and dust capacity i.e., how much particles mass they can hold.

The minimum efficiency reporting value (MERV) is a rating scale (1-16) that classifies filters according to their ability to capture different particle sizes represented by an efficiency percentage. Each MERV rating and its corresponding efficiency has its typical application (See figure 2.8).

Moreover, the filtering efficiency is simply an indication of the fraction of particles removed from the air passing through the filter. There are various particle types and sizes shown in figure (2.9). These particles are classified into three categories based on their sizes as follows:

- Range 1: 0.3 to 1.0 micron.
- Range 2: 1.0 to 3.0 microns.
- Range 3: 3.0 to 10.0 microns.

ASHRAE advises using range 1 to decide filter efficiency to protect against COVID-19 because of the relatively small size of the virus. High-Efficiency Particulate Air (HEPA) filters are the most efficient filtration with an efficiency reaching 99.97% able to remove range 1 particles at rated flow. HEPA filters correspond to a MERV rating of 17 to 20.

However, HEPA filter types have high capital costs and require higher fan speed to push the air through the filter and counteract the increased pressure drop. The pressure drop is caused by the filter's airflow resistance which varies widely between air filter manufacturers and models, primarily due to the number of pleats per inch (dense material structure) in the manufacturer's air filter model design. Therefore, a drawback to using high-efficiency filters is the significant increase in annual fan energy costs, and frequent replacement is often required. (See figure

2.10). Nonetheless, if HEPA filters are not an option, ECDC and ASHRAE recommend using **MERV-13** or higher as a compromise between filter efficiency and cost (MERV 13 filters > 90% particles of 0.3µm).]

On the other hand, low MERV filters are typically used at the outdoor air intake to prefilter the air from large particles, where the air is then refined with higher MERV-rated filters.

MERV Rating	Microparticle Performance Rating (MPR) .3-1.0 micron (µm)	Performace Rating Particles sized 1.0 to 3.0 microns (µm)	Performace Rating Particles sized 3 to 10 microns (µm)	Typical Application	Common Filter Types - Types of Particles
5	< 20%	< 20%	20% - 34%	• Industrial Workplace • Paint Booth • Commercial Buildings • Standard Residential	• Disposable/ Throwaway • Pocket Filters • Pleated Filters *Pollen, Dust Mites, Spray Paint, Carpet Fibers*
6	< 20%	< 20%	35% - 49%		
7	< 20%	< 20%	50% - 69%		
8	< 20%	< 20%	70% - 85%		
9	< 20%	Less than 50%	85% or Better	• Better Commercial Buildings • Hospital Labs • Better Residential	• Bag Filters • Pleated Filters • Box Filters *Lead Dust, Flour, Auto/Welding Fumes*
10	< 20%	50% - 64%	85% or Better		
11	< 20%	65% - 79%	85% or Better		
12	< 20%	80% - 90%	90% or Better		
13	Less than 75%	90% or Better	90% or Better	• Superior Commercial Buildings • Hospitals • Smoking Lounges	• Pleated Filters • Cartridge Filters • Box Filters *Bacteria, Smoke, Sneezes*
14	75% - 84%	90% or Better	90% or Better		
15	85% - 94%	95% or Better	90% or Better		
16	95% or Better	95% or Better	90% or Better		
17	99.97%	99% or Better	99% or Better	• Pharmaceutical Mfg. • Carcinogenetic Materials • Cleanrooms	• HEPA & ULPA *Viruses, Carbon Dust, < .30 pm*
18	99.997%	99% or Better	99% or Better		
19	99.9997%	99% or Better	99% or Better		
20	99.9997%	99% or Better	99% or Better		

Figure 2.8: Filter's MERV efficiency index, image taken from (Nelson-Jameson, 2020) reproduced from (ANSI/ASHRAE, 2017)

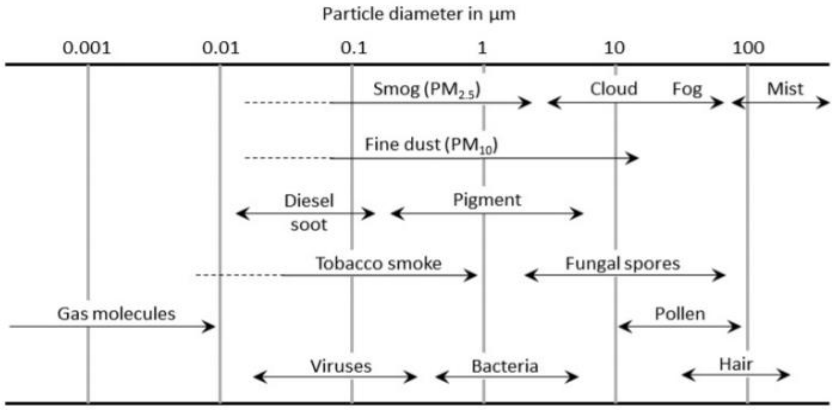

Figure 2.9:General guide to the particle size distribution of common atmospheric contaminants (Eurovent, 2017).

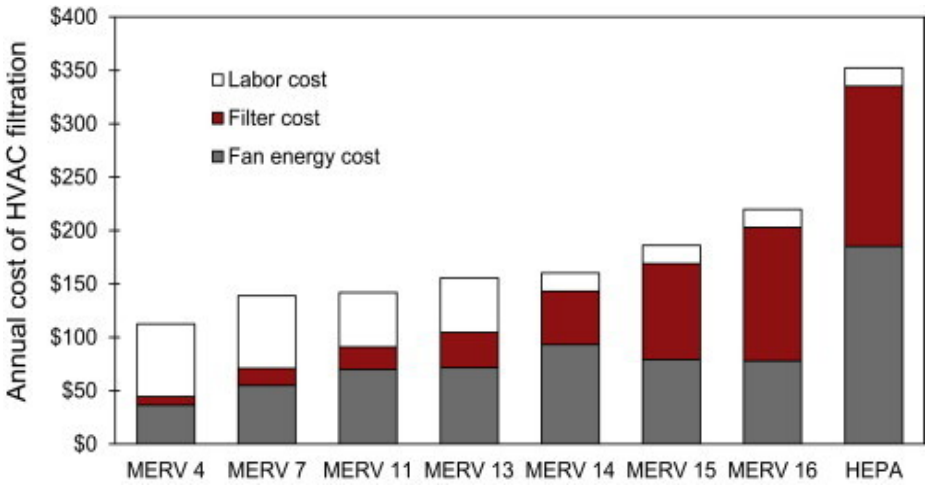

Figure 2.10: Estimated annual cost of filtration in hypothetical office environment.(Azimi and Stephens, 2013).

Furthermore, static pressure drop evolves from ducts and filters. When air passes through a duct, the difference in pressure between the two ends is referred to as pressure drop. The higher the pressure drop means more resistance to the airflow, which increases the work required, corresponding to higher fan horsepower needed to push the air through.

The static pressure drop for air ducts per meter of length is depicted on Darcy Weisbach equation:

$$\frac{\Delta p}{L} = \frac{f_D}{D} \cdot \frac{pV^2}{2} \qquad [Pa/m] \qquad (3)$$

Where:

- *Δp is the pressure drop [pa]*
- *f_D is Darcy friction factor*
- *L is the duct length [m]*
- *D is the inside diameter [m]*
- *V is the air average velocity [m/s]*
- *p is the fluid density [kg/m^3]*

2.3.1.3 HEAT RECOVERY

Similar to the recuperator working mechanism for heat in the boiler's flue gases, heat recovery at the AHU is integral to the system design. Heat recovery is an energy-efficient method to reduce energy consumption substantially by utilizing the energy contained in the exhaust air in the form of "Low-grade heat" that would otherwise be wasted and supply it back to pre/heat the incoming air stream through air-to-air heat exchangers (Zemitis and Borodinecs, 2019). The two most known forms of the heat exchanger are wheel and flat plate. Unlike flat plate HX, the

rotary HX provides high efficiency but with a potential of air leakage between the supply and extract air streams. This is due to the wheel's rotation, making it difficult to seal effectively (William Lawrance, 2020). The uncontrolled transfer of polluted air can be in the order of 1-9% (Andersson *et al.*, 1993).

However, CIBSE, 2020; REHVA, 2020b and WHO argues that there may be a possibility of viral material be transferred to the supply airflow via leaks, but there is no strong evidence. Instead, the leakage risk is outweighed by sustaining proper ventilation rates. In addition, there is a minimal risk of cross-contamination if the overall system is constructed, installed, and maintained properly.

2.3.1.4 OPERATION SCHEDULE

To reduce airborne exposures, changes in the building HVAC devices, as well as operation schedule. ASHRAE, 2020, recommends a ventilation system to operate 24/7 if possible. REHVA, 2020, recommends turning on ventilation systems to their nominal speeds at least 2 hours before occupancy and switch off or lower speed after two hours of building occupancy. Extended operation time helps to flush out contaminants.

It is worth noting that most guidelines advise avoiding demand control ventilation (DCV), in which the ventilation rate is controlled by CO_2, humidity, volatile organic compounds (VOCs) sensors or timer.

2.3.1.5 TEMPERATURE AND RELATIVE HUMIDITY

The transmission of the COVID-19 virus is governed by a number of factors such as host immune system, migration flow, medical care quality, population density, and climate conditions. Mecenas *et al.*, 2020 examined seventeen recent studies focusing on the connection of temperature and relative humidity on SaRs-CoV-2 virus viability. The study found, with low confidence, that warm and wet climates reduce the spread of COVID-19 over cold and dry climates.

Casanova et al., 2010, found that the Coronavirus's viability is reduced only when relative humidity (RH) is above 80% and temperature (T) is greater than 30°C.

On the contrary, ASHRAE and REHVA, 2020, in their final guideline, argues that humidification is not an effective measure to reduce SARS-CoV-2 stability in buildings and advises maintaining normal operating temperature and humidity setpoints. Besides, high values of RH and T are unacceptable thermal comfort levels for occupants inside the buildings and may cause condensation and microbial growth indoors (e.g. airborne fungi) which could affect occupants' health negatively (Arundel *et al.*, 1986).

2.3.2 COVID-19 RISK PROBABILITY MODEL

A risk infection probability model goal is to roughly estimate the infection probability as a function of ventilation rate given different virus exposure times.

A probability infection model is essential to relate it to the dilution effect to reduce the infection caused by ventilation and other HVAC-related measures. The probability of risk model is based on the most classic Wells-Riley equation to assess infection risk, calibrated for COVID-19. The goal is to get the order of magnitude of the infection risk rather than a sophisticated epidemiological model. There are some limitations to the Wells-Riley equation, which will be explained later.

The Wells-Riley model allows for a quick assessment to deterministically quantify the risk, which does not require interspecies extrapolation of the virus infectivity (Sze To and Chao, 2010).

According to (Sze To and Chao, 2010), the quanta “q” is not a standardized unit but rather a hypothetical infectious dose unit developed by Wells in 1995 specifically for this equation. Wells assumed that not all the droplets and aerosols inhaled by susceptible would result in an infection. Wells defined quanta as the number of infectious droplet nuclei required to infect 1-1/e susceptible people, i.e., 63% chance to be infected. (Noakes and Andrew Sleigh, 2009).

The quanta are specific for each disease. Quanta rates cannot be directly obtained but calibrated following a super spreading event of a known outbreak. This way, the concept of quanta can help lump together empirical uncertain virus parameters such as virus infectivity, deposition at the respiratory tract and immune system response, the particle size distribution. Trying to

obtain those parameters to create a detailed infection model explicitly is a daunting task, especially in the first stages of a new disease like COVID-19. Instead of a fully detailed model, the concept of quanta, although of some incomplete or uncertain virus factors, is calibrated to known outbreaks of COVID-19, as done in the following papers.

Dai and Zhao, 2020 have used a reproductive number-based fitting approach to estimate the COVID-19 quanta generation rate (q) from previous viruses. The generation rate is needed to form a correlation between the infection probability and ventilation rate. The study estimated the COVID-19 generation rate to be in the range of 14 – 48 (q/h).

Buonanno, Morawska and Stabile, 2020 estimated the quanta emission rate (q/h) emitted given different activity levels, type of respiratory activity, and viral load concentrations (expressed in RNA copies in mL−1) (Figure 2.11).

ER_q (quanta h^{-1}) and $\log(ER_q)$ statistics for SARS-CoV-2 as a function of the expiratory activity and activity level. The log-transformed ER_q values follow a log-normal distribution; thus, the average and standard deviation values of the $\log_{10}(ER_q)$ are provided.

		Resting, oral breathing	Heavy activity, oral breathing	Light activity, speaking	Light activity, singing (or speaking loudly)
ER_q	5th percentile	2.4×10^{-2}	1.6×10^{-1}	3.2×10^{-1}	2.1×10^{0}
	25th percentile	1.2×10^{-1}	8.2×10^{-1}	1.6×10^{0}	1.0×10^{1}
	50th percentile	3.7×10^{-1}	2.5×10^{0}	5.0×10^{0}	3.2×10^{1}
	75th percentile	1.1×10^{0}	7.7×10^{0}	1.5×10^{1}	9.8×10^{1}
	90th percentile	3.1×10^{0}	2.1×10^{1}	4.2×10^{1}	2.7×10^{2}
	95th percentile	5.7×10^{0}	3.8×10^{1}	7.6×10^{1}	4.9×10^{2}
	99th percentile	1.7×10^{1}	1.2×10^{2}	2.4×10^{2}	1.5×10^{3}
$\log_{10}(ER_q)$	Average	-4.29×10^{-1}	3.99×10^{-1}	6.98×10^{-1}	1.50×10^{0}
	Stand. dev	7.20×10^{-1}	7.20×10^{-1}	7.20×10^{-1}	7.20×10^{-1}

Figure 2.11: Quanta emission rates (q/h) for SARS-CoV-2 as a function of the activity level. (Buonanno, Morawska and Stabile, 2020).

Figure (2.1) shows there is a two order of magnitude difference between the 5th percentile and 95th**.** For comparison, the quantum emission rate for measles is between 570q-5600q (Riley,

C.E., Murphy, G. and Riley, 1978) and (15-500q) for Influenza (Lee, Golinski and Chowell, 2012). So COVID-19 is much less transmissible through the air than measles. Still, aerosols can be transmitted under the right circumstances (indoors, lower ventilation, crowding, longer duration, activities that favor higher emission rates of respiratory aerosols such as singing, talking, aerobic exercise (Zafra and Salas, 2020).

Generally, infection models consist of two main components:

a) Estimation of the generation of the infectious intake dose.

b) Estimation of the probability of infection given the infective dose.

So, knowing the infectious dose, the likelihood of infection can be modeled. This is shown in the Wells-Riley equation as follows:

$$p = \frac{C}{S} = 1 - exp(-n) = 1 - exp(-\frac{I \cdot q \cdot p \cdot t}{v}) \qquad [\%] \qquad (4)$$

Where:

- *-P probability of infection.*
- *-C number of infected cases*
- *-S number of susceptible*
- *-n is the quantity of quanta inhaled (dose).*
- *-v is the outdoor air ventilation rate [ACH].*
- *-I number of infectors*
- *-q quanta generation rate [q^{-1}]*
- *-P breathing rate [m^3/h]*
- *-T exposure time [h]*

The term in the brackets in equation (4), $\left(-\frac{Iqpt}{v}\right)$, refers to the risk of infection in a room. It assumes a constant well-mixed concentration which increases with time from an initial value of zero. The numerator indicated the pollutant generation rate (source), while the denominator evaluates the ventilation removal rate (sink).

2.3.2.1 TOTAL FIRST-ORDER LOSS RATE

Besides the denominator Q (ventilation removal) in equation (4), which only considers ventilation, other control measures that affect the infection risk measure have been incorporated in previous studies; to include air filtration ($\lambda_{filtration}$), virus decay (λ_{decay}), and deposition

rates ($\lambda_{deposition}$). These sink terms can be added, and all terms sum is referred to as Total first-order loss rate, λ_{total} (Fisk *et al.*, 2004; Sze To and Chao, 2010).

$$p = 1 - exp(-\frac{I \cdot q \cdot p \cdot t}{v + \lambda_{decay} + \lambda_{deposition} + \lambda_{filtration}}) \qquad (5)$$

According to the COVID-19 online decay rate calculator (DHS, 2020a), the virus decay rate is dependent on the UV index, relative humidity, and temperature. The UV index is 0 for indoor spaces, 20°C as average temperature, and 40% RH. All of these parameters give a virus decay (half-life) of 0.98 h^{-1}. This value is in the same order of magnitude found in the New England journal article shown in the figure below.

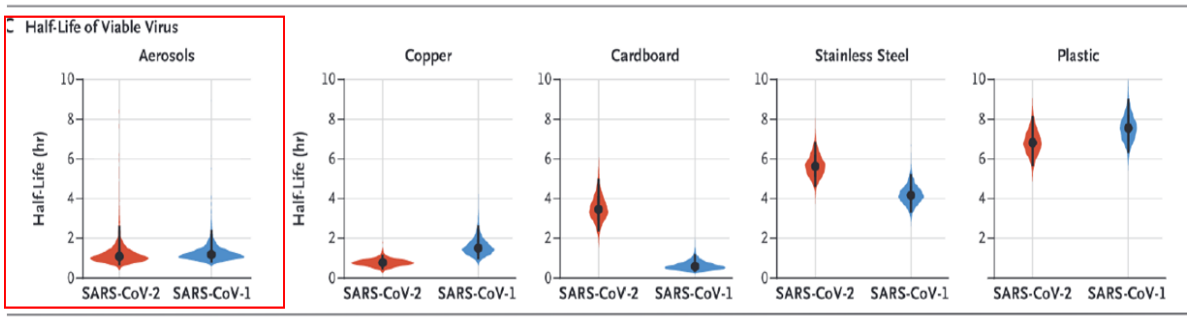

Figure 2.12: SARS-CoV half-life decay rates for different mediums (van Doremalen et al., 2020).

For the SARS-CoV-2 deposition rate, (Miller *et al.*, 2020) estimate the deposition rate following a super spreading event using Monte Carlo simulation, the loss rate due to deposition values ranges from 0.3 to 1.5. This rate varies due to the different particle size ranges and heights of the emission source. Another study evaluated deposition to 0.24h^{-1} (Buonanno, Stabile and Morawska, 2020).

The final term in equation (5), $\lambda_{\text{filtration}}$ is proportional to the filter efficiency i.e., MERV rating, and the amount of air passing through the filter. Hence, $\lambda_{\text{filtration}}$ equals:

$$\lambda_{filtration} = \eta_{filter} \cdot \frac{Q_{OA}}{V} \qquad [h^{-1}] \qquad (6)$$

Where:

- Q_{OA} *is the amount of outdoor airflow in* $[m^3/h]$
- V *is the space volume* $[m^3]$.
- η_{filter} *is the primary filter efficiency*

2.3.2.2 INHALATION OF VIRAL PARTICLES:

As explained in (*COVID-19: SARS-CoV-2 Aerosol Mechanisms- The Aerosol Society*, 2020), to evaluate the infection risk probability of susceptible, an estimation of the quanta concentration evolution time is needed to predict how much quanta is inhaled. Based on Miller *et al.*, 2020 equation (4), the average quanta concentration C_{avg} is determined as follows:

$$C_{avg} = \frac{1}{D} \cdot \int_0^D C(t)dt = \frac{E}{\lambda \cdot V} \cdot \left[1 - \frac{1}{\lambda \cdot D} \cdot \left(1 - e^{-\lambda \cdot D}\right)\right] \qquad [\, q/m^3] \qquad (7)$$

Where:

- *E is the net emission rate and equals to*

  $E = number\ of\ infectors \cdot quanta\ emitted\ per\ person \cdot (1 - \eta_{mask})$.

- *λ is the total first-order loss rate [h^{-1}].*
- *D is the time duration [h].*
- *V is the room volume [m^3].*
- *-t time [h].*

Therefore, the number of the infective dose is the quanta inhaled in a given concentration and breathing rate of susceptible and is determined as follows:

$$q_{inhaled} = C_{avg} \cdot t \cdot b \cdot (1 - \eta_{mask}) \qquad [\, q\,] \qquad (8)$$

Where:

- *$q_{inhaled}$ is the quanta inhaled per person*
- *Cavg is the average concentration [q/m^3].*
- *t is the time duration [h].*
- *η_{mask} is the receptor mask efficiency.*
- *b is the breathing rate [m^3/h].*

Finally, equation (8) number of quanta is substituted into equation (4) to evaluate the probability of risk infection. Yet, the risk probability percentage whether to be considered high or low is subjective. However, studies suggest an acceptable risk probability to be less than 1%.

Furthermore, the net emission rate E shall also incorporate the mask efficiency of the infectors to mimic a real-life situation. Face masks are recommended by WHO to interrupt the potential transmission route from the source, which can significantly reduce infection probability and reduce ventilation costs.

$$Net\ Emission\ rate = \eta_{mask} \cdot q \cdot n_{inf} \qquad [\ h^{-1}\ ] \qquad (9)$$

Where:

- η_{mask} *is the mask efficiency*
- *q is the quanta*
- n_{inf} *is the number of infectors inside the space*

There are different types of masks. Each has unique collection efficiency depending on the material and its built structure. Lindsley *et al.*, 2020 conducted a quantitative comparison in efficacy to different source control devices like face masks, neck gaiters, face shields at different aerosols particle sizes. Figure (2.1) shows N95 respirators have the highest collection efficiency. Other filter types range from 40% to 60%. Yet, N95 respirators are not a common choice for the general population.

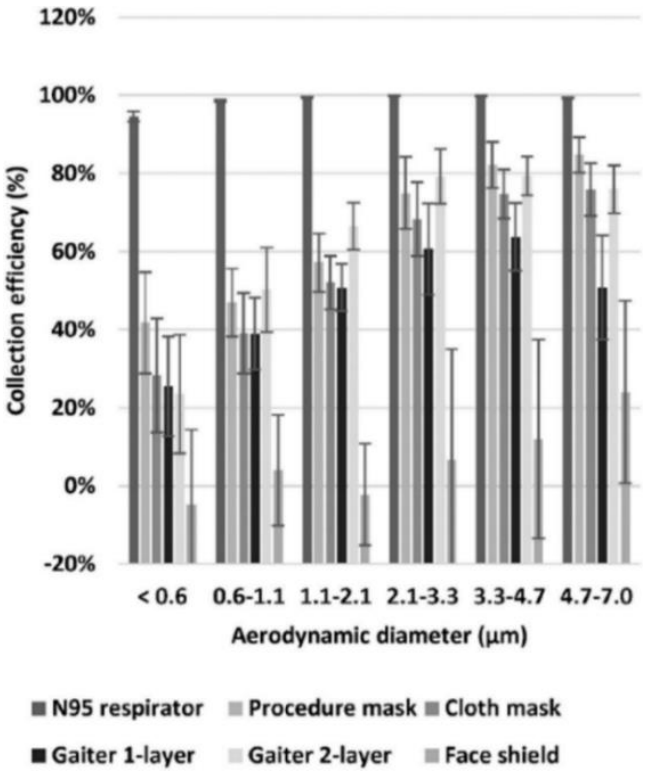

Figure 2.13: Collection efficiency of face masks, neck gaiter, and face shield (Lindsley et al., 2020).

In addition, Davies *et al.*, 2013, show different face masks filtration efficiency, the study reports from 25% to 75%, an average of 50% for homemade masks—besides, 23% efficiency for face shield (Lindsley *et al.*, 2020).

2.3.2.3 LIMITATION

The SARS-CoV-2 virus transmission is novel and an active research topic. Therefore, the uncertainties involved in the calculations are high. The quantifications of risk probability in this study are not absolute or precise but may fall within the order of magnitude.

The model considers individuals are apart and only focuses on airborne aerosols neglecting large droplets, fomite transmission, and other routes. In practice, excluding different transmission paths may lead to overestimating the quanta, which is evaluated based on known outbreaks. However, the quanta emission rates are usually back-calculated from scenarios where the probable major infection factor is caused by long-range transport.

Besides, the hypothesis of perfect mixing and steady-state of contaminants are best applicable for small volume spaces. In contrast, for large open spaces, the results of the risk probability are underestimated as it does not consider spatial variations of virus concentration and treat all the susceptible people to have the same concentration (same virus exposure level). Overall, the Wells-Riley risk assessment model is a good tool for understanding how effective the building measure like ventilation system affects the infection risk.

CHAPTER 3. OBJECTIVES

Ensuring the recommended ventilation rates through mechanical air systems increases energy consumption. Consequently, the study target is to look at the different ventilation rates' consumption and the associated electricity cost. The sufficiency of the air supplied to reduce the viral aerosol risk is evaluated using the Wells-Riley risk probability model. Additionally, although ventilation and other indoor comfort parameters such as heating have different use functions, they are interrelated parameters. The research will cover the cost implication of maintaining the recommended ventilation rates on space heating and the influence of applying heat recovery devices to reduce the cost penalties **(O1)**[2]**.**

Besides, adequate ventilation rates combined with a proper air delivery mechanism improve the overall effectiveness of air systems to reduce pollutants inside an enclosed space. The study will highlight the influence of indoor airflow patterns on the space end-users **(O2).**

Lastly, using a renewable source to power the ventilation and heating systems is beneficial to reduce the energy consumption from the grid and carbon emissions. The study will conclude by examining the feasibility to install a renewable source. The renewable integration analysis will explore the profitability to install a renewable system and examine the carbon emissions that could be saved **(O3).**

The research will conduct an array of different simulations for ventilation and space heating, air distribution, and renewables integration on a case study building. Eventually, all objectives' results will build up general recommendations to operate the building under the COVID-19 context.

[2] O1 = abbreviation to denote the sequence of the research objectives

CHAPTER 4. METHODOLOGY

The chapter starts with the introduction of a case study building and the existing ventilation condition. Subsequently, the chapter presents the process to estimate COVID-19's risk probability and cost. Following this, ventilation and heating, air distribution, and renewables different scenarios formation and calculation methods are discussed consecutively.

4.1 CASE STUDY

The rectorship building of the University of Basque Country is located in Leioa municipality in the autonomous community of the Basque country in northern Spain (Figure 4.1). The building is primarily considered an office type. However, it also includes other functions such as a nursery, server, and storerooms.

The building was chosen as a case study because it holds various zone types that require different ventilation requirements. Besides, office buildings are a focus of interest to study during the COVID-19 pandemic because of their special economic value in the urban fabric and considering the challenging task for decision-makers to reopen such buildings due to the prolonged exposure times of occupants and the high risk of transmission.

Figure 4.1: The University of the Basque Country (UPV), rectorship building.

The building is oriented in the north-south direction and has a total area of 2500m^2. The rectorship building layout comprises four stories, including the ground floor. The ground floor serves as multi-use space for the nursery and store, while the upper floors are reserved as open office spaces (See figure 4.2).

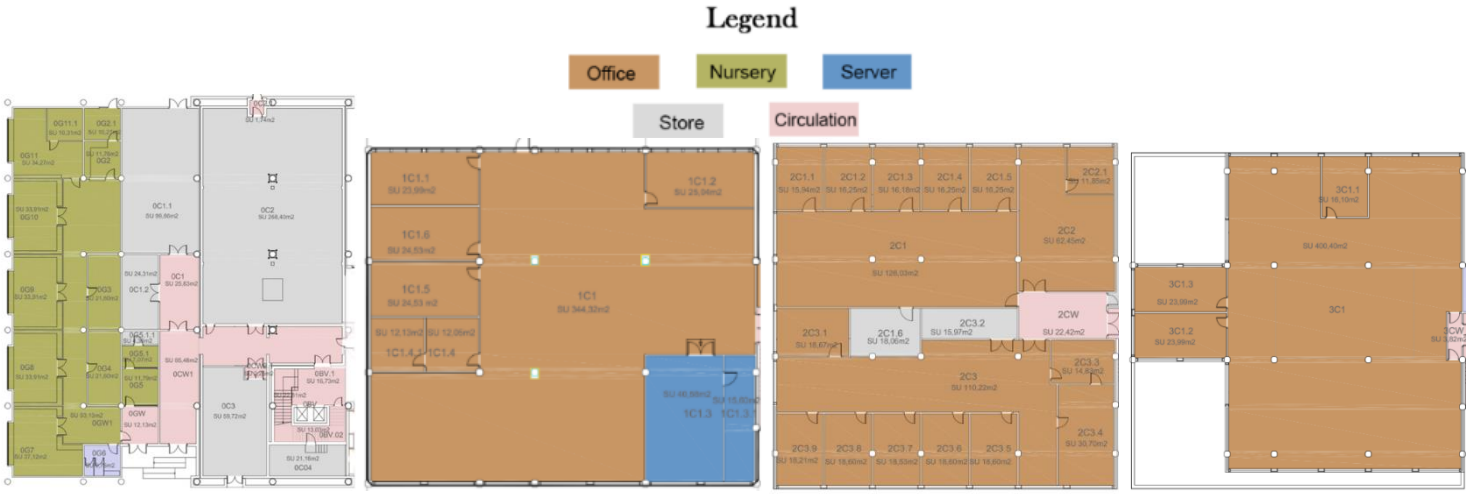

Figure 4.2: Case study floor plans

The two terms “space” and “zone” are sometimes interchangeably used, but the difference shall be highlighted. Space is a part of a building that is not necessarily separated by walls or floors, which can be big or small and subjective to identify. While a zone, always coupled in HVAC literature, contains several spaces. A zone is fundamentally chosen depending on the space/s thermal gains affected by orientation, function, and location within the building layout. Each zone is independent and assigned a thermostat that controls the thermal and indoor air quality needs (McDowall, 2006).

In figure (4.3), the ground floor of the rectorship building is distributed into three zones: nursery, store, and circulation. First, the spaces are classified by function to form custom areas, each with its own use settings and occupant’s activity. The nursery, for instance, is further divided into subzones to separate it thermally as each subzone is situated on different orientations and has a different window-to-wall ratio, thus, variable thermal gains.

On the other hand, the upper office spaces are divided into two zones because the northern and the southern zones each experience a period of solar gains different from the other while other factors such as space use, internal loads from the equipment’s lights, and occupancy are the

same within the office zone. This way we avoid too few zones which results in unacceptable performance and excessive zoning which increases the investment and maintenance costs that add to the complexity of the HVAC system.

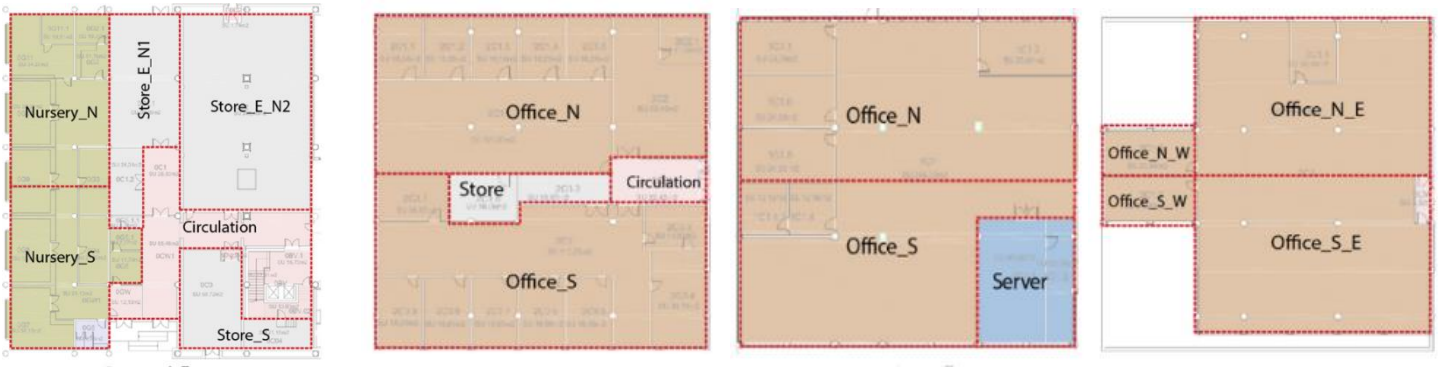

Ground floor First floor Second floor Third floor

Figure 4.3: Assigning zones for case study's spaces

4.2 SCOPE AND BASELINE VENTILATION

The rectorship building has different space uses, as shown in figure (4.2). Nevertheless, the focus of the study is to compare different ventilation rate costs and their influence on infection risk probability, risk costs, and space heating.

Spaces like circulation, server, and store do not have the same high exposure time compared to that of office and nursery. Therefore, providing high ventilation rates to circulation, store, and server is not a top priority to analyze, and are excluded from this work.

Similarly, the rectorship building has more than one office and nursery room. So, simulating more than one office and nursery does not add any significant information to the results. Therefore, the chosen spaces are Nursery_N and Office N_E, better refer to both as *"Focused zones"*.

The following points highlight the study boundaries to conduct ventilation, heating, and risk of infection.

- *Only mechanical ventilation:* the simulation does not consider natural ventilation or building infiltration, exfiltration, or any air leakage mechanisms neither through the building envelope (ex/infiltration) nor mechanical ventilation system's components.

- *Focusing on critical zones in the case study:* the rectorship building includes various use spaces. However, the focused zones include a Nursery and an Office. Other zones like the store, server and circulation are neglected.
- *Four hours of occupancy per day (8:00 – 12:00):* the simulation considers 4 hours of occupancy five days a week from Monday to Friday for one year.
- *Fixed occupancy density:* The Office density is fixed and set to have 1.5m and Nursery 2m of circle radius around each occupant. This corresponds to 7.07m^2/person and 12.57m^2/person, respectively.
- *Homogenous viral concentration:* based on the Wells Riley hypothesis, the level of concentration of SARS-CoV-2 is assumed to be the same at every location within the indoor environment.
- *Ten percent are infected:* this work assumes 10% of the space occupants are infected and constant quanta generation per infector throughout the occupancy duration.

Figure (4.4) depicts a schematic of the HVAC system for the case study building. A centralized VAV air system is chosen. It is widely used for multizone applications because it can reduce energy consumption than CAV and adds to the flexibility of operation. Generally, VAV terminal units are equipped with an air damper with an automatic actuator controlled by a thermostat to vary the amount of air for each zone.

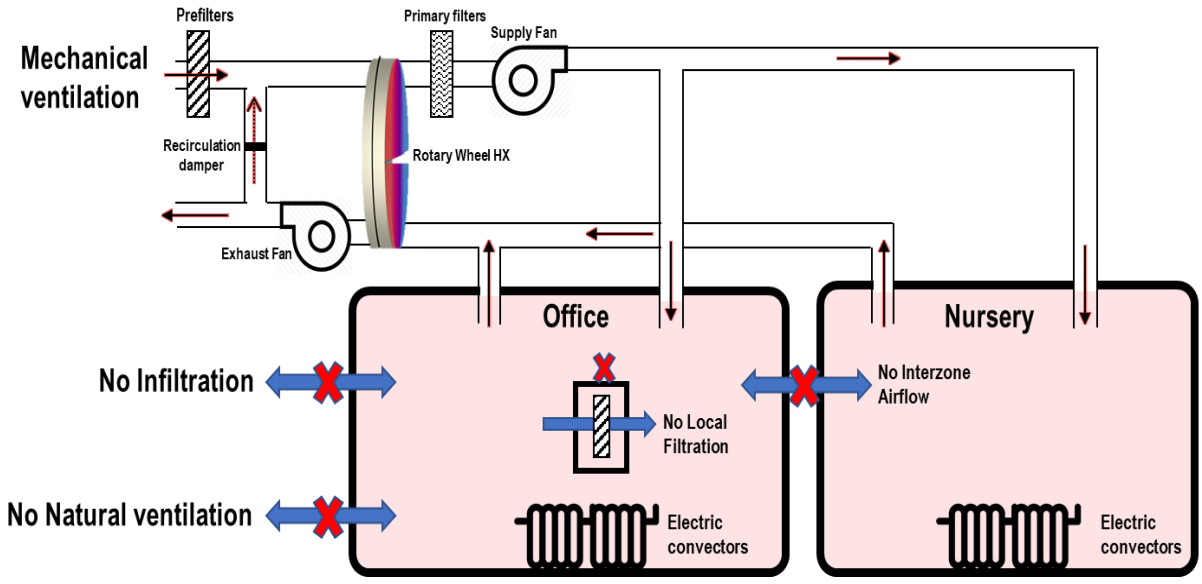

Figure 4.4: Case study's HVAC system illustration diagram

Furthermore, the baseline ventilation refers to the current air requirements for the focused zones before COVID-19 prevalence. Baseline ventilation is evaluated using ASHRAE's Ventilation Rate Procedure (VRP) to examine and compare the minimum air requirements of the focused zones. Table 4.1 shows a breakdown of the focused zones parameters. The quantity of air per person implies poor existing ventilation rates because it fell below the recommended ventilation for COVID-19 of at least 40 l/s and 15 l/s for Nursery and Office, respectively.

Table 4.1: Focused Zones baseline ventilation rate using VRP

Parameter	Office	Nursery
Area (m^2)	203.81	174.03
Height (m)	3.95	5.5
Density (#/m^2)	0.14	0.08
Number of occupants	28	14
Rp	2.5	7.5
Ra	0.3	0.6
Equivalent ACH for baseline	0.6	0.8
Ventilation per person (l/s)	4.6	15

4.3 COVID-19 RISK COST MODELLING

This section will redraw the process of quantifying the risk based on the Wells-Riley equation. It is worth mentioning that there are aerosols transmission online calculators to roughly estimate the infection probability including the University of Cambridge, 2020, NIST, 2020, and REHVA, 2020a. These calculators are not fully tailored to the research's information needed to fulfill the objectives. Instead, the online aerosols calculators' scientific approach is explored and adapted to a spreadsheet using the recent information found in the literature review, section 2.3.2.

Furthermore, the quanta value varies significantly with the activity, e.g., talking, loud speaking, signing, and the metabolism rate, e.g., resting and light or heavy exercise. The chosen quanta emission rate (q/h) is based on the 99^{th} percentile of SARS-CoV-2 taken from the latest study of Buonanno, Stabile, and Morawska, 2020.

For the face masks, 50% is assumed to be an average efficiency for the general public since not everyone wears a respirator mask with efficiency higher than 90% such as FFP3, N95, N99 nor low-efficiency masks such as neck gaiters or cloth masks. However, the 50% is lowered to 40% due to leaks resulting from improper wearing (fit, tight, or loose), and long-term use of masks. All of which influence the mask's effectiveness.

The probability of infection for a given ventilation rate (i.e. ACH) is calculated analytically through the following steps:

A. Establish the space environment parameters such as the type and volume of the space, number of occupants, breathing rate, number of infectors, and mask efficiency (Table 4.2).
B. Calculate the total first-order loss rate (λ_{total}), including ventilation, virus deposition, decay rates, and air filters to evaluate the total removal rate for the infectious quanta.
C. Calculate the infectors' net emissions using equation (9)
D. Calculate the average quanta concentration per m^3 of air using equation (7).
E. Obtain the number of quanta inhaled using equation (8).
F. Calculate the estimated probability of infection equation (4).
G. Translate the risk probability to treatment cost.

Converting the infection risk probability to risk expenses estimates the risk price to be paid out for treating an infected person given a ventilation rate supplied in space. This helps to form a balance between the ventilation costs and risk cost, cost-effectively.

After figuring out the probability of risk from equation (4), the risk percentage is multiplied by the total number of susceptible people to obtain the fraction of people infected. However, not all people infected must go to the hospital to get treatment. The hospitalization rate varies enormously and is subjected to age, immune system, and the existence of chronic disease on the individual level and influenced by the prevalence of COVID-19 in the community on a larger scale.

The hospitalized rate is determined by dividing the number of cases admitted to the hospital by the total number of cases. Daily reports from 9/05/2020 to 16/04/2021 for the province of the

Basque region were obtained from Centro de Coordinación de Alertas y Emergencias Sanitarias (CCAES). Plotting the ratio to see the trend in (Figure 4.5).

The hospitalization rate range fell from 52% during the early period of the pandemic to 9%. Additionally, the cost of treating a COVID-19 patient varies considerably. According to a news report (Business Insider España, 2021), the worst-case scenario costs more than one hundred thousand euros, and on average, the cost is between (66,000 € to 76,000 €) per patient. Add to it the transportation cost to the hospital obtained from the Basque department of health (Oskidetza Libro de tariffs 2021), which is 876€ for an ambulance trip distance of less than 100km.

Hence, equation (10) evaluates the probability of the infected people receiving treatment by adding the prevalence of the disease in the area, i.e., the hospitalization rate.

$$Risk\ Cost = H_r \cdot T_c \cdot P \cdot N_s \qquad [\,€/yr\,] \qquad (10)$$

Where:

-H_r is the hospitalization rate.

-T_c is the treatment and transportation cost for an infected person.

-P is the probability of infection.

-N_s the number of susceptible people in space (Total number of people minus infected)

Figure 4.5: Hospitalization rate of the Basque Country, Spain.

Therefore, the higher the ventilation rate supplied, the less the probability of infection, and the fewer expenses needed to treat and transport the patients. Table 4.2 compiles the selected space medical-related parameters used to quantify the probability of infection and evaluate the risk cost.

Table 4.2: Model parameters summary

Parameter	Value
Quanta rate	5.7 h^{-1} for Office (resting, breathing) 76h^{-1} for Nursery (Light activity, speaking)
Decay rate*	0.15h^{-1}
Deposition	0.3h^{-1}
Mask filtration (inhalation and exhalation) ***	40%
Percentage of people wearing the masks	100%
Breathing rate***	0.96 m^3/h for Office (resting, speaking) 1.74 m^3/h for Nursery (Light activity, speaking)
Number of infectors	10% of the total occupants in each zone
Hospitalization rate	10%
Medical treatment for COVID-19 Per patient	66000€
Ambulance cost (>100km)	876€

***** *Using (DHS, 2020b)*

****** *The physical flows during exhalation and inhalation are different and affect aerosol particles differently. Therefore, the efficiencies are typically different. For simplification, the mask efficiency during exhalation and inhalation is given the same percentage.*

**** For the breathing rates, the chosen rates are according to the intensity activity level according to table 6-2 in (Wang et al., 2015).*

4.4 STUDY SCENARIOS

The following sections introduce the scenario formulation method of ventilation and heating and air distribution. It also explores the potential of renewables integration. All study scenarios are applied to the focused zones of the case study building.

4.4.1 VENTILATION AND HEATING

The ventilation scenarios are based on the two approaches discussed by REHVA to supply outdoor air as much as reasonably possible and ASHRAE's to upgrade filters to at least MERV-

13. Both ventilation and filtration are two methods effectively used to counteract COVID-19 propagation.

Ventilation and filtration are often regarded to achieve the same goal, reducing indoor generated contaminants. Therefore, two distinct ventilation operational settings are drawn for the focused zones as follow:

-*Scenario "A"* is characterized by Low filtration (MERV 8), with 100% outside air.
-*Scenario "B"* is characterized by High filtration (HEPA), with 10% outdoor air (90% recirculated).

The two scenarios do not necessarily give the same effect, yet both can reduce the indoor contaminants. Scenario "A" represents the REHVA approach to introduce outdoor air to dilute indoor contaminants by maintaining a higher air renewal rate. Scenario "A" incorporates a MERV 8 filter index because outside air does not necessarily mean fresh air all the time. Outdoor air can contain coarse contaminants. Hence, a low- MERV ranked filter is employed as a primary filter.

On the other hand, Scenario "B" represents the ASHRAE strategy to recycle air with the existing outdoor air fraction and to upgrade the filters. Scenario "B" depicts the typical outdoor air intake fraction in many air systems (10 to 30% outdoor air intake) which were commonly applied before the pandemic spread and suggested to be an adequate fraction to balance the indoor air quality and maintain energy-efficient operations. When the fraction of recirculated air is high i.e., 90%, the probability of viral pathogens disseminating throughout the space to be transported increases which necessitates upgrading air filters to a highly efficient filter such as HEPA to filter out smaller particles. Additionally, a prefilter is also added in scenarios "A" and "B" to prevent larger outside objects from clogging up the primary filter and air ducts. It is worth noting that is no specific filtration level proven to filter out the SARS-CoV-2.

Each scenario, the amount of supplied air i.e., the ACH is increased by a magnitude of half an ACH beginning from the baseline ventilation rate up to 16 ACH (See figure 4.6). Ventilation in the diagram refers to supplying uncontaminated air either from outdoor or through filtration of recirculated air.

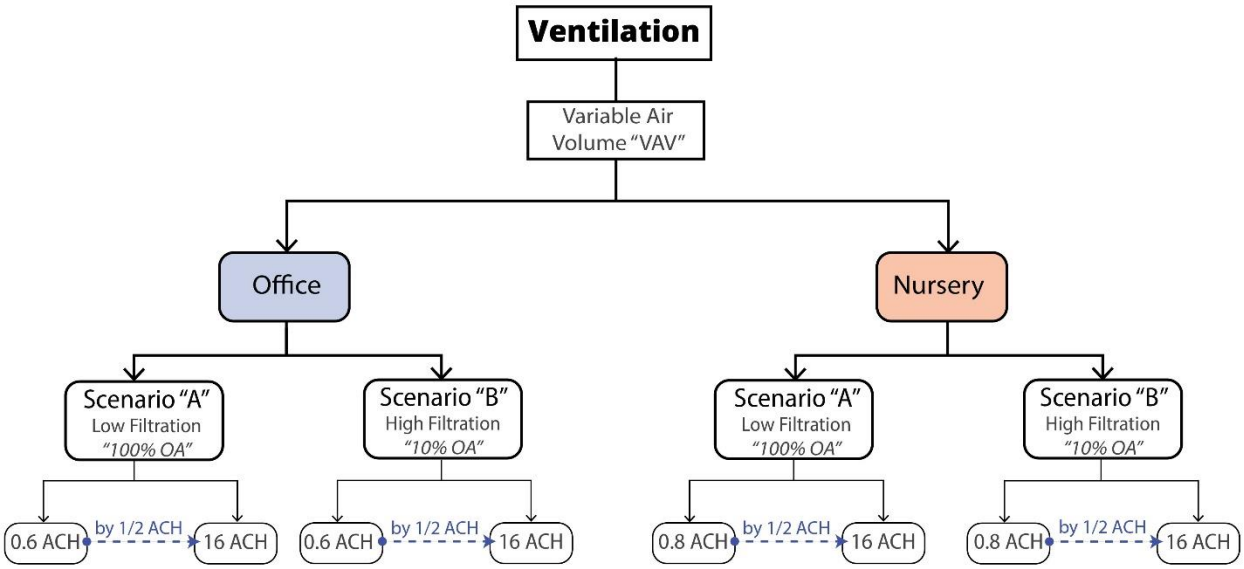

Figure 4.6: Ventilation scenarios diagram

Moreover, space heating is considered the second-ranked consumer of energy after lighting in office buildings. The evaluation of space heating consumption in this study is crucial to examine the ventilation effect on heating inside the focused zones. Unlike ventilation which aims to maintain clean air indoors, heating technologies accomplish heating the air to the preferred temperature.

The heating setpoint temperature, the temperature that the thermostat is set to maintain thermal comfort, is taken from the "Codigo de la edificacion" (CTE), the Spanish standard regulating energy efficiency. The indoor air temperature (Tin) following CTE particularly the "Reglamento de Instalaciones Termicas de los Edificios" (RITE) is 20-23°C. Therefore, a median of 22°C is adopted as the default heating setpoint for the entire heating simulation.

Figure (4.7) shows the average monthly temperature where wicks indicating the highest and lowest temperature. The heating load is more significant than the cooling load throughout the year. More specifically, the hourly ambient temperature in the case study building site is below 22°C eighty-five percent of the total yearly hours and is above or equal to 22°C fifteen percent of the total annual hours Additionally, the heating and cooling degree days (HDD, CDD) which is a calculation method to estimate the energy demand for heating and cooling in buildings, shows an annual total of 720 and 305 for HDD and CDD respectively. Thus, the cooling will be neglected for this study for low demand and the fact that it can also be fulfilled by natural means.

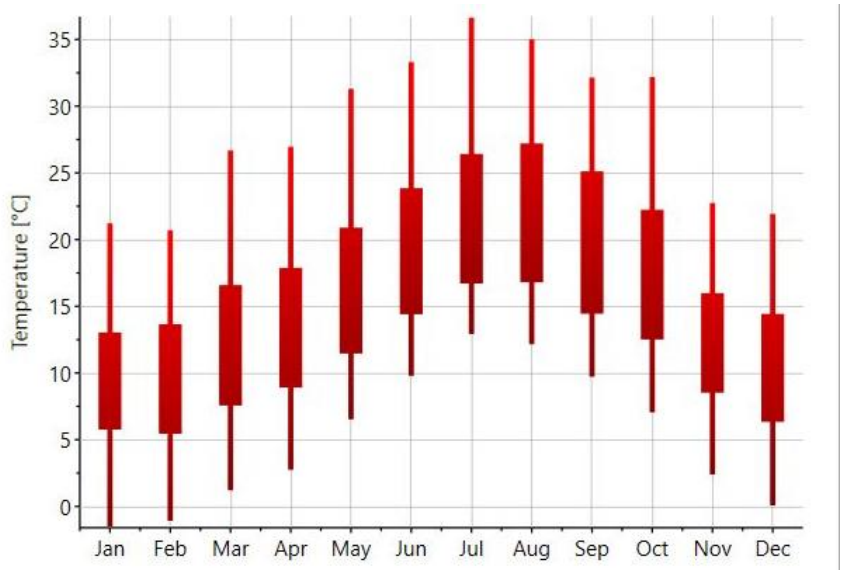

Figure 4.7: Monthly Air Temperature, Leioa, Basque Country, Spain (Meteonorm)

In wintertime, buildings typically become less ventilated in order to maintain warm conditions indoors. Therefore, heating is separated rather than integrated at the AHU heating coil to keep a stable supply of ventilation while not affecting the thermal comfort of space users. The heating is delivered through electric convectors.

Heating analyses follow the same ventilation scenarios with the addition of heat recovery (HR).

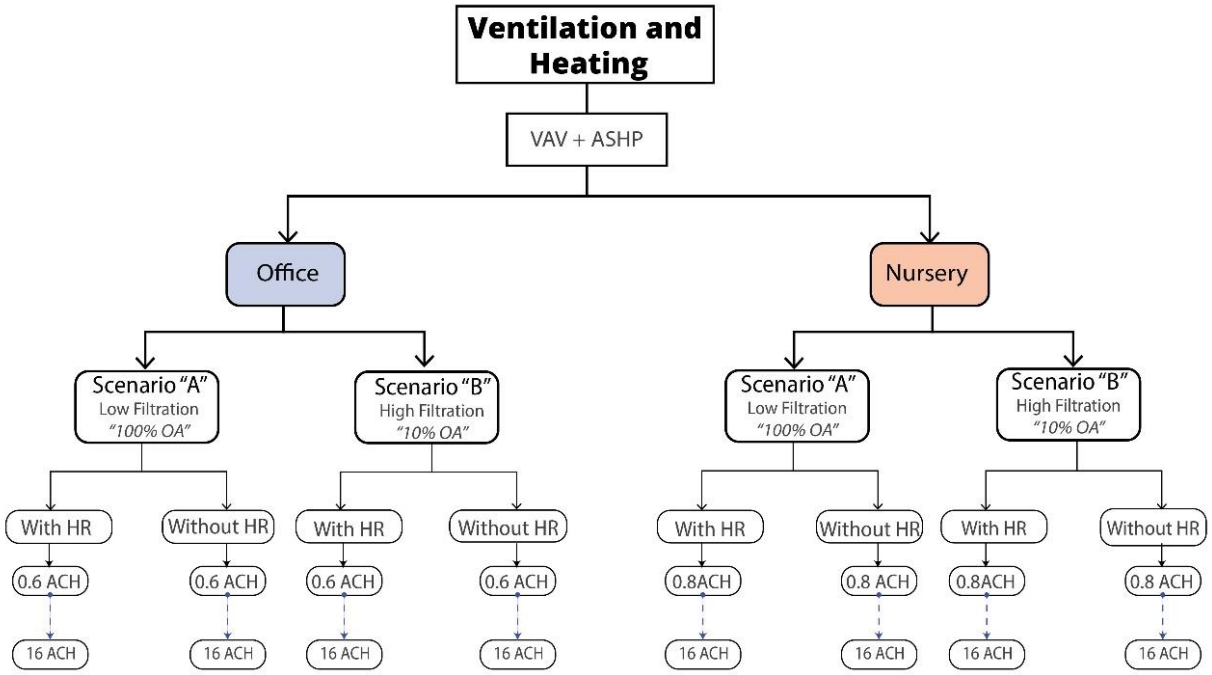

Figure 4.8: Heating scenarios diagram

HR is fulfilled by a rotary type heat exchanger (HX), and its effectiveness is set to 70% taken from (Roulet *et al.*, 2001). Figure (4.8), shows the integration of HR to the ventilation scenarios. "With HR" refers to the adoption of HR in the simulation while "Without HR" describes a simulation carried out without heat recovery. This is to show the effect of HR on the amount of electricity consumption savings.

4.4.2 AIR DISTRIBUTION

Air distribution systems play an important role to maintain the indoor comfort level and to flush out pollutants properly. It is a one-sided view to focus only at supplying adequate ventilation while neglecting the air patterns behaviors around the end users. Computational Fluid Dynamics (CFD) analysis is used to test airflow direction, velocity, and temperature distribution inside space. After searching in the literature to find general concepts about the relationship between building internal airflows and viral transmission, we found that the number of buildings where the literature focused on airflow behavior and viral transmission, making it hard to generalize concepts on building population at large.

The European Centre for Disease Prevention and Controls, 2020, addresses the possibility that airflow generated by HVAC units may facilitate the spread of viral materials. However, the relative contribution is uncertain whether to be attributed to airflow patterns or poor ventilation, such as the outbreak that happened in the Guangzhou restaurant in China. Accordingly, a careful analysis of interior airflow is needed.

When an occupant generates viral particles, the virus aerosols may be carried by the movement of air to be inhaled by a neighboring occupant inside the same space. Thus, improper air supply mechanism may create air turbulence which compromise the ventilation effect and unintentionally increases the risk of airborne viral transmission. In this study, a simple CFD analysis aims to examine the effects of microcurrent around the occupants and assess roughly whether the air currents are accumulated near the occupant plume or flushed out to the extract.

We assume a well-mixed of air approach employed in this analysis. Hence, the approach implies that mixing between air and viral aerosols happens fast, and so viral materials are dispersed homogenously in the room.

The model is created for the Office zone only (Figure 4.9). The equivalent air quantity (l/s) corresponds to 5ACH. The ceiling supply and exhaust air diffuser is a four-way, square ceiling type with the dimension of 300mmx300mm determined using a manufacturer catalog (PrudentAire, 2018) which is best accompanied with VAV applications. The selection of ceiling supply of air is best applicable to ensure a well-mixed air distribution according to ASHRAE 62.1 (Table 6-4). Despite the displacement (stratification) air distribution technique is known to provide better indoor air quality, mixed air distribution helps protect people more efficiently from high exposure of viral material from the source according to Nielsen *et al.*, 2008; Li, Nielsen, 2011.

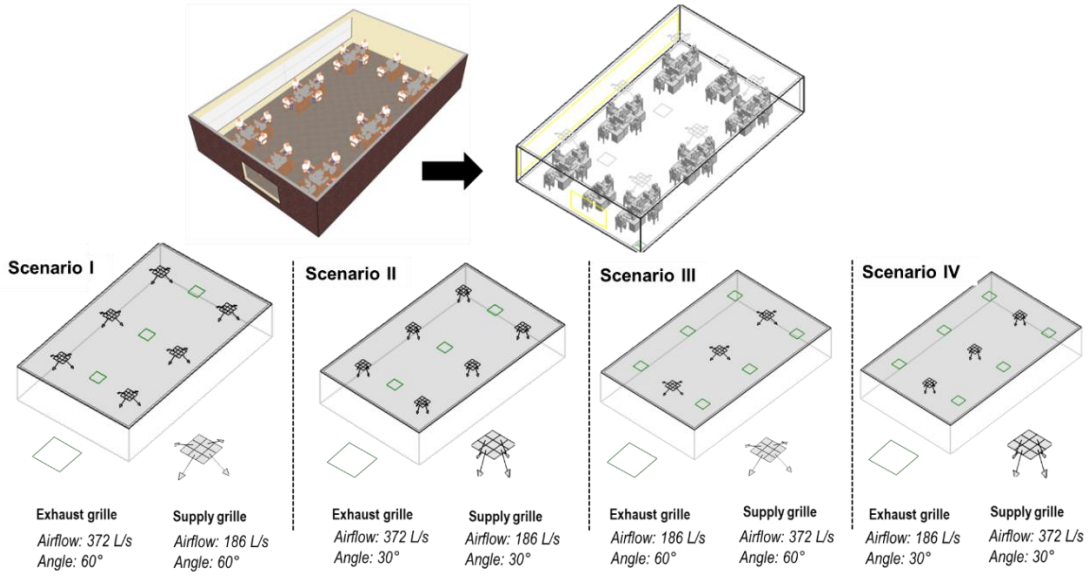

Figure 4.9: Air distribution scenarios for the Office zone

The placement of the indoor furniture in the office as well as diffusers is according to the author's choice for a typical office layout. The number of occupants is kept fixed at 28 occupants. Figure (4.9) shows four scenarios based on changing the diffuser's placement, air-jet angle and amount of air per diffuser. Overall, the amount of incoming air flow must equal extract flow. It is worth noting that these scenarios are independent from the previous heating and ventilation scenarios.

Scenario "I" and "II" have the same diffuser layout. There are six supply diffusers and three exhausts located in the center of the space. The variation of the supply and exhaust diffusers number dictates to vary the amount of air (l/s) per diffuser. Similarly, Scenario "III" and "IV" have the supply diffusers in the middle and exhaust on the space edge. The diffusers' angle is altered by 30° and 60°.

4.4.3 RENEWABLES INTEGRATION

This section aims to view how feasible and profitable a renewable source could be if installed to power ventilation and heating energy consumption. This section has no scenarios but to investigate the potential to integrate a renewable source.

Looking at the wind and solar data in the case study building site, both renewable resources have the potential for electricity generation, generally speaking.

The average wind power density is *385 W/m²* (Figure 4.10) while the average wind speed is *6.5m/s* (World Bank Group, 2018). According to the Renewable Energy Laboratory wind assessment handbook (NREL), both the wind speed and power density fall into class 3 (AWS Scientific Inc., 1997). Power classes range is from Class 1 to Class 7, with Class 4 or greater being suitable for most wind turbine applications. Class 3 is suitable only if wind turbines' hub is tall i.e., large projects considering high-rated capacity wind turbines typically above four megawatts. Hence, the wind source is technically not feasible to establish aside from other social constraints such as noise, safety and environment at the university campus.

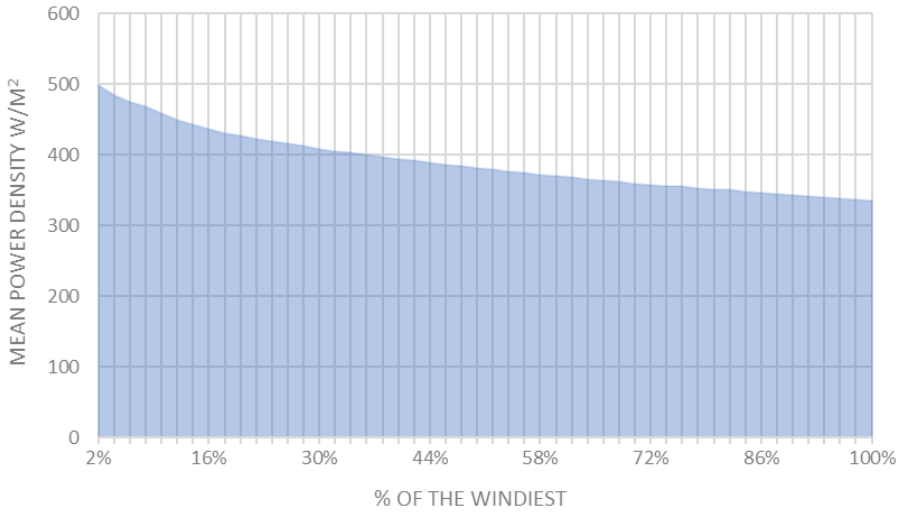

Figure 4.10: Mean power density at 100m hub height (World Bank Group, 2018)

On the other hand, the yearly global solar irradiance is **1237 kWh/m²** (Figure 4.11), which could potentially produce high PV yield per installed PV capacity (kWh/kWp) (World Bank Group, 2020). This suggests a considerable amount of solar potential of the site, beneficial for implementing a photovoltaics power system. Unlike wind turbines, solar panels are easier to install and maintain, and possible to mount on the roof of the rectorship case study.

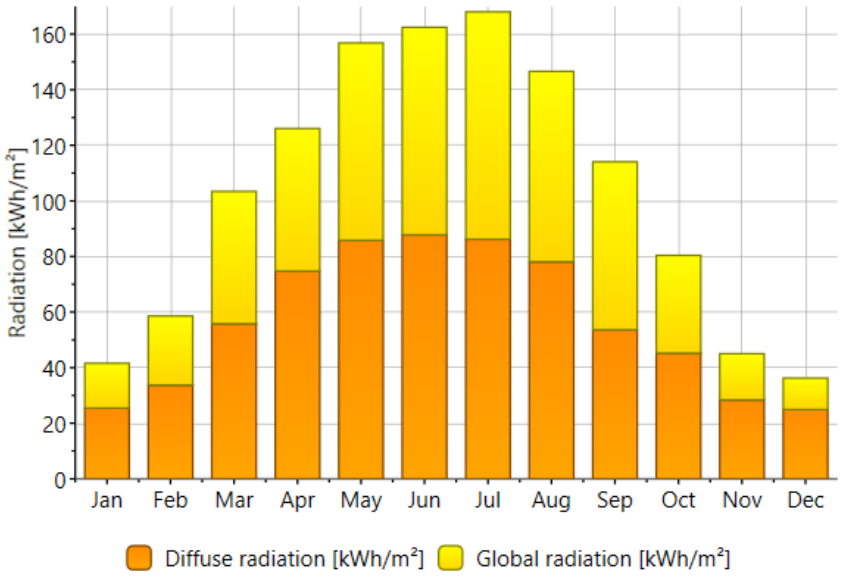

Figure 4.11: Monthly global radiation at Leioa, Basque Country (Meteonorm)

4.5 SIMULATION METHODS

The following sections present the calculations process and tools to conduct ventilation, space heating, air distribution, and photovoltaics scenarios and the associated costs.

4.5.1 VENTILATION AND HEATING

Supplying higher ventilation rates and upgrading filters as the recommendation entails, requires more fan power and energy consumption. In addition, filters upgrade not only consumes a higher fraction of energy to operate but also other associated costs of ownership.

4.5.1.1 ENERGY COST

The total pressure drop consists of duct and filter pressure drops. It is calculated for each ACH step to obtain the energy consumption of the fan and consequently the electricity cost per year. The Darcy Weisbach equation (3)is used to determine the pressure drop per meter multiplied by the total length of the ducts in focused zones of the rectorship building. The Darcy friction factor (f_D) is calculated graphically by Moody chart using the following values:

-Absolute Surface roughness (ε) *= 0.15mm for galvanized steel (The Engineering Toolbox, 2015).*

-Dynamic Viscosity (η) = 0.000018 kg/ms for air at 20C (Osborn, 1985).

- L is the duct length [m] and is set to 156m for only the focused zones ducts (the length is multiplied by two to account for the supply and return duct).

-D is the inside diameter [m] and is by default 500mm.

-V is the air average velocity [m/s] derived from each ACH's air quantity and divided by duct cross-sectional area.

- p is the fluid density, 1.225 kg/m^3.

The Darcy Weisbach equation shows that pressure drop is proportional to the square velocity of the air and inversely proportional to the cross-sectional area of the duct. Figure (4.12) shows the evolution of the pressure drop per meter of duct length.

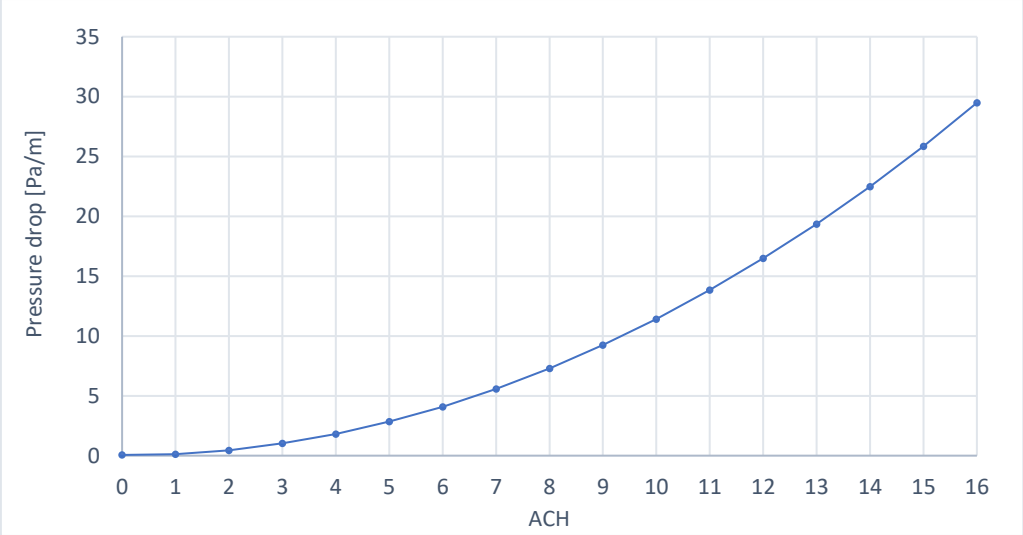

Figure 4.12: Focused zones duct pressure drop per meter

Moreover, the pressure drop caused by filters is calculated using the manufacturer catalog (Camfil, 2016). *For scenario "A"*, a "M5" rated filter class is selected (medium filtration rating). On the contrary, *Scenario "B"* is equipped with an "H-13" filter class to account for a high filtration rating (HEPA filter).

Table (4.3) indicates the chosen filters' dimensions and a comparative classification of air filters according to different standards rating. According to the Camfil catalog, each H-13 and M5 air filter has a maximum airflow of 4250 m^3/h per filter. When the equivalent air quantity reaches the maximum capacity of the filter, the number of filters is increased incrementally to extend the surface area and operate according to the manufacturer's maximum recommended settings.

The number of filters is increased evenly by two filters to be consistent with a real filter housing design. The filter pressure drop and the number of filters are calculated from 1 to 16 ACHs.

Table 4.3: Ventilation air filters type

Filter type	Dimensions	Max capacity	ISO 16890 Std.*	EN779 Std.	ASHRAE 52.2 Std.	Eurovent
Prefilter**	W=59.2cm H=59.2cm D=98 mm	4250 m^3/h (88 Pa)	N/A	G4	MERV 1-6	EU4
Scenario "A"	W=59.2cm H=59.2cm D=64 cm	4250 m^3/h (60 Pa)	ePM1 $\eta < 20\%$	M5	MERV 8-10	EU5
Scenario "B"	W=59.2cm H=59.2cm D=64 cm	4250 m^3/h (297pa)	ePM1 $99.95\% \leq \eta$	H13	MERV 19	EU13

**Note: Taken particle efficiency range of (≤ 1 μm).*

*** Prefilter is included in scenario "A" and "B".*

Finally, using the Camfil pressure drop calculator for the prefilter, M5, and HEPA and inputting the air quantity corresponding to each ACH for the focused zones, we obtain the following pressure drops (Figures 4.13, 4.14, and 4.15).

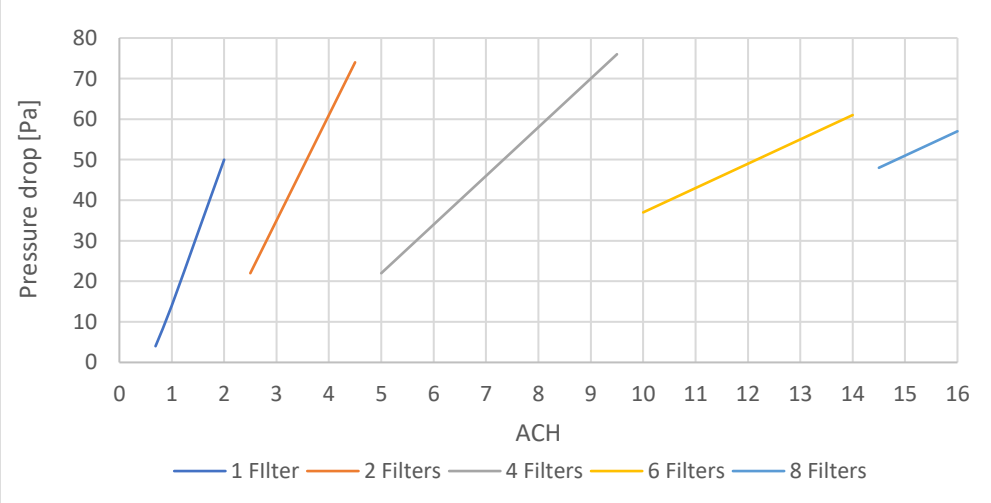

Figure 4.13: Pressure drop across the prefilter (G4), calculated using (Camfil, 2016)

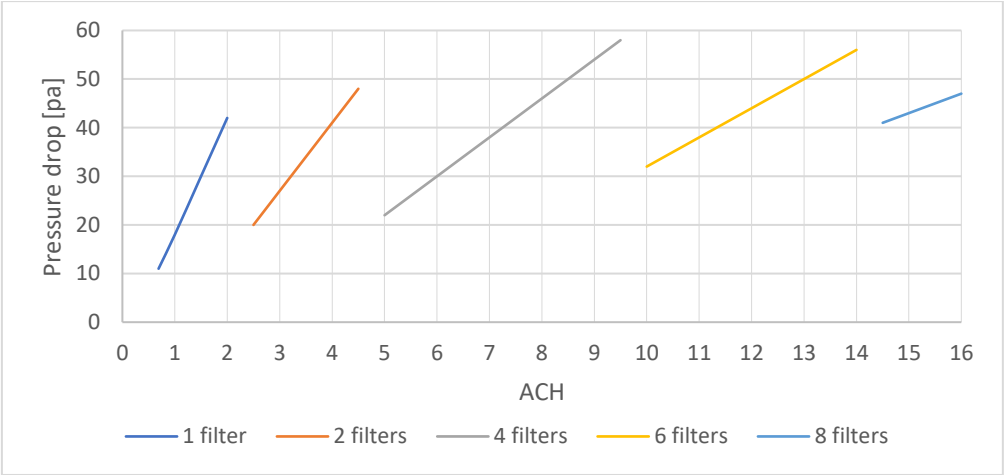

Figure 4.14: Pressure drop across medium filter index (M5), calculated using (Camfil, 2016)

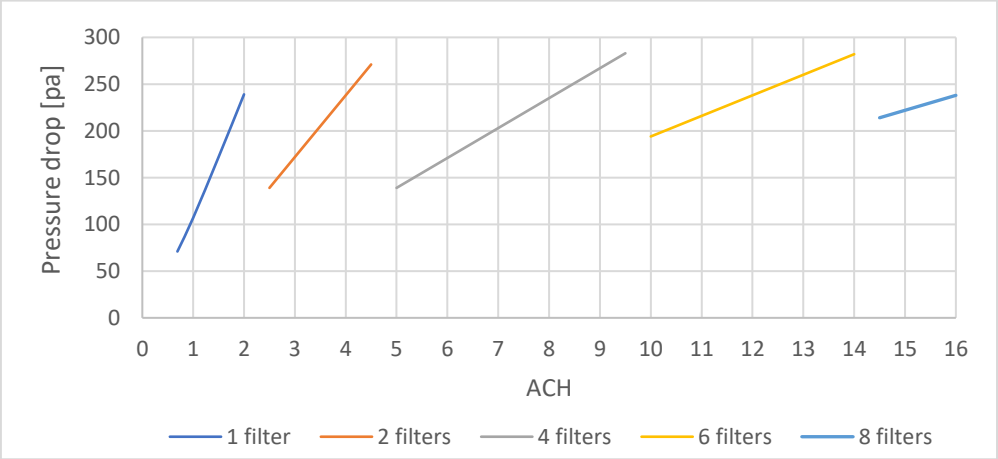

Figure 4.15: Pressure drop across high Index filter (HEPA), calculated using (Camfil, 2016)

Finally, combining the pressure drops from filters and duct, figure (4.16) is obtained.

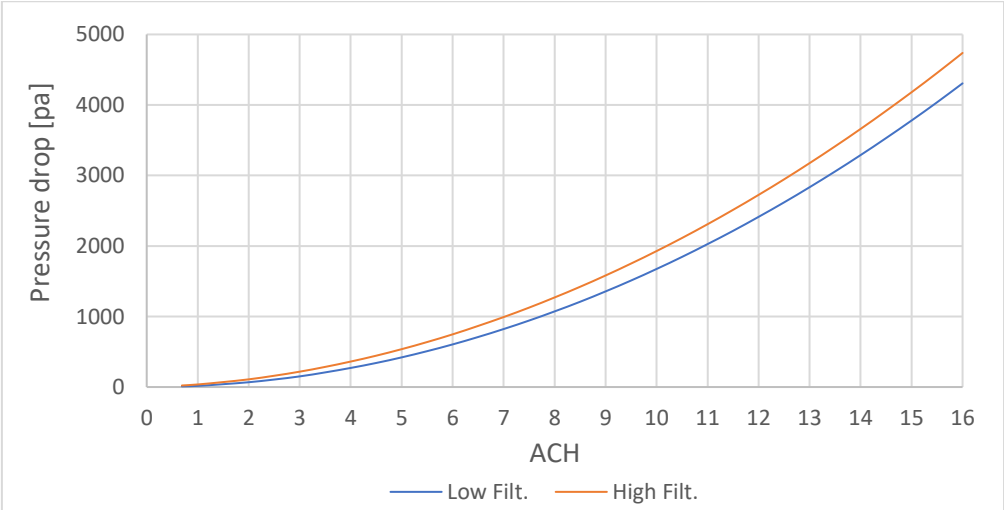

Figure 4.16: Total pressure drop

Furthermore, the fan power needed to push the air to overcome the resistance caused by filters and ducts for every half ACH is determined using equation (11). The fan energy consumption is fan power multiplied by number of the operating hours over the year. The fan electricity cost per year is computed using equation (13).

$$W_{fan} = \frac{Q_{air} \cdot \Delta p_{total}}{\eta_{fan\ total}} \qquad [\ KW\ ] \qquad (\ 11\ )$$

$$E_{fan} = W_{fan} \cdot t \qquad [\ Kwh/yr\ ] \qquad (\ 12\ )$$

Where:

-E_{fan} fan energy consumption *-Q_{air} airflow volume [m^3/h]*

-η_{total} total fan efficiency including the motor impeller and belt efficiencies and is assumed 70% taken from (Bekö, Clausen and Weschler, 2008).

-Δp_{total} total pressure drop [pa] *-W_{fan} fan power*

-t fan operation time [h].

$$C_{fan} = E_{fan} \cdot P_{elec} \qquad [\ €/yr\ ] \qquad (\ 13\ )$$

Where:

-C_{fan} total fan electricity cost per year

-P_{elec} is the electricity tariff (€/KWh) and is fixed to 0.08 €/kWh (Electricity price for non-household final consumers in Spain excluding tax, the first half of 2020. (Eurostat, 2020).

4.5.1.2 FILTRATION COST

The annual ventilation cost includes the cost of fan electricity and the total cost of filter ownership.

$$C_{vent} = C_{fan} + TCO \qquad [\ €/yr\ ] \qquad (\ 14\ )$$

Where:

- C_{vent} Total ventilation cost per year.

- TCO Total cost of ownership.

The filter total cost of ownership includes the cumulative costs of filter investment and replacement.

$$TCO = [\mathrm{C_{filter}} + \mathrm{C_{lm}}] \cdot \mathrm{N_c} \cdot \mathrm{N_f} \qquad [\ €/yr\ ] \qquad (\ 15\ )$$

Where:

-C_{lm} labor and maintenance cost

-C_{filter} filter cost

- N_f number of filters per change

-N_c number of Changes per year

Table (4.4) summarizes the values used for the filter cost calculation and lifetime. The expected filter lifespan (i.e., replacement frequency) was taken from a commercial contact advise in the filtration industry as a "best building practice norm". Quantifying the exact filter replacement periods is a complex task that depends on various variables such as the outdoor air environment, cleanliness of the indoor air, amount and temperature of the air stream, filter design, and pleats' material and structure on a micro level.

Table 4.4: Filter's lifetime and cost break-up

Parameter	Value		
	G4 filter	**M5 filter**	**HEPA filter**
Filter cost (€) *	15	34	125
Replacement cost (€) **	12	12	12
Disposal cost (€) **	5	5	5
Expected filter life	6 months	8 months	12 months
Changes per year	2	1.5	1

**the values are derived from the Camfil product catalog and similar filter costs from (Escoda, 2012).*

*** directly taken from (Bekö, Clausen and Weschler, 2008).*

4.5.1.3 HEATING COST

The heating simulation is based on Design Builder's EnergyPlus weather data for Bilbao, Spain. From the weather data, the highest heating load referred to as "Winter Design Day" is used to determine the sizing of convectors with a relative 25% oversizing margin used as a safety factor.

The heat generation uses an electric convector and calibrated to an Air Source Heat Pump (ASHP). The electric convector converts electric to heat energy with 100% efficiency. The electric convector consumption is divided by the yearly mean value of ASHP's Seasonal Performance Factor (SPF), equation (16). The annual mean value of SPF is estimated as three for ASHP (Nouvel, Cotrado and Pietruschka, 2015). It is worth noting that the heat delivery

mechanism inside the focused zones is the same for the two heating technologies i.e., using convectors.

$$ASHP = \frac{Electric\ Convector\ KWH}{Average\ ASHP\ SPF} \qquad [\ Kwh\ ] \qquad (16)$$

Similarly, the electricity consumption is multiplied by the fixed electricity tariff to obtain the heating cost per year. Finally, a summary of the key parameters data discussed used in the ventilation and heating Design-Builder simulation are displayed in the following table.

Table 4.5: Summary of input data used in the ventilation and heating simulation

Parameter	Value	
DB Simulation timeframe	One year- hourly timestep	
Total ventilation rate	From 1 to 6 ACH, step of 0.5ACH in between.	
Number of Occupants	Nursery: 14	Office: 29
Zone Volume area (m^3)	Nursery: 956	Office: 804
Cost of electricity	0.08 €/Kwh	
Fan efficiency	70%	
Operation time per year	4h/day, 5d/week, =11% of the total year hours.	
Heating setpoint T Heating setback T	22°C 12°C	
Heat recovery Efficiency	70% (Rotary air to air heat exchanger)	

4.5.1.4 PENALTY FUNCTION

The ventilation rate is inveserly proportional to the probability of risk and vice versa. This relation is also valid to the respective cost of ventilation and and probability of risk. Hence, balancing the ventilation costs and risk cost is crucial to determine and select a cost-effective ACH by minimizing the two costs using L^2 norm. Norms in mathematics are typically used to measure the magnitude (length or size) of a vector, a matrix, or a function. In this study context, the ventilation and risk costs make up the vector magnitude.

L^2 norm looks at the shortest path in the vector space referred to as Pythagorean distance or Euclidean distance. The L^2 norm is a function that takes the square root of the sum of the absolute values squared, expressed as follow:

$$\|x\|_2 = (\sum_{i=1}^{N} |x_i|^2)^{\frac{1}{2}} \quad (17)$$

Substituting the ventilation and risk costs gives equation (18).

$$f(ACH) = [(Risk\ €(ACH)^2 + Vent\ €(ACH)^2]^{\frac{1}{2}} \quad (18)$$

Equation (18) will return a certain value for each half step of ACH which we can then minimize. The minimum value from the 1 to 16 ACH set would be our cost-effective ACH solution.

4.5.2 AIR DISTRIBUTION

Air distribution scenarios are carried out using DB's CFD tool which is based on the RNG k-epsilon turbulence model.

The model is first created by defining the zone geometry, and air quantity linked to each supply and exhaust diffuser. Then the creation of internal and external boundary conditions which include surface temperature, finite volume grid spacing, and monitor point located in the center of the office space (See figure 4.17). The finite volume grid axes (X, Y, Z) are generated by using key vertices of the indoor space objects and static occupants models, i.e., non-uniform 3D grid.

The grid spacing is set to 50cm and the grid line merge tolerance of 5cm. The grid tolerance is to avoid small grid sections and produce a more uniform grid. Additionally, the monitor point function located in the center of the space is to monitor the variations of the calculated variables during iterations until reaching a convergence (DesignBuilder, 2019).

The average metabolic rate per occupant is 60Watt (=1met), which corresponds to the sedentary office activity level (ASHRAE, 2013). The metabolic rate corresponds to the heat emitted,

affecting the heat gain, which in return increases temperature and thus air direction and intensity.

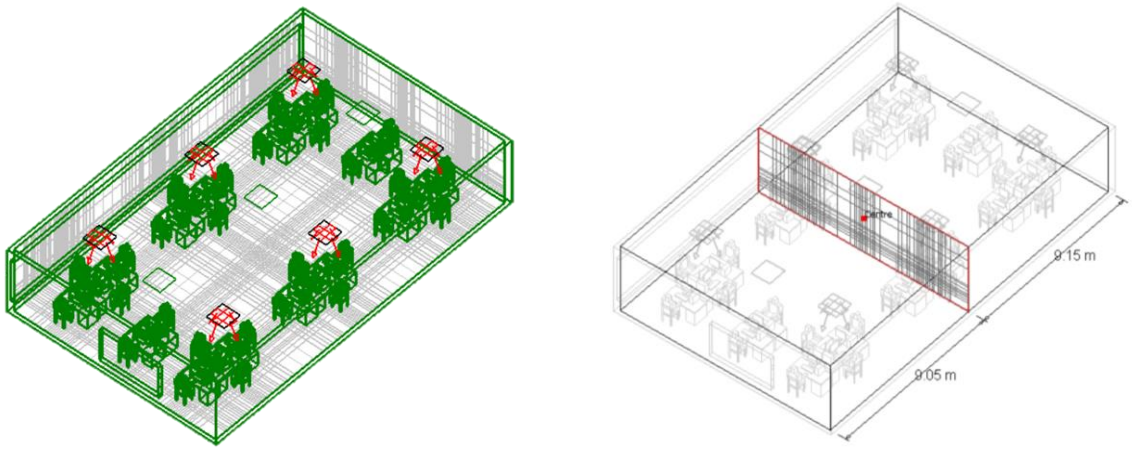

Figure 4.17: Creation of the finite volume grid (left) and monitor point (right)

Nevertheless, this study's air distribution analysis highlights the importance of supplying air properly to minimize the probabilities of infection to the lowest possible. The created CFD results is unique for this setup and does not incorporate virus transport behavior. Modeling a full airborne model to simulate the virus characteristic, level of contamination, and spatial variations of viral concentration is a complex task and often returns highly uncertain results due to the novelty of this field. Additionally, the model does not consider air entrainment, which may occur due to the dynamic indoor activities such as people walking, opening doors, and windows.

4.5.3 RENEWABLES INTEGRATION

Solar energy was found to have a potential to install a photovoltaics system in the case study building site. The photovoltaic system is designed using PVsyst Software based on the hourly irradiance data extracted from the site coordinates and altitude using Meteonorm software.

The focused zones' demand profile (KW) will be determined after conducting the ventilation and heating assessment and applying the penalty function to evaluate the range of the ventilation rate (ACH) and the least scenario energy consumption (i.e., scenario A or B). The analysis will also discuss the profitability to install a renewable source as well as the carbon savings using a life cycle emissions approach.

4.5.3.1 PHOTOVOLTAICS DESIGN

Generally speaking, the solar system design for self-consumption takes two pathways in terms of sizing; the first is oversizing the PV array capacity above the electricity demand. Oversizing is used because of solar intermittency and the fact that PV does not operate under rated power (Wp) in actual conditions all the time. The other option is to size the PV modules' capacity to meet occasional peak demands throughout the year to reach a cost-effective investment and performance arrangement. The former option is typically used for standalone (off-grid) systems commonly associated with energy storage to meet 100% of electricity demand for a selected period of autonomy, whereas the latter for grid-connected solar systems to meet partial demand and sell the surplus back to the grid.

The case study building is in an urban area, making it more viable to select a grid-connected solar system with no need for an energy storage medium. The photovoltaic rated capacity (KWp) is sized to meet the highest hourly power demand of the year theoretically**.**

Figure (4.18) shows the energy flow scheme of the grid-connected PV system. When there is enough energy output from the modules, the energy is consumed by the local load (E_used). However, if the PV modules output is not sufficient to meet the total demand, the deficit is supplemented by the grid (E_backup). Nevertheless, the PV energy is injected into the grid (E_over) during times of no demand or energy surplus from the PV output.

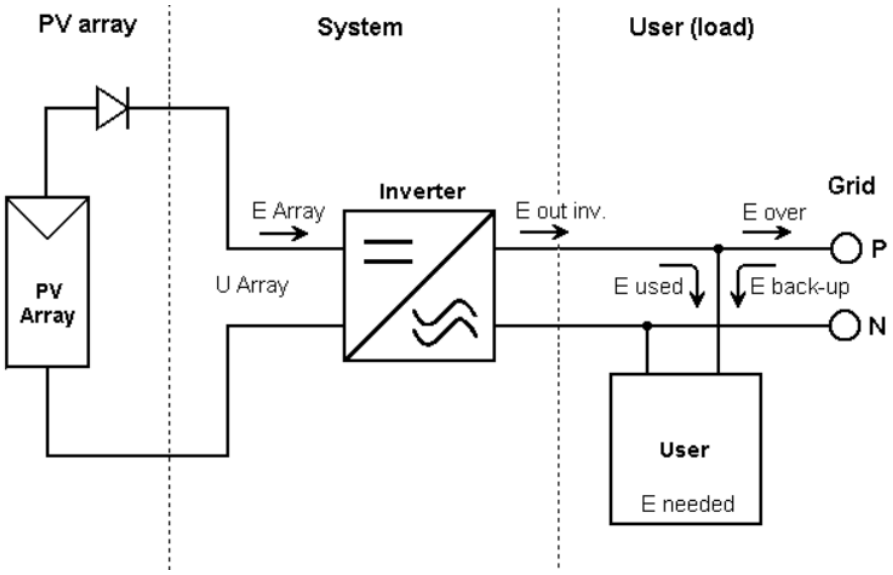

Figure 4.18: Simplified PV system energy flow scheme (PVsyst)

The price per kWh is 0.08€ from the grid (Eurostat, 2020), while 0.051 € is the feed-in tariff to the grid (IBERDROLA, 2021).

Furthermore, to ensure system high efficiency, a seasonal tilt angle adjustment [3] (winter tilt at 55°, summer tilt at 24°) was decided to be the most optimal, being a compromised solution (Performance/cost) between the fixed tilt and the two-axis tracking panels. The two seasonal tilt angles and the azimuth angle were determined using PVsyst and PVGIS inclination angle optimization tools for the site coordinates (Commission, 2019).

4.5.3.2 ECONOMIC ASSESSMENT

The economics of the solar system is a cash flow analysis based on the difference between electricity costs from the local grid and the PV system.

$$CF_s = C_i - \left|(E_t \cdot C_f) - \left(E_R \cdot C_f\right) - (C_m) + (E_s \cdot C_t \cdot D_r)\right| \qquad [€] \qquad (19)$$

Where:

$\boldsymbol{CF_s}$ ***Cash flows***

$\boldsymbol{C_i}$ ***is the intial ivestment*** (€)

$\boldsymbol{E_t}$ ***is the total energy demand*** $(\boldsymbol{kwh})$

$\boldsymbol{E_R}$ ***is the residual demand supplied by grid***$(\boldsymbol{k}$

E_S *is the PV injected energy to grid* (kwh)

C_m *is the maintennace cost per year* (€)

[3] Winter months (October to March), Summer (April to September)

$\boldsymbol{C_f}$ ***is the electricity tarrif from grid*** (€) C_t *is the electricity tarrif to grid* (€)

$\boldsymbol{D_r}$ ***is the PV modules degradation rate per year*** (%)

The calculations are based on the euro per watt total cost value. The capital cost "CAPEX" is the initial cost that must be accumulated at the start of the project; this cost covers the equipment (panels, inverters, wiring, etc.) and the installation cost. According to PvXchange, 2021, the average cost of monocrystalline modules from April 2020 to April 2021 is 0.33€/Wp. Inverters and other equipment cost 0.15€/Wp while maintenance cost is 0.18€/kwh/yr (IRENA, 2020). Additionally, a PV performance degradation rate of (0.08%) is incorporated in the 25 years of PV modules' lifetime. The Payback period (PP) and internal rate of investment (IRR) metrics are used to evaluate the profitability of PV installations.

Finally, the capital cost can usually be reduced by government grants and incentives for such renewable projects; however, with the uncertainty around the Spanish "tariff-deficit" [4] described in (López Prol and Steininger, 2017) and its consequent restrictive measures to reduce green prosumers profitability, the economic assessment will not consider any external subsidies.

4.5.3.3 CARBON SAVINGS

The carbon balance analysis estimates the amount of reduction in CO_2 emissions if solar energy is implemented. The analysis is based on comparing the life cycle carbon emissions (LCE) difference between the system using solely an existing grid and a PV system to replace the same amount of electricity. If the carbon footprint of the PV installation per kWh is smaller than the one for the grid electricity production, there will be a net saving of CO_2 emissions (PVsyst, 2020). The previous description is expressed in equation (20)

$$Saved\ Carbon = LCE_{grid} - LCE_{PV\ system} \qquad [tCO_2\text{-}eq^5] \qquad (20)$$

[4] An accumulated debt of 30€ billion since 2001 caused by financing the difference between costs and revenues in the regulated activities derived when the retail price of electricity is set lower than the corresponding costs borne by energy companies.

[5] [tCO_2-eq] tons of carbon dioxide equivalent

Where:

- $LCEgrid = Total\ amount\ of\ electricity\ consumption\ (kwh) \times 25yr \times 207gCO2/kwh$ [6]
- $LCEpv\ system = which\ includes\ PV\ modules\ and\ system\ support\ LCE\ (See\ Appendix\ C)$.

[6] Spain greenhouse gas emissions intensity of electricity generation (European Environment Agency, 2020).

CHAPTER 5. RESULTS

The chapter presents the ventilation, space heating, air distribution, and photovoltaics different simulations' findings and analyzes the key differences.

5.1 VENTILATION AND COVID-19 PROPAGATION RISK

The annual ventilation costs stated expressed in this section corresponds to the cost described in equation (14). Figures (5.1), and (5.2) show that the ventilation costs curve is increasing non-linearly. With each step of ACH, i.e., higher air quantity, the total pressure drop increases which is proportional to the square of the average air velocity. This results in the fan's high electricity consumption and cost. The Nursery has overall higher ventilation costs than the Office because of the larger volume requiring more airflow rate (m^3/s) to be delivered. Nursery and Office constitute 54% and 46%, respectively, of the total air supplied by the central VAV AHU unit.

Overall, scenario "A" is relatively cheaper than Scenario "B". Scenario "B" has more additional pressure drop from the HEPA filter, requiring extra energy to push the air through the filter. Besides, the high ventilation costs in scenario B are attributed to the HEPA filter investment and replacement costs.

On the other side, the difference in the risk probability between the two scenarios is relatively minor. This is because the Wells Riley equation considers both ventilation and filtration with the same weight to reduce the infection. In scenario "A", the Wells Riley equation sink terms incorporated the effect of ventilation ($\lambda_{Vent.}$) for 100% of air together with the additional measure of the M5 filter ($\lambda_{filtration}$) whose efficiency to filter out particles of 0,3 µm up to 1 µm is less than 20%[7].

On the other hand, scenario "B" incorporated the HEPA filter ($\lambda_{filtration}$) which can filter out particles with an efficiency of 99.95% for 90% of the total air, recirculated, and the remaining 10% of fresh air accounts for ventilation effect to reduce airborne particles (λ_{Vent}). Therefore,

[7] See Figure 2.8 for filter efficiency

both scenarios “A” and “B” yield little difference in the total first-order loss rate (λ_{total}) and consequently the risk probability difference magnitude. It is worth noting that the virus deposition and decay rates are equal in both scenarios.

Moreover, although the lower density and bigger volume the nursey has, the Nursery poses a higher probability of risk than the Office. Nursery starts as high at 12.5% at 0.8ACH while the Office starts at 2.5% at 0.6ACH, baseline ventilation. The quanta generation rate magnitude of (76q) for the Nursery compared to (5.7q) for the Office explains the initial high percentage of risk, i.e., high quanta generation translates to higher SARS-CoV-2 aerosols concentration in the air and higher probability of infection for susceptible occupants. However, at 16ACH, the probability of infection significantly decreased to 1.57% and 0.3% for nursery and office, respectively.

Additionally, the trend of the risk probability tends to fall drastically from the initial concentration of 2.5% and 12.5% to 1.3% and 7% at 2ACH for Office and Nursery, respectively. Therefore, 2ACH can reduce the risk by at least 40% of the initial risk percentage both in scenario “A” and “B”. This is due to the low initial average concentration of quanta (q/m^3), consequently lowering the probability to inhale viral particles per air volume by susceptible people. However, the risk after 2ACH is relatively high even with an initial reduction. Hence, the amount of money spent to dilute and reduce the probability of risk (i.e., Risk probability/ventilation costs) is lower and more profitable until 2ACH than above 2ACH. Eventually, with higher ventilation rates, the slope plummets with a slight decrease because of the nature of the exponential function in the Wells Riley equation.

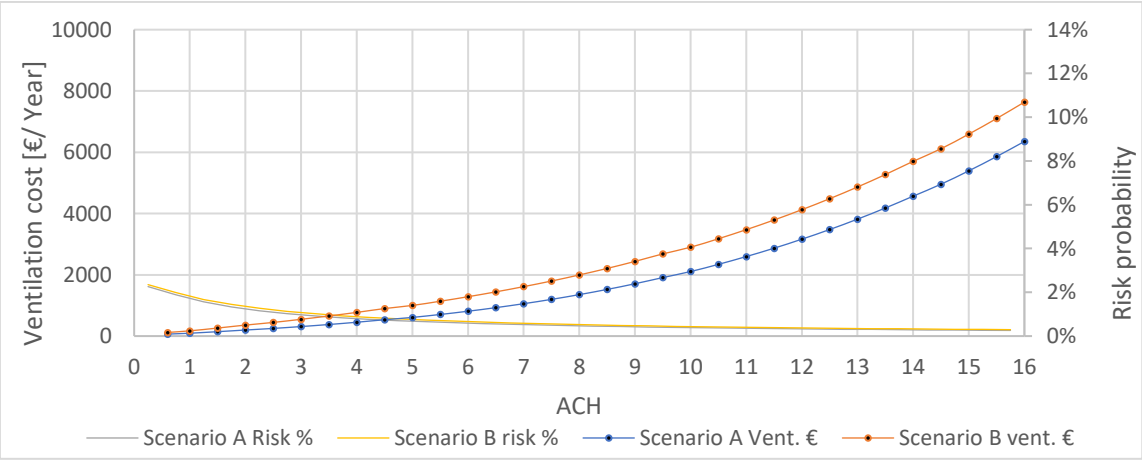

Figure 5.1: Office ventilation costs and risk probability (Scenario A vs. Scenario B)

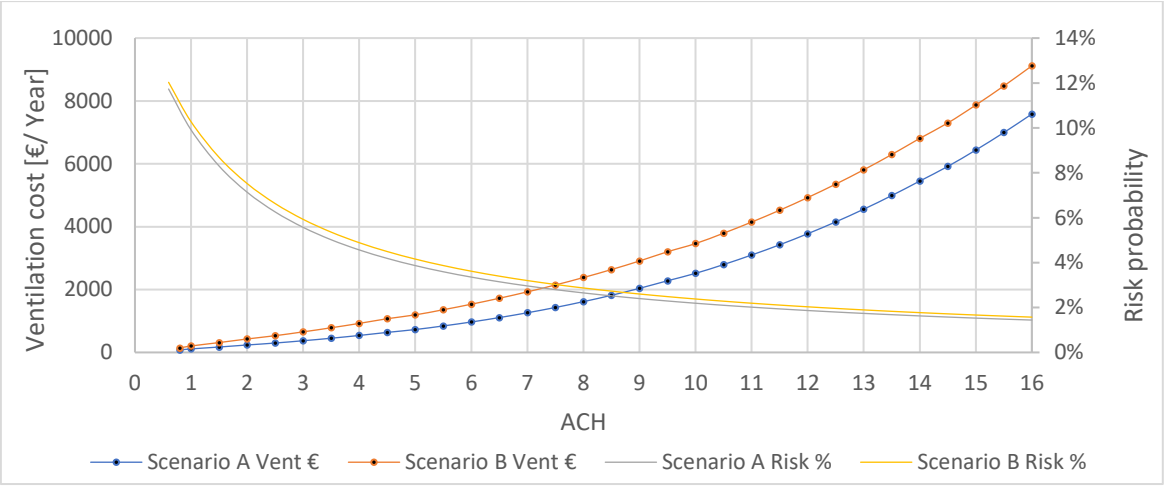

Figure 5.2: Nursery ventilation costs and risk probability (Scenario A vs. Scenario B)

Furthermore, the penalty function from equation (18) is implemented for each ACH step to calculate the minimum value of ventilation and the risk costs. The minimum value is drawn corresponding to the ACH bin shown in the following table:

Table 5.1: L^2 norm minimum ACH

Zone	Scenario A	Scenario B
Office	6 ACH (= 46 l/s/pers.)	5 ACH (= 38 l/s/pers.)
Nursery	8 ACH (= 152 l/s/pers.)	7 ACH (= 133 l/s/pers.)

** The Graphs of the L^2 norm are found in Appendix A*

On one side, in the Office, a ventilation rate of 6ACH and 5ACH for scenario "A" and "B", respectively, yields the lowest minimum based on the L^2 norm method. On the other side, the nursery L^2 norm returns 8ACH and 7ACH for scenario "A" and "B", respectively.

Additionally, taking the highest and lowest ACHs in (Table 5.1), both 5 and 8ACH would take 58minutes and 35minutes, respectively, to remove 99% contaminant removal efficiency based on the CDC removal rates.

Furthermore, figures (5.3) and (5.4), show the evolution of supplying 5 ACH and 8 ACH to the risk probability evolution in the focused zones over the exposure hours of 10 hours. The extended exposure duration shows the linear increase in the probability risk from 4h and 10h of by a factor of 2.5. As a result, ventilation costs would increase correspondingly to keep a constant infection probability.

The value of the quanta determines the magnitude of the risk probability reduction. Figure (5.3) shows the Office zone is less sensitive when the ventilation supply is increased from 5ACH to 8ACH. Unlike the Office, Nursery has 70 more quanta production per person inside the space resulting in a considerable difference in reducing the risk probability from 10% to 7% on the 10th hour of exposure. Hence, the higher the exposure time with a constant ventilation rate, the higher the risk of infection.

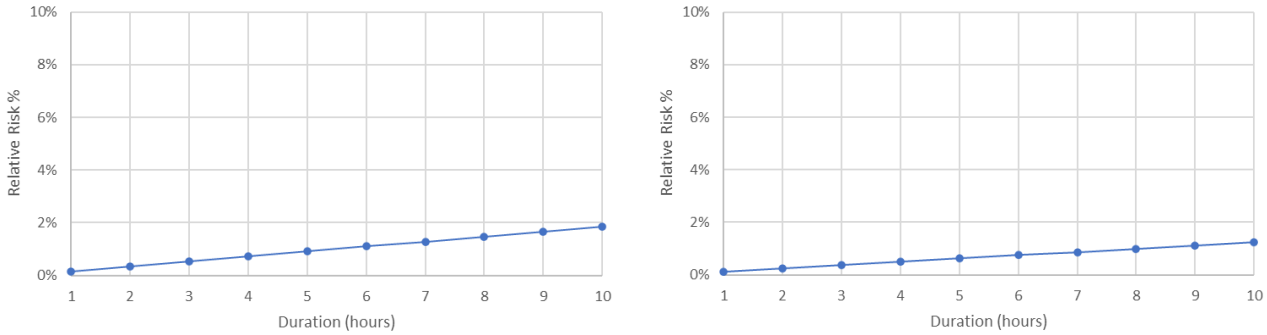

Figure 5.3: Office infection risk evolution, left: 5ACH, Right: 8ACH – Scenario A

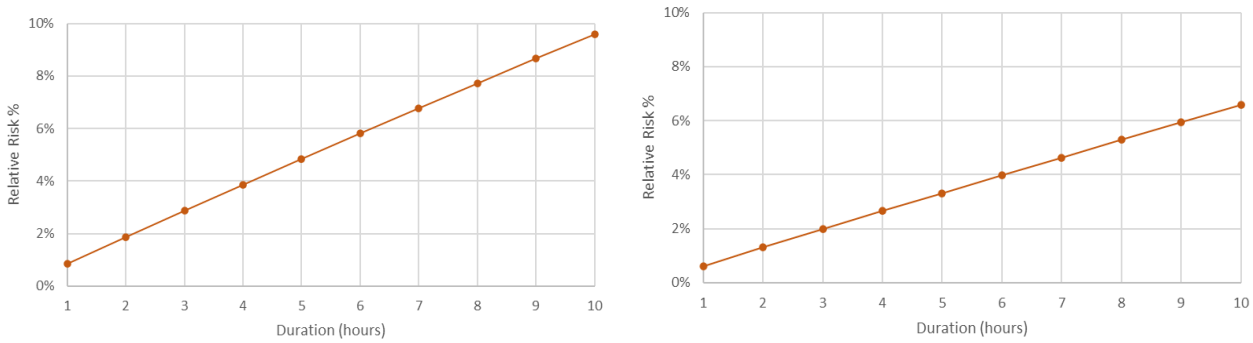

Figure 5.4: Nursery infection risk evolution, left: 5ACH, Right: 8ACH – Scenario A

5.2 HEATING

In the previous section, we found that Scenario A's ventilation costs are less than Scenario B for all ACH steps. This section will compare the two scenarios in terms of increased ventilation rates' implications on space heating cost and the effect of heat recovery.

Ventilation and heating systems are not directly connected technologies. Nevertheless, when air is being supplied and extracted to and from space by the centralized AHU, the air temperature should fall within the heating setpoint to maintain the thermal comfort of occupants. Evidently, more outdoor air quantity means more energy is needed to heat the air.

Figure (5.5) shows the annual heating cost for scenario “A” characterized by 100% outside fresh air, is the most energy-intensive option when the heat recovery is off. Without the heat recovery activated, the amount of air needed to be heated increases with each incremental step of ACH. Likewise, The Nursery heating cost is higher than the Office because of the Nursery’s larger space volume and orientation (more thermal gains) in the building layout.

In scenario “A”, figure (5.5) shows turning on heat recovery in scenario “A” reduces energy consumption by a factor of 3 to 5 (i.e., huge spread) over the 1 to 16 ACH range. Additionally, the difference between “with HR” and “Without HR” modes, reaches 2811€ for the focused zones at 16ACH, corresponding to 35130 KWh per year.

On the contrary, scenario “B” cost reduction factor over the 1-16 ACH range is 1.2 to 1.5 (i.e., small spread), (See figure 5.6). Additionally, Scenario B's highest cost difference between the two heat recovery modes at 16ACH, for the focused zones is only 205€ corresponding to 2560 KWh per year. Hence, the benefit of heat recovery is not as significant as in scenario “A” because heat recovery is effectively utilized to preheat the incoming remaining 10% of the outdoor air while the 90% recirculated air still possesses a fraction of the sensible heat.

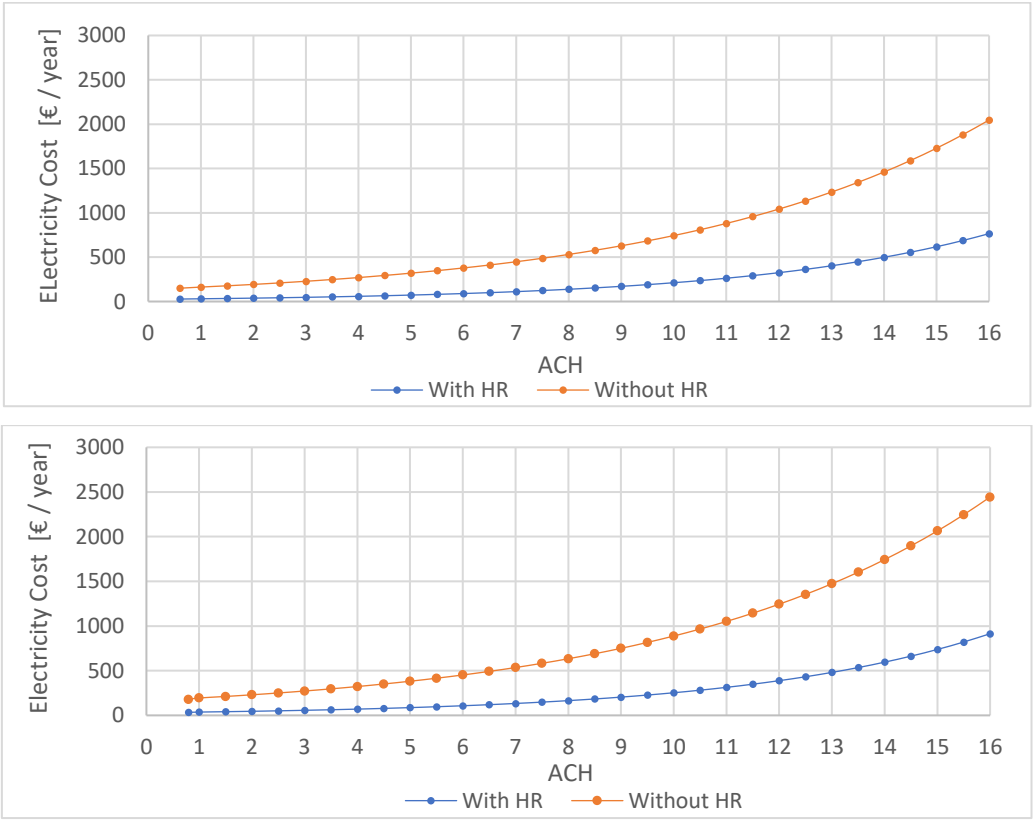

Figure 5.5: Scenario A space heating cost per year for ASHP - Office (Top)-Nursery (Bottom).

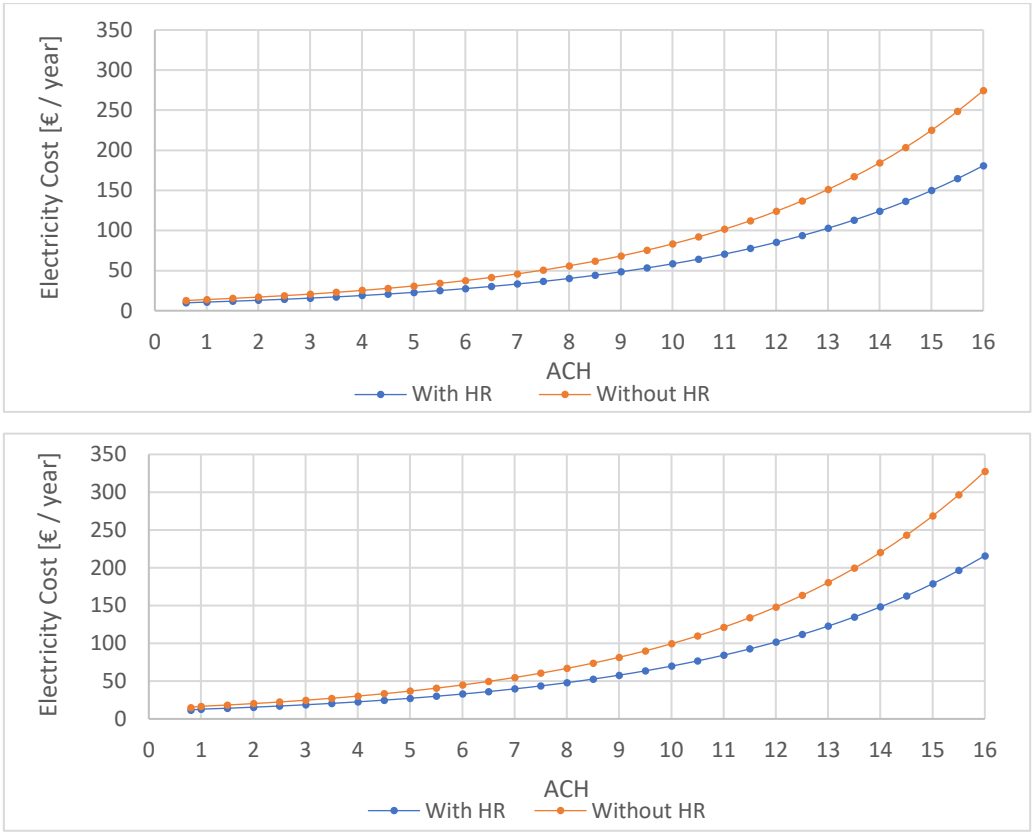

Figure 5.6: Scenario B space heating cost per year for ASHP - Office (Top)-Nursery (Bottom).

Finally, based on the results mentioned above, table (5.2) summarizes the compiled annual total cost of ventilation and heating for scenario "A" and "B" between the range of 5 to 8ACH determined by the L^2 norm and compared to 16ACH. It is evident that scenario A is less costly in terms of ventilation than scenario "B" especially when heat recovery is activated. Nevertheless, at 16 ACH, scenario "B" has less total cost than scenario "A" when heat recovery is switched off. This is because the heating consumption in scenario "A" becomes exponentially high at 16 ACH. After all, the heating generation COP is 3 compared to 70% of the fan efficiency. In addition, the operation time of the fan is constant all year long for 4 hours 5 days a week while heating works for a limited number of hours over the year during wintertime. This makes heating has a low impact on the overall total cost, i.e., heating savings from scenario "B" is low to offset ventilation costs. Consequently, Scenario "A" is a plausible option to be used at lower ACHs (<16ACH) for the focused zones.

Table 5.2: Focused zones scenario "A" and "B" yearly ventilation and heating Cost

Scenario	**Parameter**	**5 ACH**	**6 ACH**	**7 ACH**	**8 ACH**	***16 ACH***
Scenario A	Ventilation + Heating *with* HR (€)	1497	1977	2564	3272	*15600*
	Ventilation + Heating *without* HR (€)	2039	2611	3303	4133	*18420*
Scenario B	Ventilation + Heating *with* HR (€)	2245	2878	3614	4466	*17150*
	Ventilation + Heating *without* HR (€)	2263	2901	3642	4500	*17356*

Finally, tables (5.3) and (5.4) show the summary of ventilation, risk probability, and heating for office and nursery, respectively. Each scenario indicates the equivalent ACH calculated by the L^2 norm. Undoubtedly, for both zones, scenario "A" with HR is cheaper to operate. If scenario "A" is not a plausible option to implement, Scenario "B" can be another alternative. The difference in the risk probability in Scenario A and B in the two zones is also not significant.

Table 5.3: Office ventilation, risk probability, L^2 norm, and heating summary

Parameter		**Scenario A : 6ACH**	**Scenario B : 5ACH**
Risk (%)		1%	1.2%
Ventilation (€)		1057	1284
Heating (€)	With HR	112	28
	Without HR	450	38

Table 5.4: Nursery ventilation, risk probability, L^2 norm and heating summary

Parameter		**Scenario A : 8ACH**	**Scenario B : 7ACH**
Risk (%)		2.9%	3.2%
Ventilation (€)		1615	1926
Heating (€)	With HR	165	33
	Without HR	633	46

5.3 AIR DISTRIBUTION

Each scenario explained in the air distribution methodology has two distinctive differences: the placement and angle of supply and exhaust diffusers and the quantity of air per diffuser. The total air supply quantity is equivalent to 5 ACH i.e., 1117 l/s, and is divided by the number of

the supply and return diffusers. The focus of this analysis is to examine the airflow patterns around the end-users by changing diffusers settings.

The red lines drawn over the figures in this section are indicative to illustrate the major air flow movement trend. It is worth noting that the discussed results for this section are based solely on the author's air movements analysis to further employ ventilation appropriately and avoid the transmission risk as much as possible. There is no scientific basis to confirm or refute the occurrence of infection.

Looking at Scenario “I” and “II” in figures (5.7), and (5.8), the arrows show the direction and the intensity of the air stream. Scenario I’s supply diffuser (at 60° angle) throw distance, which is the distance from the diffuser to the point where the airstream reaches, is shorter than the 30° supply diffusers of scenario “II”. Scenario “I” air pattern from the supply diverts from hitting directly the occupants but eventually creates a turbulent zone on the right side of the space. This may stimulate the transfer of viral aerosols from the left to the right side of the space.

On the other hand, scenario “II” has a smooth airflow movement diluting the air around the occupants and extracting it in the center of the space. However, air direction arrows indicate a portion of the air is transferred to other zones in the center and around the corners.

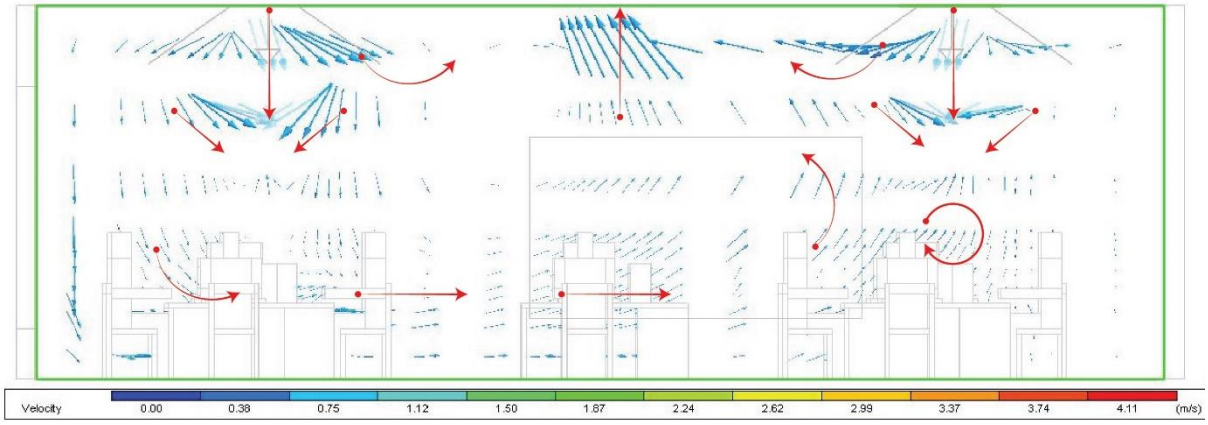

Figure 5.7: Scenario I -Cross-sectional view of air patterns around occupants

Furthermore, in scenarios “I” and “III”, it is noticed that a portion of the supply air is short-circuited to extract because of the short distance between supply and extract air streams. Scenario “III” is similar to “I” where air turbulence happening in the corners instead of the center of the space. The initial horizontal spread in Scenario “I” and “III” discharged by the

supply diffuser caused by the 60° tilt results in the air eventually being dropped vertically, which then induces the existing stagnant air in the room and creates turbulence in the center due to air density and temperature difference.

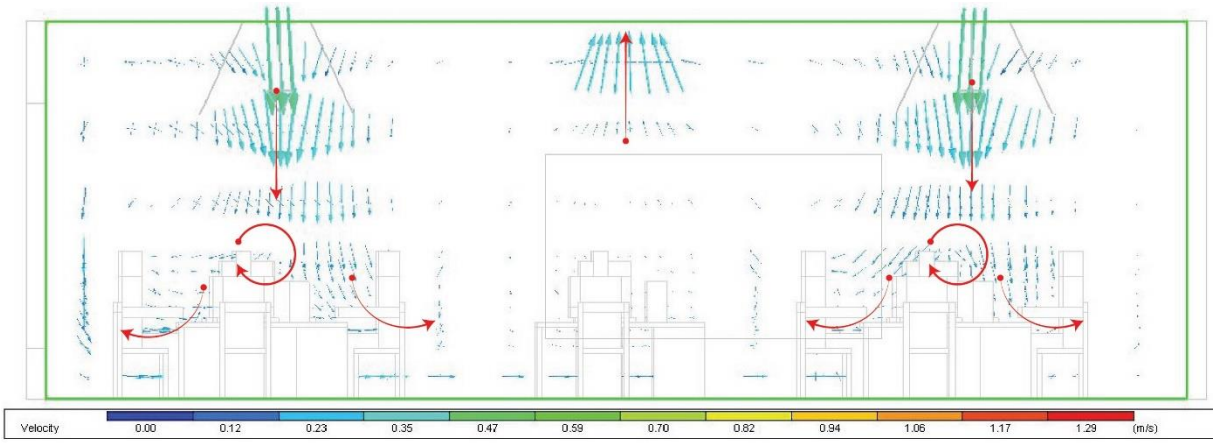

Figure 5.8: Scenario II - Cross-sectional view of air patterns around occupants

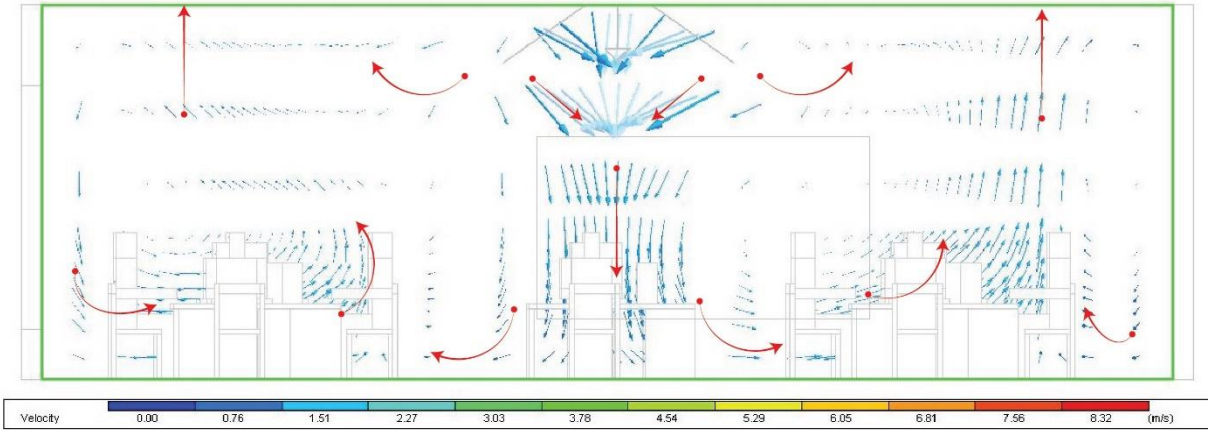

Figure 5.9: Scenario III - Cross-sectional view of air patterns around occupants

Finally, Scenario "IV" air movement has a vertical drop, passing through occupants' plume and directly extracted upward. This air behavior gives less probability of infection for circulation in the room center and also for seated occupants in the corners. All scenarios' turbulence level findings around the occupants are analyzed more in-depth using several CFD slices in the model itself and are estimated in table (5.5).

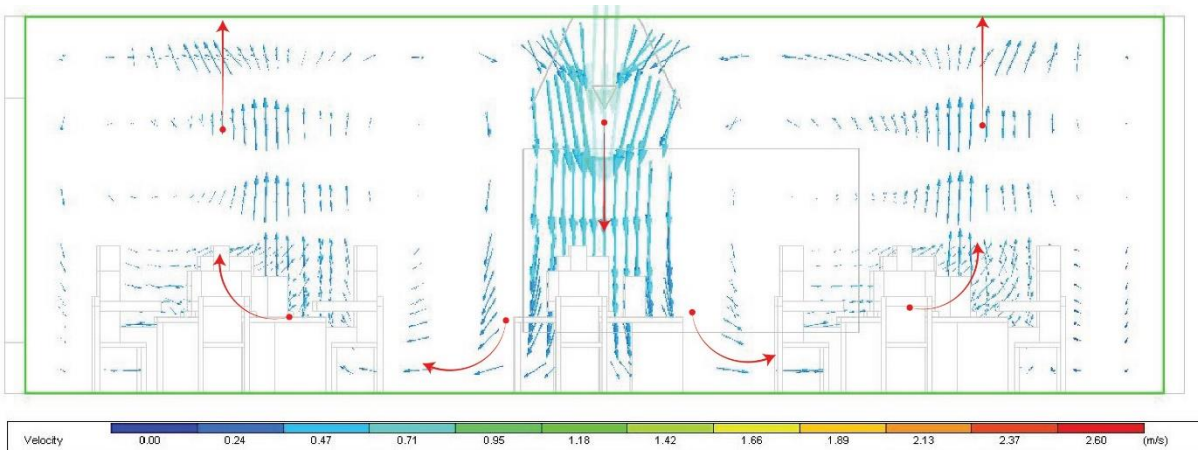

Figure 5.10: Scenario IV – Cross-sectional view of air patterns around occupants

Table 5.5: CFD scenario turbulence assessment summary

Scenario	Level of turbulence around occupants
Scenario "I"	High - (Air is short circuited)
Scenario "II"	High
Scenario "III"	Low - (Air is short circuited)
Scenario "IV"	Low

5.3.1 PHOTOVOLTAIC SYSTEM

The section will first draw out the focused zone annual hourly power demand profile for Scenario A in the focused zones. Scenario "A" is selected only to design the PV system because it returned a lower annual operation cost than scenario "B". The power profile incorporates scenario's "A" ventilation and heating with a heat recovery power demand over a year and is used to size the PV capacity. The demand profile is created for 5ACH and 8ACH, selected as the lowest and the highest range of air change rates found to have the minimum cost for ventilation and risk in the table (5.1). Also, 16ACH is added to compare the 5 and 8 ACH to higher ventilation rates if to be used. The section starts with an overview of the PV system design and components and explains the different losses during operation. The economic assessment and the saved carbon footprint are discussed subsequently.

Figures (5.11) and (5.12) illustrate the hourly power demand profiles over the year for 5ACH and 8ACH, respectively. The highest power peaks are 11.2KW and 29KW for 5ACH and 8ACH, respectively, and taken as the PV-rated installed capacity.

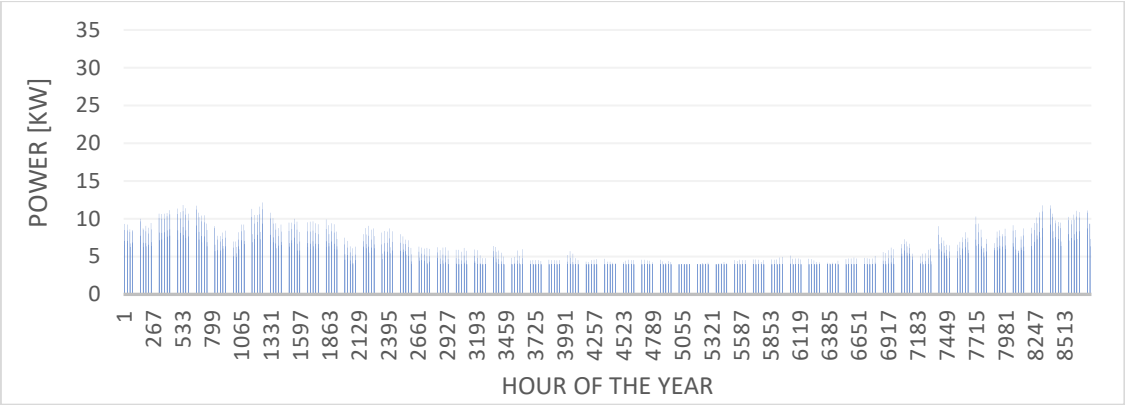

Figure 5.11: Focused zones annual hourly power demand at 5ACH.

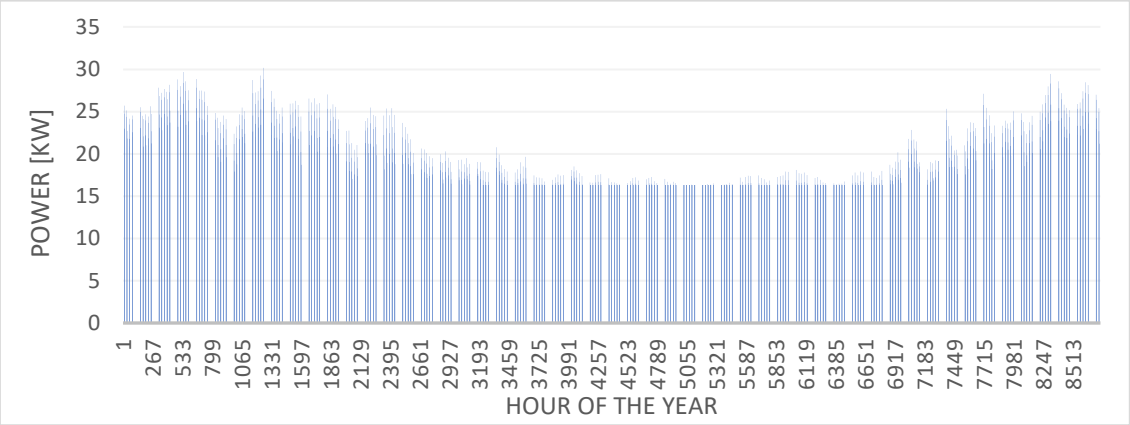

Figure 5.12: Focused zones annual hourly power demand at 8 ACH.

The PV system consists of monocrystalline modules, with rated efficiency of 19% and a nominal power of 400Wp according to the manufacturer, PowerSun[8]. For 5ACH, the PV system comprises of 28 modules connected in 7 in series, and 4 in parallel to make up the 11.2 KWp of nominal PV capacity under Standard Test condition (STC) with a total area of 61m^2. On the other hand, the 8ACH's system includes 72 modules connected as 9 in series and 8 in parallel with a total area of 156m^2.

Additionally, the number of PV modules can be mounted on the roof of the Rectorship building (Figure 5.13). It is found that the roof can accommodate up to 200 PV modules which can support a maximum of 12ACH of ventilation rate.

[8] PV module Model : Si-mono - SPR-400-WHT-D

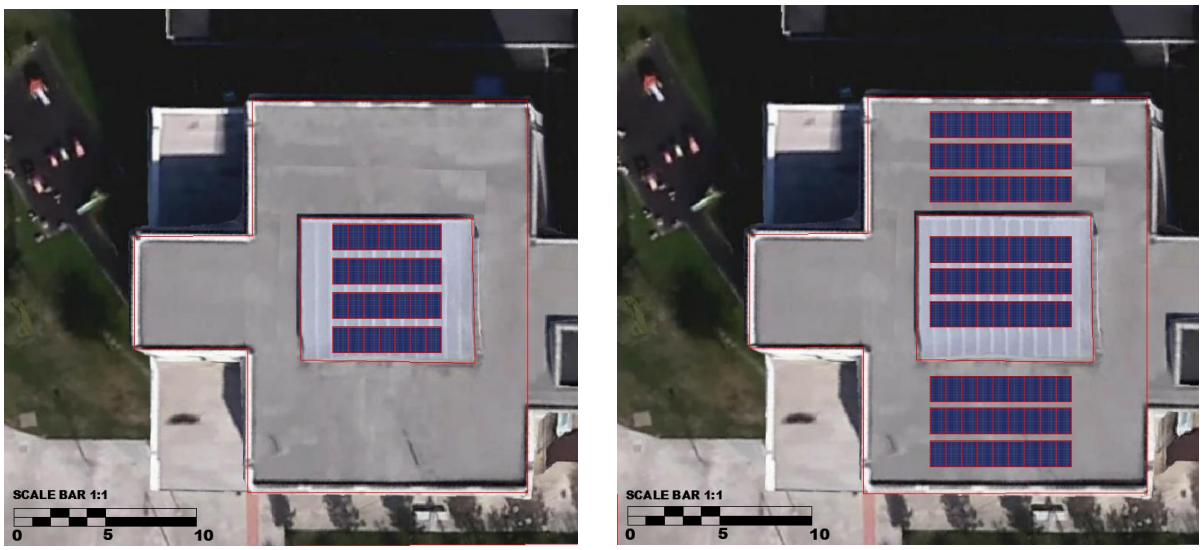

Figure 5.13: Illustration of the case study's roof and PV modules mounting area proportion - Photo and PV modules to scale- Left: 5ACH, Right:8ACH

Furthermore, the inverter is sized to achieve a DC to AC ratio [9] of 1.15, which is ideal for significantly minimizing clipping losses (Good and Johnson, 2016). Table (5.6) shows a breakup a summary of photovoltaic components for 5ACH and 8ACH. The solar fraction indicates the percentage of the amount of energy consumed by demand from photovoltaics. It is found that PV meets an average of 51% of the total demand. In other words, the demand and PV generation mismatch causes around 49% of PV energy not effectively utilized by the building due to solar intermittency and is fulfilled by the grid.

Table 5.6: PV system components and solar fraction

Parameter	5ACH	8ACH
Nominal installed power (KWp)	11.2	28.8
Number of modules	28	72
Module's connection	4 strings, 7 in series	8 strings, 9 in series
Yearly energy demand (KWh)	6089	20660
Solar fraction	53%	48%

Moreover, figure 5.14 shows a breakdown of power flows to and from the grid as well as the different losses. The surplus of electricity is injected back to the grid or can be also stored using

[9] Also called "PV to inverter Load" is the ratio between the PV rated capacity under STC and inverter capacity. A rule of thumb is to have a ratio between 1.1 to 1.2 since PV is very rarely operating under optimum conditions in real life settings.

any storage technology. The energy flows from and to the grid at 8ACH is approximately 3 times higher than at 5ACH.

Manufacturers use the Standard Testing Conditions (STC) to give the rated capacity KWp of the module. STC assumes no losses, and thus an ideal array/module yield is helpful to determine system losses using STC as a reference. Figure (5.14) shows a breakup of the yearly flow diagram of losses, system, and collection losses. Another metric to evaluate the losses is the Performance ratio. PR is the ratio of the energy effectively produced to the energy which would be produced if the system was continuously working at its theoretical STC efficiency (PVsyst, 2020), i.e. the production of energy under STC minus losses. The system PR for both ACHs reaches 83%, i.e., system loss is 17%. The total losses are justified by several factors.

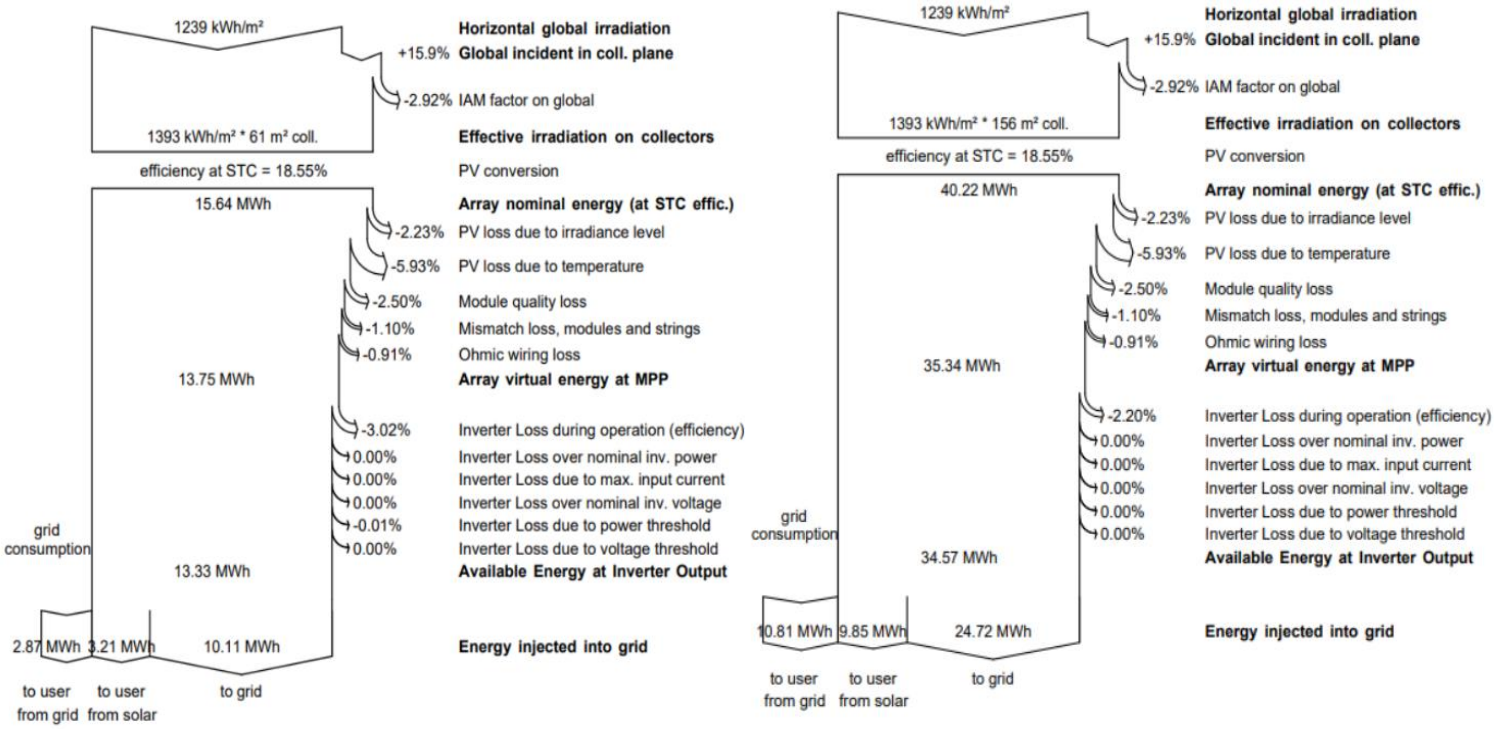

Figure 5.14: Loss diagram over the whole Year, Left: 5ACH, Right: 8ACH (PVsyst)

Firstly, the orientation and tilt of the modules might not be at their optimum all the time. Also, climatic conditions change occasionally, especially during the winter months (high precipitation), and partial shading caused by nearby terrain.

The collection losses of the modules are estimated *at 0.57 kWh/kWp/day*; these are caused due to the differences between the cell operating temperature and their STC conditions.

.

Furthermore, the system losses of *0.11 kWh/kWp/day* include losses from electrical support devices such as inverters, charge controllers, and wiring.

5.3.2 ECONOMIC ASSESSMENT

A cash flow analysis was conducted for 5ACH and 8ACH using equation (19) to examine the payback period and profitability applied to 4 and 8 hours of building operation. It is worth noting that the study assumed power injection to the grid is permissible all the time regardless of real operations constraints such as voltage regulations.

Figures (5.15) and (5.16) show the annual cashflows and the payback period for 5ACH and 8 ACH respectively. The graph indicates that going to a higher ACH and extending the operation period, results in a decrease in the payback period. In 5ACH, the payback period is cut down from 13 to 10 years whereas a decrease from 11 to 10 years for 8ACH when demand is increased from 4 hours to 8 hours.

Additionally, table (5.7) summarizes the payback periods and the IRR results. At 5 ACH, the IRR returns 0% which means project unprofitability and loss of the principal amount invested. Conversely, at 8 hours of operation, the IRR grew to 3.3%. Similarly, 8ACH, the IRR increases from 0.5% and 5.6% on the 4 and 8 hours of operation, respectively. The minor improvement in 16ACH's payback period and the IRR marginally is attributed to the exponential increase in power and energy demand. Besides, even if the system is over/undersized, the fact that investment's components cost calculations are incremental and based on euro/Wp which does not significantly affect the payback period i.e., high installed PV capacity yields high investment. Hence, an IRR value of less than 10% considering the system's lifetime of 25 years implies low demand to offset the investment by large, i.e., economies of scale do not break down. This is compounded by the fact that the selling price to the grid is only 64% of the buying price (i.e., huge spread).

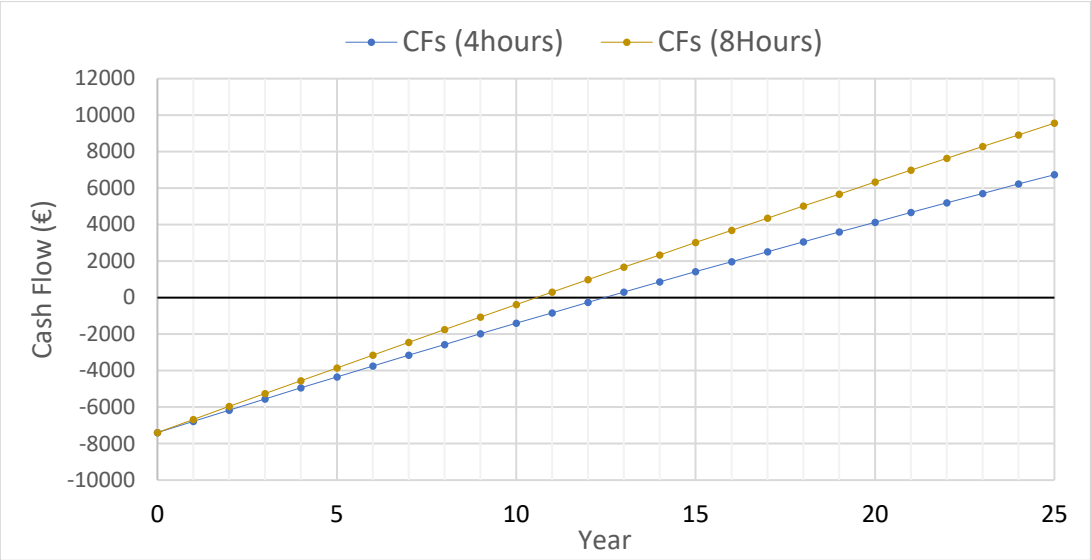

Figure 5.15: Cashflows at 5 ACH

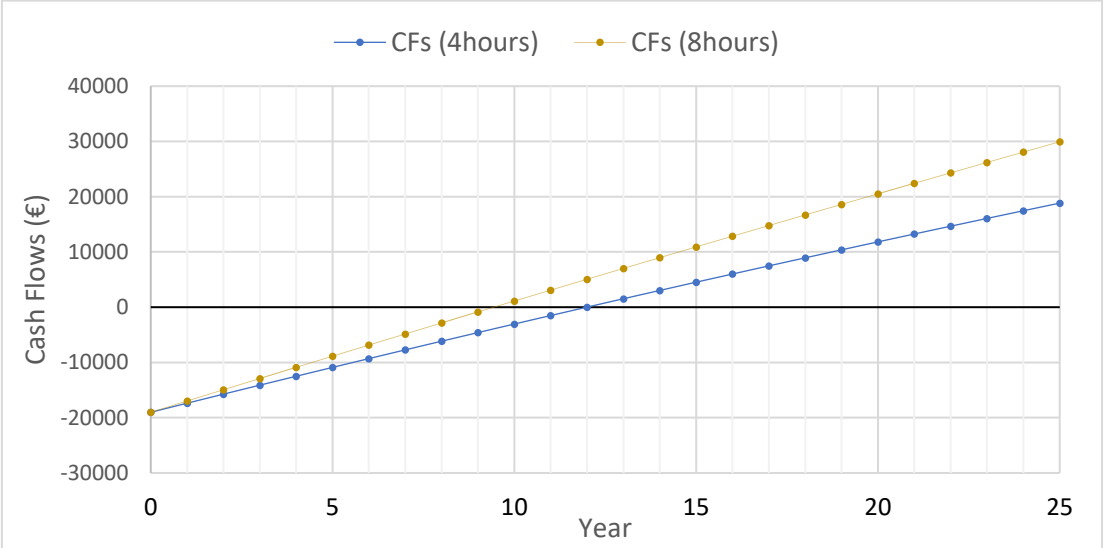

Figure 5.16: Cashflows at 8 ACH

Table 5.7: Photovoltaics economic assessment summary

`	5ACH		8ACH		16ACH*	
	4 h	**8 h**	**4h**	**8h**	**4h**	**8h**
Payback period (PP) – (Years)	13	11.	12	10	12	9
Internal rate of return (IRR) %	0%	3.3%	0.5%	5.6%	0.8%	5.9%

* *16ACH demand profile and cash flows chart in Appendix B*

5.3.3 CO_2 SAVINGS

Based on the LCE method, see equation (20). The results in figures (5.17) and (5.18) indicate that the total amount of saved carbon emissions during the installation lifetime of 25 years when operating 4 hours per day. The study found that 5ACH saves 45 (tCO_2 -eq). On the contrary, 8ACH carbon saving is 118 (tCO_2 -eq). Nevertheless, both 5 and 8ACHs reach a carbon balance within six years. On the other hand, 16 ACH saves 550 (tCO_2 -eq). This is due to the energy demand profile from 1 to 16 ACH is nonlinearly increasing, and thus, more carbon savings acquired, estimated to be 112%. increase every 1ACH step

Note that the calculations estimated the grey energy use of transportation and include 1% degradation of the PV efficiency. However, it did not incorporate the embodied emissions from maintenance and dismantling at the end of its lifetime.

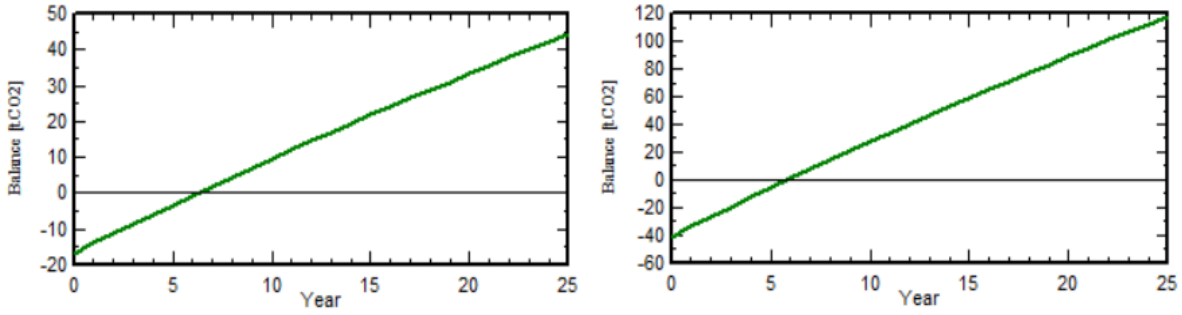

Figure 5.17: Carbon Balance; saved tons of CO_2 versus PV lifetime, Left: 5ACH, Right: 8ACH

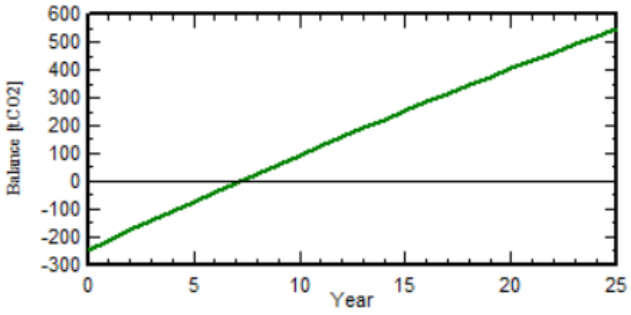

Figure 5.18: Carbon Balance; saved tons of CO_2 versus PV lifetime, 16ACH

CHAPTER 6. RECOMMENDATIONS

The study estimated the worst-case scenario risk probability of infection if ten percent of the indoor users are infected with an exposure duration of four hours. The study conducted the simulations within a range of ventilation rates from 1 to 16 ACH on an office and nursery zone in two distinct settings; Scenario "A" with 100% outdoor air intake with a M5 filter and Scenario "B" operating on 90% of the total air recirculated with a HEPA filter integrated.

Typically, the more we increase the outdoor air, the less the recirculation and the more the air that goes to the filters. Hence, if we look into the overall cost impact, there is a tradeoff between the removal of indoor air contaminants by ventilation and removal by filters. However, both ventilation and filtration techniques were found to reduce the COVID-19 probability of risk with the same order of magnitude. The higher the ACH, the lower the risk probability but higher energy consumption. Scenario "A" has lower ventilation costs to achieve the same risk reduction as scenario "B" due to the latter scenario requiring a higher filtration investment, and operation cost (higher pressure drop).

However, the space heating results suggest that heating cost savings are significant in Scenario "B" due to 90% of air is recirculated while still possessing sensible heat to reheat the space again reducing the convectors heat generation. However, the magnitude of the heating electricity consumption is relatively insignificant to ventilation consumption because of the high COP and lower operation periods throughout the year. Hence, the lower the COP of the heating technology and higher heating demand, the preferable Scenario "B" becomes. Hence, scenario "A" with a heat recovery device is the most profitable option to operate in the focused zones at this point.

Furthermore, it is found that the Nursery shows a higher risk probability than the Office starting from 12% at baseline ventilation rate to 1.5% at 16ACH. In the Nursery the L^2 norm returns 7ACH for Scenario "B" and 8ACH for scenario "A" which meets the 6 to 12 ACH range of healthcare facilities recommended by the CDC, and WHO and falls within the 83 to 278 l/s/ per infector according to Dai and Zhao, 2020. Accordingly, applying 7ACH or 8ACH in the Nursery zone is not only medically adequate but also technically cost-effective.

Similarly, the Office poses a low-risk probability starting at 2.5% at a baseline ventilation rate reaching 0.3%. The 5ACH and 6ACH for Scenario A and B, respectively, meet the minimum of 40 l/s/patient recommended by the CDC, and WHO but not the study of Dai and Zhao, 2020. However, unlike the Nursery, the Office zone is not a healthcare facility where stringent ventilation requirements are necessary. Hence, the 5 to 6 ACH obtained can be lowered to a minimum of 2ACH (equivalent to 14 l/s/person) to meet REHVA's guidance of 10-15 l/s/person. The study found that at 2ACH can decrease the initial risk probability to at least 40%. Nevertheless, the Office zone can still operate at 5 or 6 ACH following the healthcare facilities standards as ASHRAE suggests if deemed necessary. Besides, if the building operator decides to extend the 7ACH in the Nursey and 2ACH in the Office for an additional hour to dilute any remaining airborne contaminants after space occupancy, then it would take 40 and 138 minutes for Nursery and Office respectively to remove 99.9% of indoor airborne contaminants.

Moreover, the results show that by extending the exposure time from four to ten hours, leads to more accumulation of infectious quanta in the room and consequently a higher probability to be inhaled, requiring even higher ventilation rates to dilute (See figure 5.3 and 5.4). Hence, in principle, decreasing the exposure time by reducing the occupancy schedule, i.e., exposure time is a priceless practical approach to consider first.

Undoubtedly, there is not any scenario more cost-effective than the other. It depends on the indoor settings, outdoor air conditions, and building conditions. The maximum possible outdoor air rate that we can bring in is dependent on the weather condition. Scenario "A" is a favorable option only if outdoor conditions are compatible with indoors, reducing the heating loads while not affecting indoor conditions adversely. Alternatively, scenario "B" is an applicable option with high heating load, low efficient heating technology used, and high ACH operation. Besides, scenario "B" is also a good choice to apply with existing HVAC systems where there are no operable windows.

The amount of air recirculated is dependent on the outdoor air conditions to achieve energy savings on the one hand and to eliminate contaminants through filters on the other hand. Hence, a "good practice" approach is to determine the maximum fraction of the outdoor air intake based on the outdoor conditions and the building administrators' energy efficiency tolerance and to upgrade the air filters to a higher index accordingly. Filter upgrade is generally less

feasible to implement than adjusting AHU air intake operational settings because of existing fan capacity. This approach would provide the desired exposure control while minimizing energy penalties. Besides, it is advisable to operate with a heat recovery especially when the fraction of outdoor air intake is high **(O1)**.

Furthermore, ventilation and filtration are not the only strategies to reduce indoor pollutants per se. Viral aerosol concentration control is a new consideration in indoor spaces. Air distribution system designs have a crucial effect on the concentration of viral material inside the confined space which can minimize the possibility of direct person-to-person transmission. The study suggests if ceiling mixing type air distribution is used in the office zone, it is advised to use a supply diffuser with a jet angle of 30° placed away from occupants. The supply diffusers should supply high mass flow rates than the extract grilles with air movement updrafting around the occupants to mix the contaminants at the source on one hand and provide a vertical draft to exhaust on the other hand. This would effectively dilute and remove viral material locally from an unknown point of infection inside the space. Hence, minimizing the uncertainties associated with the impact of air turbulence that may cause virus-laden particles' re-suspension and deposition. Nonetheless, the revision of air distribution is highly dependent on existing space-specific parameters which differ from one case to another (**O2**).

Moreover, the solar energy in the case study building site was found to be suitable for photovoltaics installations. The study found that the IRR and PP values obtained for 5ACH, 8ACH, and 16ACH indicated in the table (5.7) are considered low, and the grid electricity may be a preferable option to consider at this point unless the share of electricity self-consumed increases, and governmental subsidies or other financing schemes for renewables are incorporated to find a better price to sell to the grid. All of which, if implemented, would return higher cash flows relative to the initial investment that deduct the original investment leading to higher renewable project profitability (i.e., IRR) and a lower payback period. Additionally, improving PV efficiency and lowering maintenance cost are additional factors to consider in the long term.

Above all, if a PV installation is decided to be used, it is advisable to supply ventilation above the rate of 5ACH to be profitable under the determined settings used in this study.

Finally, on the carbon emissions side of the PV analysis, the study revealed an exponential increase of 111% in the carbon emissions savings with each 1ACH step reaching 550 (tCO_2-eq) at 16 ACH throughout the system lifetime for the focused zones combined. Hence, if PV is installed to power the focused zones whether in scenario "A" or "B", the CO_2 savings are substantial. In short, PV installation is recommended at higher ventilation rates for the reduction of carbon emissions and the expansion of profits. (**O3**).

CHAPTER 7. CONCLUSION AND FUTURE WORK

The SARS-CoV-2 virus airborne transmission is efficacious in confined spaces with poor ventilation and an insufficient supply of uncontaminated air. Adequate ventilation has always been important, and now we just became even more aware during the COVID-19 pandemic with a swift focus on modeling airborne infection risk. Evidently, removing viral aerosols via ventilation and filtration is necessary to reduce exposure to viral particles.

Despite the limitations and uncertainties attached to quantifying the infection risk using the Wells Riley equation, this research approach to defining infection risk is based on the current information found in the literature that is not definitive or absolute because of the rapid research progress in this field. However, it gives a fair approximation to compare the infection reduction effectiveness and the associated cost to different ventilation strategies. Besides the study provides an insight into how much increase in ventilation the building needs during an outbreak as well as other implications on heating and photovoltaics.

Although there are many ongoing studies to investigate how much ventilation is needed to reduce the infection risk, the current information has no strong scientific evidence. If the SARS-CoV-2 virus and its variants' characteristics are proven with high confidence in future studies, it is recommended to conduct a Computational Fluid Dynamics analysis to obtain a deeper understanding of how air moves around space and to show the different levels of viral concentrations given the spatial variations. Air distribution design and airflow patterns are as important as supplying adequate ventilation to achieve an effective ventilation system design.

Buildings are diverse. Likewise, building systems like design and controls, occupant activities, layout, operation are different. This study is oriented to a specific building site and specific zones setup where heating demand, solar irradiance, and air distribution vary largely from one building to another. However, the methodology remains the same and can be applied to different environments.

Finally, since the beginning of the pandemic, several organizations have produced guidelines (REHVA, ASHRAE, CIBSE) for temporal mitigation purposes. This renewed focus on ventilation and airborne viral transmission will have a significant impact on creating and

revising building codes and standards preparedness for future epidemics and its implications on the design of air handling systems.

REFERENCES

Andersson, B. *et al.* (1993) 'Mass Transfer Of Contaminants In Rotary Enthalpy Exchangers', *Indoor Air*, 3(2), pp. 143–148. doi: 10.1111/j.1600-0668.1993.t01-1-00009.x.

ANSI/ASHRAE (2017) *ANSI/ASHRAE Standard 52.2-2017, Method of testing general ventilation air-cleaning devices for removal efficiency by particle size*, *ASHRAE Standard*.

ANSI/ASHRAE (2019) 'ANSI/ASHRAE Standard 62.1-2019, Ventilation for Acceptable Indoor Air Quality', *Ashrae*, 2019.

Arundel, A. V. *et al.* (1986) 'Indirect health effects of relative humidity in indoor environments', *Environmental Health Perspectives*. National Institute of Environmental Health Sciences, VOL. 65, pp. 351–361. doi: 10.1289/ehp.8665351.

ASHRAE (2013) *ANSI/ASHRAE Standard 55-2010*. Available at: www.ashrae.org (Accessed: 15 May 2021).

ASHRAE (2020) 'ASHRAE Position Document on Infectious Aersols', p. 17.

Atkinson, J. *et al.* (2016) 'Natural ventilation for infection control in health-care settings', *World Health Organization*. Available at: http://www.who.int/water_sanitation_health/publications/natural_ventilation/en/ (Accessed: 14 May 2021).

AWS Scientific Inc. (1997) 'WIND RESOURCE ASSESSMENT HANDBOOK; Fundamentals for Conducting a Successful Monitoring Program', *National Renewable Energy Laboratory (NREL)*, (April), p. 79.

Azimi, P. and Stephens, B. (2013) 'HVAC filtration for controlling infectious airborne disease transmission in indoor environments: Predicting risk reductions and operational costs', *Building and Environment*. doi: 10.1016/j.buildenv.2013.08.025.

Bar-On, Y. M. *et al.* (2020) 'Sars-cov-2 (Covid-19) by the numbers', *eLife*. eLife Sciences Publications Ltd, 9. doi: 10.7554/eLife.57309.

Bekö, G., Clausen, G. and Weschler, C. J. (2008) 'Is the use of particle air filtration justified? Costs and benefits of filtration with regard to health effects, building cleaning and occupant productivity', *Building and Environment*, 43(10), pp. 1647–1657. doi: 10.1016/j.buildenv.2007.10.006.

Bischoff, W. E. *et al.* (2013) 'Exposure to influenza virus aerosols during routine patient care', *Journal of Infectious Diseases*, 207(7), pp. 1037–1046. doi: 10.1093/infdis/jis773.

BizEE Software (2017) *Heating & Cooling Degree Days - Free Worldwide Data Calculation*. Available at: https://www.degreedays.net/ (Accessed: 26 May 2021).

Buonanno, G., Morawska, L. and Stabile, L. (2020) 'Quantitative assessment of the risk of airborne transmission of SARS-CoV-2 infection: Prospective and retrospective applications', *Environment International*. Elsevier Ltd, 145(June), p. 106112. doi: 10.1016/j.envint.2020.106112.

Buonanno, G., Stabile, L. and Morawska, L. (2020) 'Estimation of airborne viral emission: Quanta emission rate of SARS-CoV-2 for infection risk assessment', *Environment International*. medRxiv, 141, p. 2020.04.12.20062828. doi: 10.1016/j.envint.2020.105794.

Business Insider España (2021) *Cuánto cuesta el tratamiento de un paciente con COVID en un hospital público*, *Business Insider España*. Available at: https://www.businessinsider.es/cuanto-cuesta-tratamiento-paciente-covid-hospital-publico-803913 (Accessed: 17 March 2021).

Camfil (2016) *Hi-Flo XLS*. Available at: https://www.camfil.com/en/products/general-ventilation-filters/bag-filters/hi-flo/hi-flo-xls-_-6094 (Accessed: 18 March 2021).

CDC (2003) *Guidelines for Environmental Infection Control in Health-Care Facilities. Appendix B: Air*. Available at: https://www.cdc.gov/infectioncontrol/guidelines/environmental/appendix/air.html (Accessed: 15 February 2021).

CDC (2015) '"Hierarchy of controls".', *The national Institute for Occupational Safety and Health (NIOSH)*. doi: 10.1097/00000446-200312000-00030.

CIBSE, T. C. I. of B. S. E. L. (2020) 'COVID-19 Ventilation Guidance', (Version 4), p. 19.

Commission, E. (2019) *JRC Photovoltaic Geographical Information System (PVGIS)*. Available at: https://re.jrc.ec.europa.eu/pvg_tools/en/#PVP (Accessed: 1 April 2021).

COVID-19: SARS-CoV-2 Aerosol Mechanisms- The Aerosol Society (2020). Available at: https://aerosol-soc.com/covid-19/ (Accessed: 16 March 2021).

Dai, H. and Zhao, B. (2020) 'Association of the infection probability of COVID-19 with ventilation rates in confined spaces', *Building Simulation*. Tsinghua University Press. doi: 10.1007/s12273-020-0703-5.

Davies, A. *et al.* (2013) 'Testing the efficacy of homemade masks: would they protect in an influenza pandemic?', *Disaster medicine and public health preparedness*. Cambridge University Press, 7(4), pp. 413–418. doi: 10.1017/dmp.2013.43.

DesignBuilder (2019) *Help Manual v6*. Available at: https://designbuilder.co.uk/helpv6.0/ (Accessed: 16 June 2021).

DHS (2020a) *Estimated Airborne Decay of SARS-CoV-2 | Homeland Security, Department of Homeland Security*. Available at: https://www.dhs.gov/science-and-technology/sars-airborne-calculator (Accessed: 16 March 2021).

DHS (2020b) *SARS-CoV-2 Airborne Decay Calculator, Technical Report*. Available at: https://www.dhs.gov/science-and-technology/sars-airborne-calculator (Accessed: 26 April 2021).

van Doremalen, N. *et al.* (2020) 'Aerosol and Surface Stability of SARS-CoV-2 as Compared with SARS-CoV-1', *New England Journal of Medicine*, 382(16), pp. 1564–1567. doi: 10.1056/nejmc2004973.

Durand-Moreau, Q. *et al.* (2020) *COVID-19 in meat and poultry facilities: a rapid review and lay media analysis - The Centre for Evidence-Based Medicine, The Centre for Evidence-Based Medicine*. Available at: https://www.cebm.net/covid-19/what-explains-the-high-rate-of-sars-cov-2-transmission-in-meat-and-poultry-facilities-2 (Accessed: 4 February 2021).

Escoda, S. (2012) 'Nueva norma ISO 16890 Filtración', pp. 1–60.

European Centre for Disease Prevention and Controls (2020) 'Heating, Ventilation and Air-Conditioning Systems In The Context of COVID-19', (June), pp. 1–5. Available at: https://www.ecdc.europa.eu/sites/default/files/documents/Ventilation-in-the-context-of-COVID-19.pdf.

European Environment Agency (2020) *Greenhouse gas emission intensity of electricity generation in Europe*, *European Environment Agency*. Available at: https://www.eea.europa.eu/data-and-maps/daviz/co2-emission-intensity-6#tab-googlechartid_googlechartid_chart_111_filters=%257B%2522rowFilters%2522%253A%257B%257D%253B%2522columnFilters%2522%253A%257B%2522pre_config_date%2522%253A%255B2018%253B2019%255D%257D%253B%2522sortFilter%2522%253A%255B%2522ugeo%252 (Accessed: 30 May 2021).

Eurostat (2020) *Electricity price statistics - Statistics Explained., European Commission*. Available at: https://ec.europa.eu/eurostat/statistics-explained/index.php/Electricity_price_statistics#Electricity_prices_for_non-household_consumers (Accessed: 25 March 2021).

Eurovent (2017) *Air filters for general ventilation guidebook*. Available at: www.eurovent.eu (Accessed: 21 March 2021).

Fisk, B. *et al.* (2004) 'Economic Benefits of an Economizer System ':, (June), pp. 1–10.

Gao, X. *et al.* (2016) 'Potential impact of a ventilation intervention for influenza in the context of a dense indoor contact network in Hong Kong', *Science of the Total Environment*. Elsevier B.V., 569–570, pp. 373–381. doi: 10.1016/j.scitotenv.2016.06.179.

Good, J. and Johnson, J. X. (2016) 'Impact of inverter loading ratio on solar photovoltaic system performance', *Applied Energy*, 177, pp. 475–486. doi: 10.1016/j.apenergy.2016.05.134.

IBERDROLA (2021) *Solar plan, 2021*. Available at: https://www.iberdrola.es/en/electricity/solar-plan (Accessed: 5 May 2021).

IDAE (2010) *Guía técnica. Condiciones climáticas exteriores de proyecto., Ahorro y eficiencia energética en climatización*. Available at: http://www.idae.es/uploads/documentos/documentos_12_Guia_tecnica_condiciones_climaticas_exteriores_de_proyecto_e4e5b769.pdf%0Ahttp://www.minetur.gob.es/energia/desarrollo/EficienciaEnergetica/RITE/Reconocidos/Reconocidos/CondicionesClimaticas.pdf.

IRENA (2020) *Renewable Power Generation Costs in 2019*.

ISO (2017) *ISO 17772-1, Part 1: Indoor Environmental Input Parameters for the De- sign and Assessment of Energy Performance in Buildings*. Geneva.

Leclerc, Q. J. *et al.* (2020) 'What settings have been linked to SARS-CoV-2 transmission clusters?', *Wellcome Open Research*. doi: 10.12688/wellcomeopenres.15889.2.

Lee, S., Golinski, M. and Chowell, G. (2012) 'Modeling Optimal Age-Specific Vaccination Strategies Against Pandemic Influenza', *Bulletin of Mathematical Biology*. Springer, 74(4), pp. 958–980. doi: 10.1007/s11538-011-9704-y.

Li, Y. *et al.* (2020) 'Evidence for probable aerosol transmission of SARS-CoV-2 in a poorly ventilated restaurant', *medRxiv*, pp. 1–19. doi: 10.1101/2020.04.16.20067728.

Li, Y., Nielsen, P. V. and Sandberg, M. (2011) 'Displacement ventilation in hospital environments', *ASHRAE Journal*. American Society of Heating, Refrigerating, and Air-Conditioning Engineers, Inc. (ASHRAE), 53(6), pp. 86–89. Available at: https://go.gale.com/ps/i.do?p=AONE&sw=w&issn=00012491&v=2.1&it=r&id=GALE%7CA268310427&sid=googleScholar&linkaccess=fulltext (Accessed: 16 May 2021).

Lindsley, W. G. *et al.* (2020) 'Efficacy of face masks, neck gaiters and face shields for reducing the

expulsion of simulated cough-generated aerosols', *medRxiv*, pp. 1–19. doi: 10.1101/2020.10.05.20207241.

Liu, L. *et al.* (2017) 'Short-range airborne transmission of expiratory droplets between two people', *Indoor Air*, 27(2), pp. 452–462. doi: 10.1111/ina.12314.

López Prol, J. and Steininger, K. W. (2017) 'Photovoltaic self-consumption regulation in Spain: Profitability analysis and alternative regulation schemes', *Energy Policy*. Elsevier Ltd, 108, pp. 742–754. doi: 10.1016/j.enpol.2017.06.019.

McDowall, R. (2006a) 'Chapter 1 - Introduction to HVAC', in McDowall, R. (ed.) *Fundamentals of HVAC IP Book*. Oxford: Elsevier Science Ltd, pp. 1–9. doi: https://doi.org/10.1016/B978-012372497-7/50016-6.

McDowall, R. (2006b) *Fundamentals of HVAC Systems, ASHRAE*.

Mecenas, P. *et al.* (2020) 'Effects of temperature and humidity on the spread of COVID-19: A systematic review', *PLoS ONE*, 15(9 September), pp. 1–21. doi: 10.1371/journal.pone.0238339.

Miller, S. L. *et al.* (2020) 'Transmission of SARS-CoV-2 by inhalation of respiratory aerosol in the skagit valley chorale superspreading event', *medRxiv*. medRxiv, p. 2020.06.15.20132027. doi: 10.1101/2020.06.15.20132027.

Nelson-Jameson (2020) *MERV Ratings*. Available at: https://nelsonjameson.com/learn/sanitation-maintenance/merv-ratings/ (Accessed: 20 June 2021).

Nielsen, P. V. *et al.* (2008) 'Contaminant flow in the microenvironment between people under different ventilation conditions', *ASHRAE Transactions*, 114(2), pp. 632–638.

Noakes, C. J. and Andrew Sleigh, P. (2009) 'Mathematical models for assessing the role of airflow on the risk of airborne infection in hospital wards', *Journal of the Royal Society Interface*, 6(SUPPL. 6). doi: 10.1098/rsif.2009.0305.focus.

Nouvel, R., Cotrado, M. and Pietruschka, D. (2015) 'European Mapping of Seasonal Performances of Air-Source and Geothermal Heat Pumps', *Cisbat 2015*, (September), pp. 543–548. Available at: https://www.researchgate.net/publication/312941341.

Osborn, P. D. (1985) 'Data charts and tables', *Handbook of Energy Data and Calculations*, pp. 1–67. doi: 10.1016/b978-0-408-01327-7.50005-1.

Otter, J. A. *et al.* (2016) 'Transmission of SARS and MERS coronaviruses and influenza virus in healthcare settings: The possible role of dry surface contamination', *Journal of Hospital Infection*, pp. 235–250. doi: 10.1016/j.jhin.2015.08.027.

Pantelic, J., Kwok, & and Tham, W. (2013) 'HVAC&R Research Adequacy of air change rate as the sole indicator of an air distribution system's effectiveness to mitigate airborne infectious disease transmission caused by a cough release in the room with overhead mixing ventilation: A case study', 19, pp. 947–961. doi: 10.1080/10789669.2013.842447.

PrudentAire (2018) 'square Ceiling Diffuser'. Available at: https://www.newpages2u.com/attachments/1532758041adef32fd8fcc3f98e002555058034f12.pdf.

PVsyst (2020) *PVsyst Help manual*. Available at: https://www.pvsyst.com/help (Accessed: 7 April 2021).

PvXchange (2021) *Solar Price Index*. Available at: https://www.pvxchange.com/Price-Index

(Accessed: 5 May 2021).

Qian, H. *et al.* (2020) 'Indoor transmission of SARS-CoV-2', (41977370), pp. 1–22. doi: 10.1101/2020.04.04.20053058.

REHVA (2020) 'REHVA COVID-19 guidance document V 4.0', (4).

Riley, C.E., Murphy, G. and Riley, R. L. (1978) 'AIRBORNE SPREAD OF MEASLES IN A SUBURBAN ELEMENTARY SCHOOL', *American Journal of Epidemiology*, 107(5), pp. 421–432.

Roulet, C. A. *et al.* (2001) 'Real heat recovery with air handling units', *Energy and Buildings*, 33(5), pp. 495–502. doi: 10.1016/S0378-7788(00)00104-3.

Sze To, G. N. and Chao, C. Y. H. (2010) 'Review and comparison between the Wells-Riley and dose-response approaches to risk assessment of infectious respiratory diseases', *Indoor Air*, 20(1), pp. 2–16. doi: 10.1111/j.1600-0668.2009.00621.x.

The Engineering Toolbox (2015) 'Roughness & Surface Coefficients of Ventilation Ducts - engineeringtoolbox.com', pp. 1–6. Available at: https://www.engineeringtoolbox.com/surface-roughness-ventilation-ducts-d_209.html (Accessed: 28 May 2021).

Wei, J. and Li, Y. (2015) 'Enhanced spread of expiratory droplets by turbulence in a cough jet'. doi: 10.1016/j.buildenv.2015.06.018.

William Lawrance, T. S. (2020) *Rotary heat exchangers save energy and prevent a need for recirculation which contributes to the decrease the risk of COVID-19 transfer*, *REHVA Journal*. Available at: https://www.rehva.eu/rehva-journal/chapter/rotary-heat-exchangers-save-energy-and-prevent-a-need-for-recirculation-which-contributes-to-the-decrease-the-risk-of-covid-19-transfer (Accessed: 26 March 2021).

World Bank Group (2018) 'Global Wind Atlas', *Global Wind Atlas*, p. 28782. Available at: https://globalwindatlas.info/ (Accessed: 30 May 2021).

World Bank Group (2020) *Global Solar Atlas*, *Global Solar Atlas*. Available at: https://globalsolaratlas.info/map (Accessed: 30 May 2021).

Zafra, M. and Salas, J. (2020) *A room, a bar and a classroom: how the coronavirus is spread through the air*, *El Pais*. Available at: https://english.elpais.com/society/2020-10-28/a-room-a-bar-and-a-class-how-the-coronavirus-is-spread-through-the-air.html (Accessed: 21 June 2021).

Zemitis, J. and Borodinecs, A. (2019) 'Energy saving potential of ventilation systems with exhaust air heat recovery', in *IOP Conference Series: Materials Science and Engineering*. doi: 10.1088/1757-899X/660/1/012019.

APPENDIX A- CASE STUDY BUILDING

Figure 0.1: The University of the Basque Country - Rectorship building (side view)

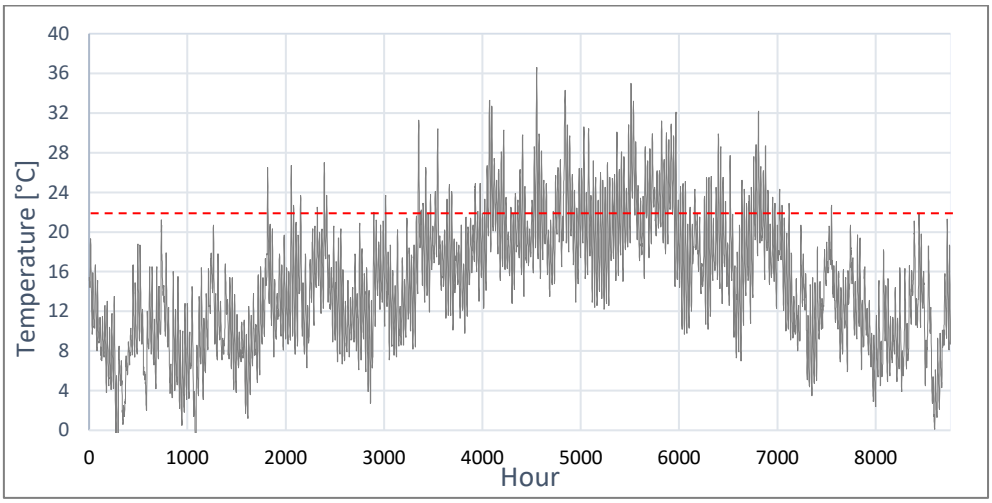

Figure 0.2: Hourly Ambient Air Temperature, Leioa, Basque country, Spain- Red line indicates the heating setpoint. (Meteonorm)

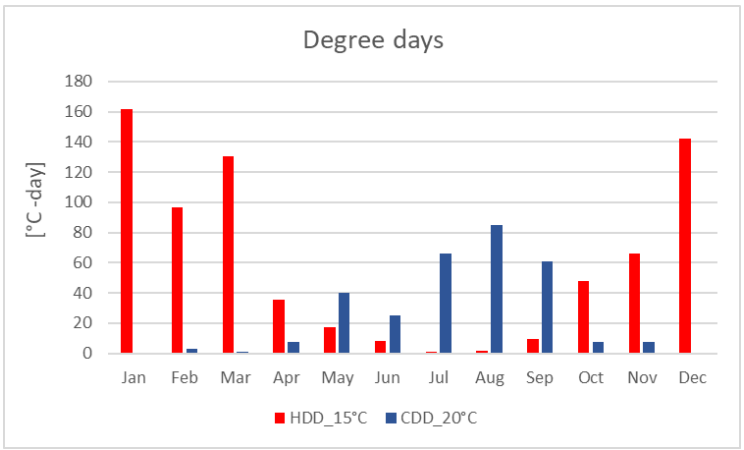

Figure 0.3 : Heating and Cooling degree days in 2020, Leioa, Basque Country (BizEE Software, 2017). Base temperatures obtained from (IDAE, 2010)

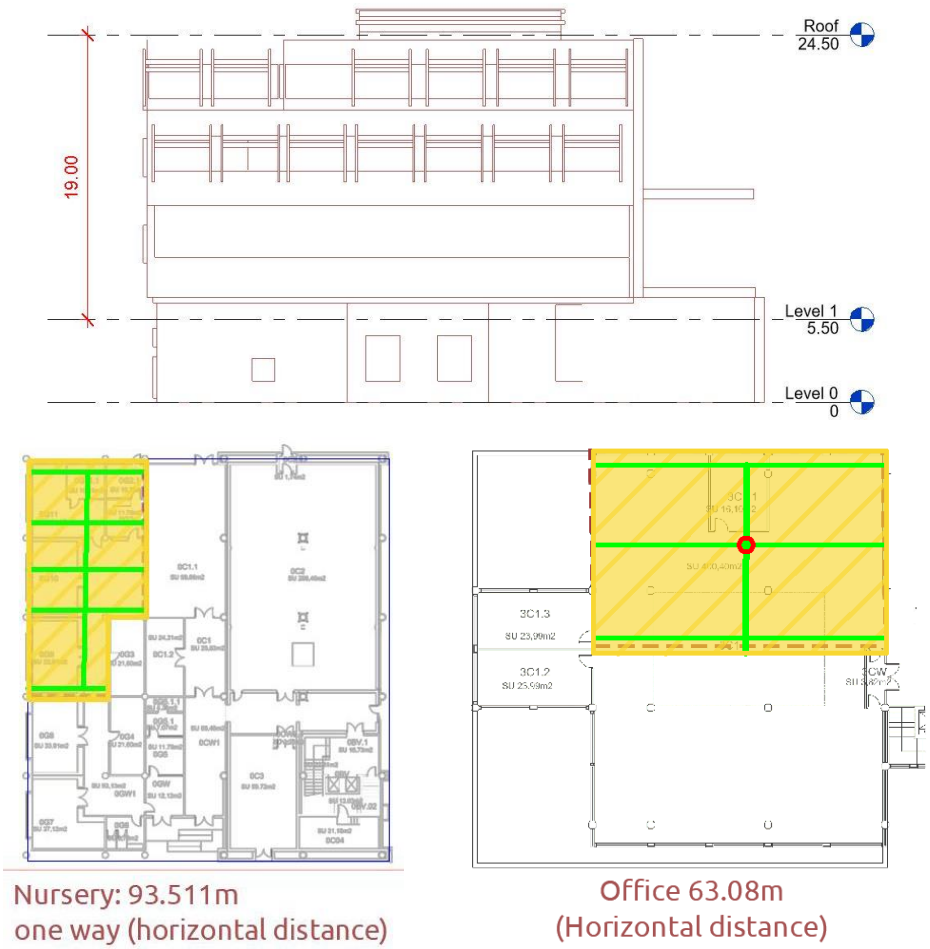

Figure 0.4: Estimating the duct length for focused zones (Vertical and horizontal length)

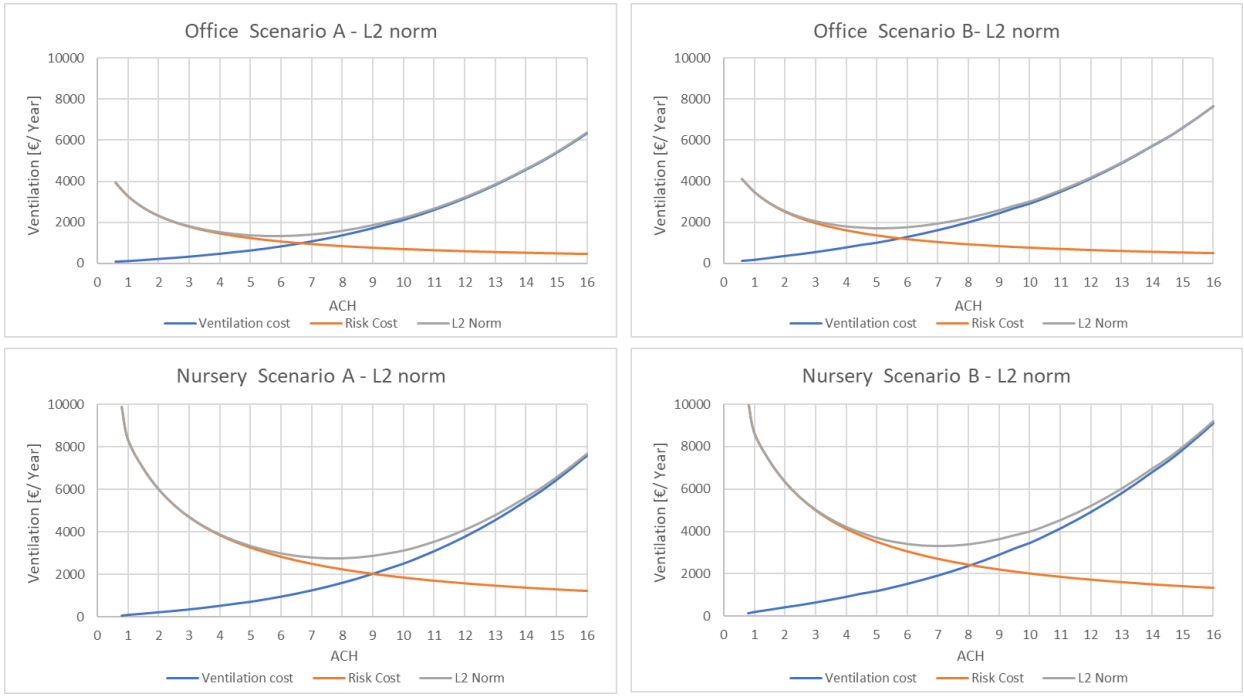

Figure 0.5: L^2 norm for Scenario "A" and "B"

APPENDIX B – PHOTOVOLTAICS SOLAR SYSTEM

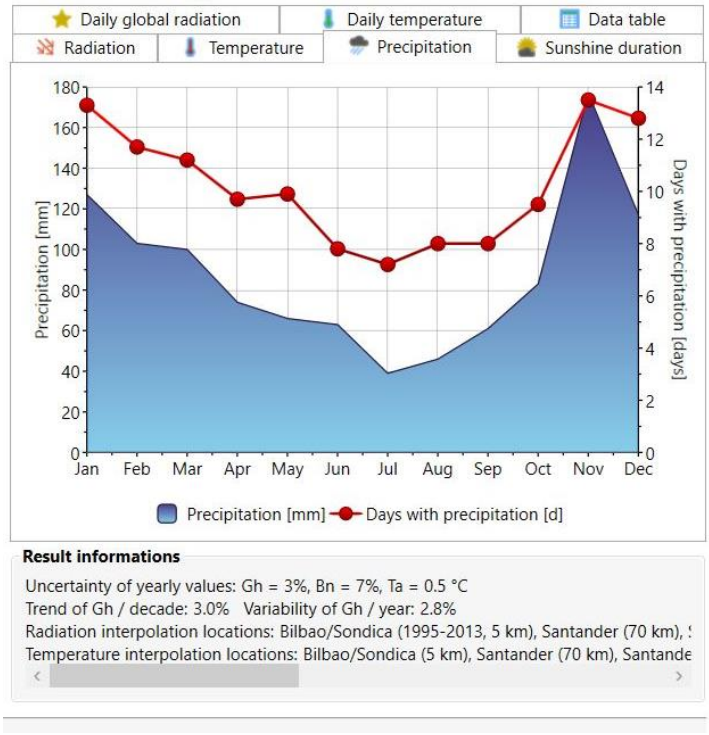

Figure 0.1: Precipitation rate, Leioa, Basque Country, Spain (Meteonorm)

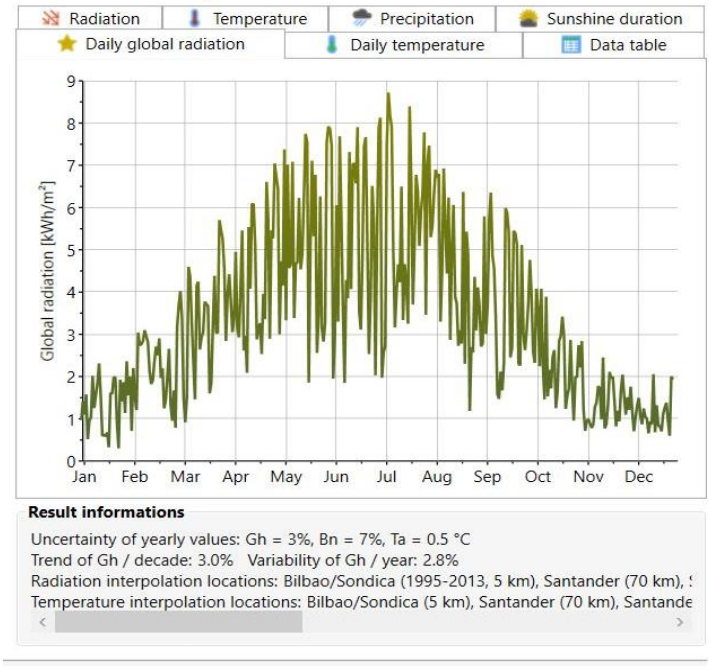

Figure 0.2: Daily global irradiance, Leioa, Basque Country, Spain (Meteonorm)

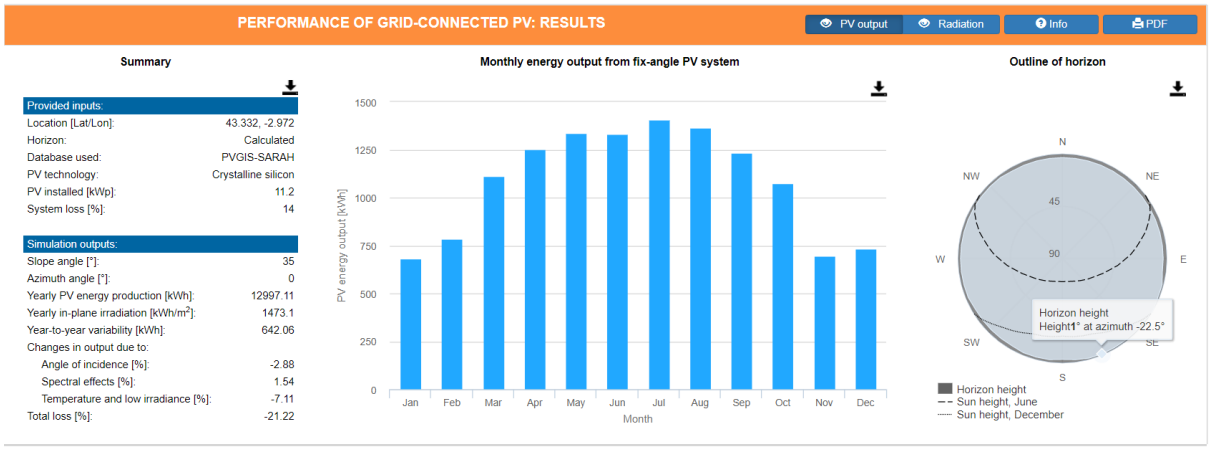

Figure 0.3: Preliminary evaluation of the PV performance potential using (Commission, 2019).

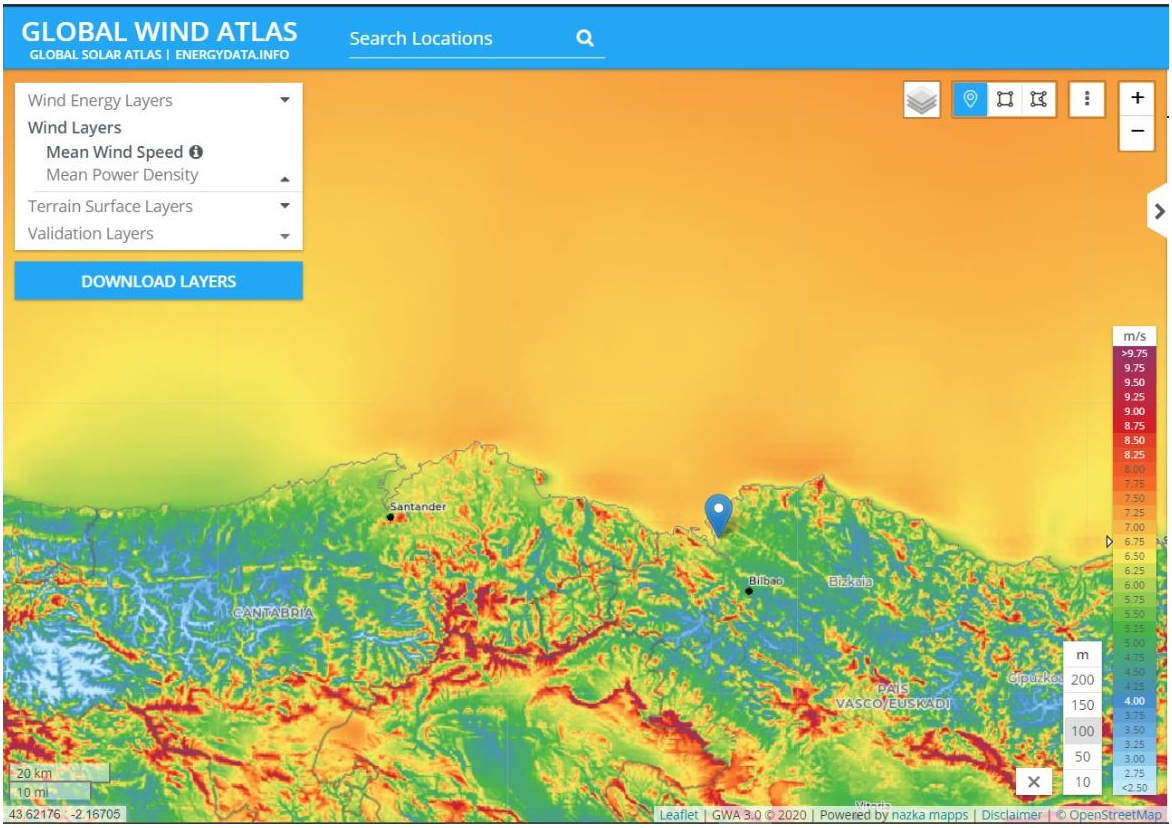

Figure 0.4: Mean wind speed at 100m height (World Bank Group, 2018)

Figure 0.5: PV system LCE calculation for 8ACH (PVsyst)

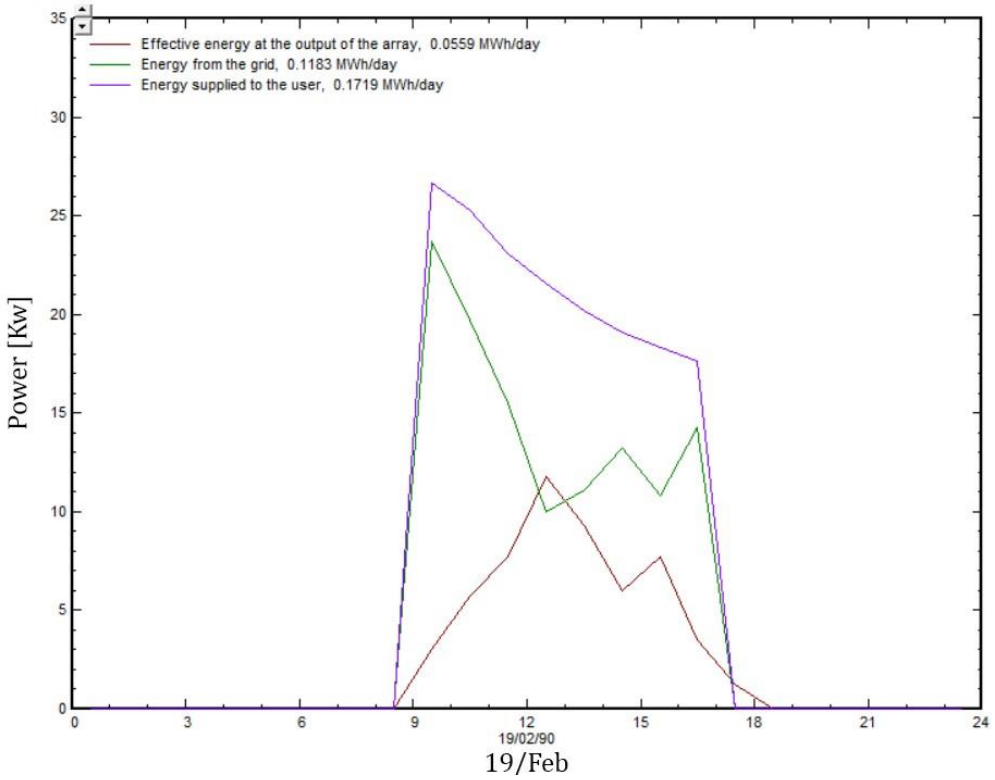

Figure 0.6: 8ACH, 8h operation, winter design day hourly power distribution (PVsyst)

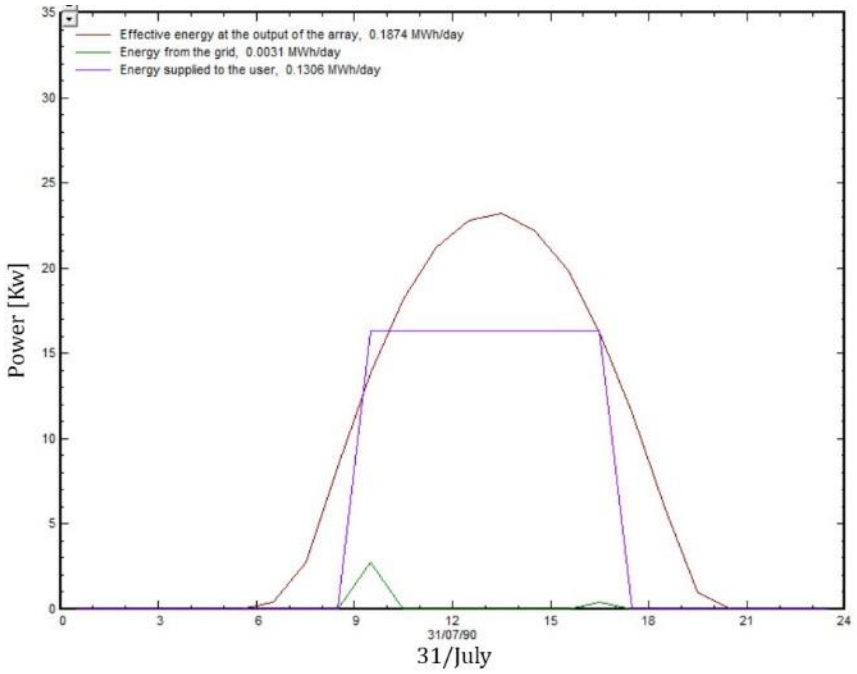

Figure 0.7: 8ACH, 8h of operation, summer design day hourly power distribution (PVsyst)

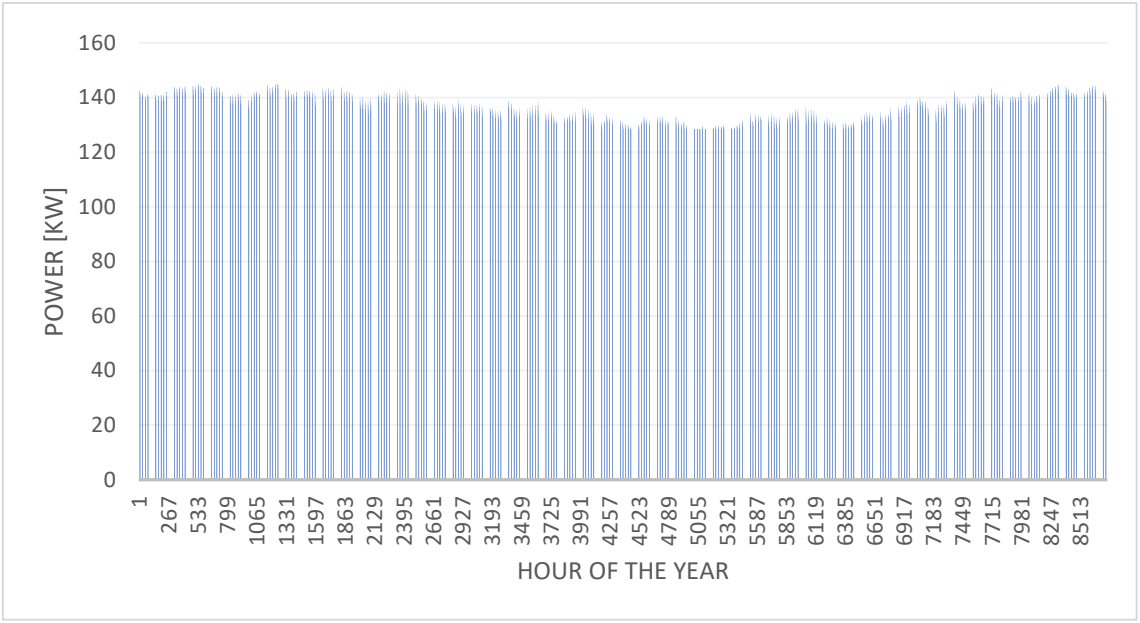

Figure 0.8: Hourly power demand profile at 16ACH

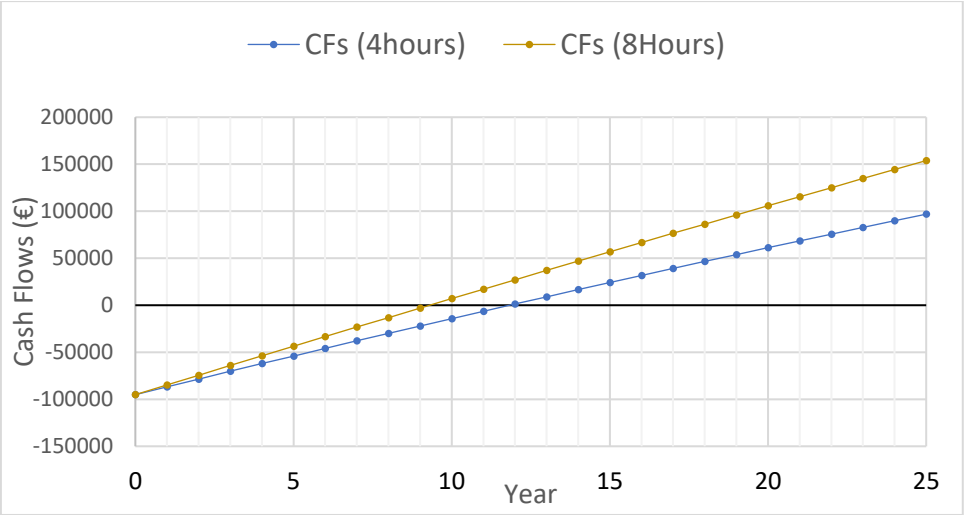

Figure 0.9: Cashflows at 16 ACH

Case study Coordinates:

Latitude: *43.33°* ***Longitude:*** *-2.97˚* ***Altitude:*** *83m above sea level*

End of report